

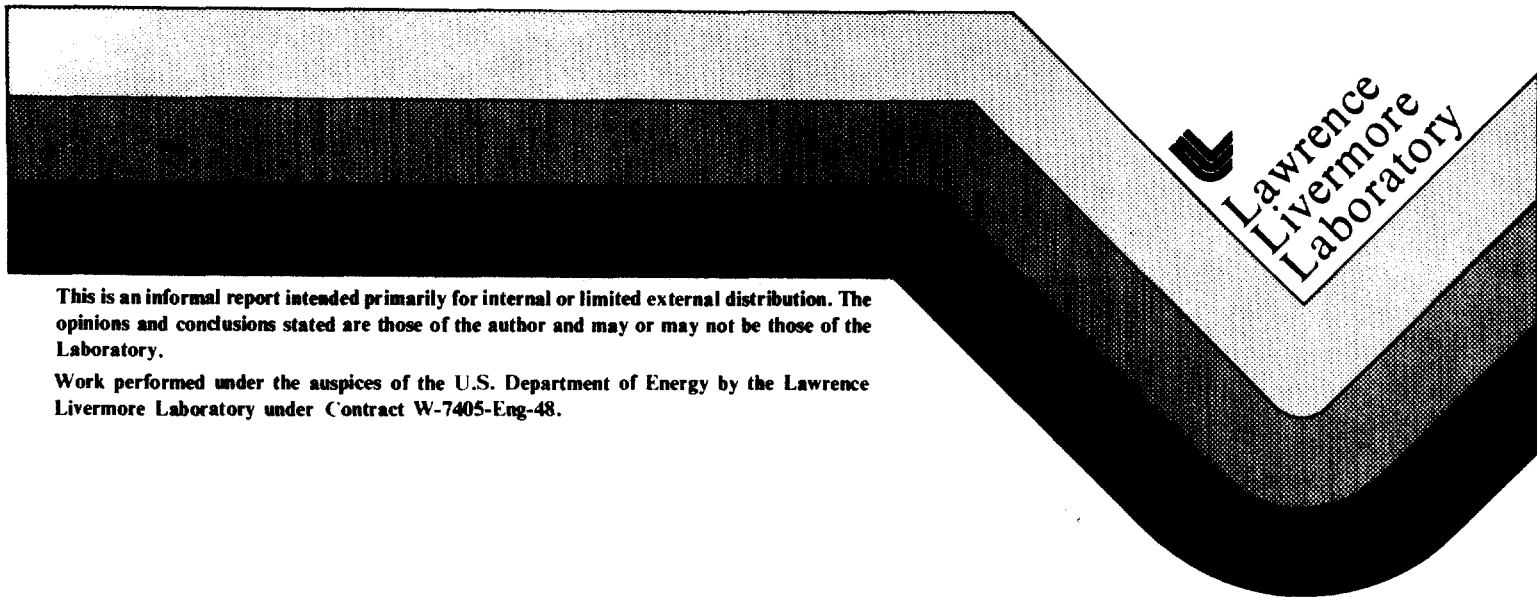
CIRCULATION COPY
SUBJECT TO RECALL
IN TWO WEEKS

UCID-20215 Part 2

PHENOMENOLOGY OF ELECTROMAGNETIC COUPLING
PART II

R. J. King
A. P. Ludwigsen
K. S. Kunz
Electronics Engineering Department
Lawrence Livermore National Laboratory

August 1985



DISCLAIMER

This document was prepared as an account of work sponsored by an agency of the United States Government. Neither the United States Government nor the University of California nor any of their employees, makes any warranty, express or implied, or assumes any legal liability or responsibility for the accuracy, completeness, or usefulness of any information, apparatus, product, or process disclosed, or represents that its use would not infringe privately owned rights. Reference herein to any specific commercial product, process, or service by trade name, trademark, manufacturer, or otherwise, does not necessarily constitute or imply its endorsement, recommendation, or favoring by the United States Government or the University of California. The views and opinions of authors expressed herein do not necessarily state or reflect those of the United States Government or the University of California, and shall not be used for advertising or product endorsement purposes.

This report has been reproduced
directly from the best available copy.

Available to DOE and DOE contractors from the
Office of Scientific and Technical Information
P.O. Box 62, Oak Ridge, TN 37831
Prices available from (615) 576-8401, FTS 626-8401

Available to the public from the
National Technical Information Service
U.S. Department of Commerce
5285 Port Royal Rd.,
Springfield, VA 22161

EXECUTIVE SUMMARY

This report is the second of a planned series which summarize efforts at Lawrence Livermore National Laboratory relating to phenomenology studies of back door coupling from several MHz to 10's of GHz. These studies are pertinent to high altitude EMP (HEMP), enhanced HEMP and microwave coupling. Part I dealt with coupling through apertures into large free-standing cavities having, at most, one interior cable.

An overview of the effort is given in Section 1, and Section 2 summarizes the effects observed in Part I. The main effort since Part I has been devoted to Facilities Development (Section 3), development of an interior coupling decomposition model (Section 4), and coupling experiments (Section 5). Projected future effort is discussed in Section 6. Sections 3 through 6 are briefly summarized here.

Facilities Development (Section 3):

The data reported in Part I only covered the frequency range from 0.1 to 2.5 GHz because of the limitations of the Electromagnetic Transient Range Facility. This facility (now called EMPEROR) has since been upgraded in several ways. Most notably, these upgrades permit cw rather than transient measurements using an automatic network analyzer. The frequency range has now been extended from 0.1 to 18 GHz. Highly resonant interior responses, predicted by a time domain finite difference code, can now be resolved experimentally. As will be seen from the results herein, these enhanced capabilities equally enhance the phenomenological understanding.

In spite of the lack of calibrated field sensors beyond 6 GHz, an empirically derived correction factor is successfully being used to correct for anomalies in the incident field. This permits highly accurate and repeatable cw experimental data to be gathered. It also permits inversion of the cw data to create the time domain impulse response (see Fig. 3.15) validated against analysis using the Numerical Electromagnetics Code (NEC).

Most of the testing was done on PLUTO (Preliminary Livermore Universal Test Object, Fig. 3.17). This object is a simple circular cylinder having a

10:1 length/diameter ratio (including the ground plane image) which generically simulates a missile at the scale model fuselage of an aircraft. PLUTO can be configured with various sizes of apertures, internal cavities, wires and metal or lossy fill, etc.

Coupling to cables in an A7 10:1 scale model aircraft was also done on the EMPEROR Facility to demonstrate the coupling effects for a more realistic system. While such a test object is not an exact scale model, it is a complex system for which the overall coupling features are expected to be like those of a real system.

An anechoic chamber facility is being installed which will operate in the range of 1 to 18 GHz. Section 3.5 describes the facility, including the microwave instrumentation and automatic position/control/recording systems. This facility will permit greater sensitivity and reduce the effects of reflected fields. It is expected to be operational in January, 1986.

Phenomenology Model Development (Section 4):

A simple interior coupling decomposition model has been developed. This model decomposes the response of an interior wire into the product of two factors, each with its own distinctive characteristics. These factors are Shielding Effectiveness (SE) which represents the shielding offered by the exterior shell at low frequencies, and the Coupling Effectiveness (CE) which represents the antenna-like f^{-1} rolloff in the induced current in the interior wires. The model (Fig. 4.1) is called SExCE. It describes the basic features in the envelope of the measured interior wire responses of simple generic test objects.

The SExCE model has been applied to data taken on PLUTO in the EMPEROR Facility. Our conclusion is that SExCE is a robust model, suitable for predicting the coupling to a wide variety of systems subjected to a wide range of stressing electromagnetic fields. These predictions have application in the areas of aerospace system design, hardening, vulnerability and survivability. It assumes some minimal critical information about the physical and electrical properties of the system, such as ports of entry, wire/cable lengths, interior fill, etc.

Experimental Coupling Results (Section 5):

Extensive testing has been done on the EMPEROR Facility using PLUTO and the A7 scale model aircraft. In these experiments the parameters varied are:

- aperture size
- test point location
- interior metal fill
- cavity height
- interior lossy fill
- dielectric loading in the aperture

The SExCE model discussed in Section 4 seems to bound the experimental results well, but considerably more effort is needed to quantify all of the possible interactions. As this work progresses, a major goal is to be able to quickly and easily sketch upper bounds on the overall receiving cross section (RCS) or normalized wire response (NWR). Obviously, this is a very ambitious goal for an exceedingly complex problem, but thus far the results suggest that it is attainable.

From the data given in Section 5, the following general conclusions are drawn:

The aperture size and shape determine the shape of the Shielding Effectiveness (SE) curve (Fig. 4.1). Apertures generally behave as high pass filters having a cutoff frequency which is determined by the perimeter (Fig. 5.2). When the aspect ratio (length/width) is large (10:1 or greater) a pronounced peaking occurs at resonance, and this effect needs further quantification. Above resonance, the SE model appears to approach unity in accordance with Fig. 4.1 if the aperture is large. For smaller apertures, SE above resonance is reduced below unity.

Lengths of the coupling wires/cables largely determine the CE portion of the SExCE model. This curve decreases as f^{-1} above the first TEM wire resonance. This strongly suggests that the CE response envelope is chiefly determined according to TEM resonances as if the wire were unshielded, i.e., it behaves as a long wire antenna. The higher order cavity resonances simply add a "picket fence" like structure to the response.

At frequencies near aperture resonance, coupling to the wire/cable is greatest when it is located near the aperture, and decreases as the wire is moved further inside the cavity. At frequencies far removed from aperture resonance ($f \gg 4f_a$), the location of the wire has little effect on the coupling (Figs. 5.3 and 5.4).

In the aperture studies to date, there is little evidence that external resonances leak into the interior to any significant degree.

Metal fill in the cavity has little effect unless it tends to block the aperture (Figs. 5.6 through 5.14). When the fill is very near the aperture, it reduces the effective size of the aperture, with a consequent increase in the aperture cutoff frequency and Perturbing Effect (PE) factor, especially if the fill is large (Fig. 5.6).

Height of the cavity has little effect on the overall coupling trend (Fig. 5.15), although the higher order cavity resonances add considerable structure to the response above aperture resonance.

Lossy fill inside the cavity can reduce the overall coupling to some degree, especially above 1 GHz. However, the reduction in coupling is not dramatic (Figs. 5.16 through 5.21). More experiments are planned for a wider variety of absorbing materials.

Dielectric windows in the aperture can either increase or decrease the coupling near aperture resonance (Figs. 5.22 and 5.23). Further experiments are also required here, and corroborating data from numerical modeling will be helpful.

Finally, tests on an A7 scale model aircraft conform to the CE of the SE_XCE model. This test object is so leaky, however, that it is not possible to identify a particular port of entry, aperture resonance or the SE portion of the model.

Future Effort (Section 6):

Until the anechoic chamber becomes operational in January, 1986, experiments will be continued using the EMPEROR Facility. Certain experiments must be done in the chamber, particularly those requiring a plane wave front and high sensitivity, because EMPEROR's wavefront is spherical and its gain is

low. Also, those calling for pattern measurements must be done in the chamber. A preliminary timetable for the various tests through 1986 is given. These tests include:

- Multiple wires and cable bundles, ● loaded wires
- including external wires ● composite fill
- thin slots ● seams and connectors
- additional lossy fill ● patterns
- multiple cavities and apertures

A wideband (2-18 GHz) coherent (homodyne) detection system (Fig. 6.3) is being developed for mapping the amplitude and phase of selected field components, particularly inside apertures and cavities. At present, there are no such instruments for mapping fields and measuring currents on wires and conducting surfaces above a few GHz. The system uses a small rectangular \vec{B} loop modulated scatterer as the probe. This probe has negligible effect on the field being measured, and can be easily positioned to measure any desired component of the magnetic field on the exterior or interior of the test object. This system is not yet operational although the components are on hand.

The technology base and the associated phenomenology of electromagnetic coupling presented in this report span issues in all three programmatic areas of electromagnetic effects; namely high altitude EMP, enhanced high altitude EMP and high power microwaves. The focus in this report is on linear coupling effects. In subsequent reports, we will start addressing the equally important nonlinear coupling phenomena associated with high fluences.

PREFACE

Recent advances in the development of electromagnetic weapons have increased interest in vulnerability and lethality of such weapons. A key factor in being able to predict the vulnerability of military systems to such threats involves understanding the phenomenology of how electromagnetic energy couples into cavity-like objects, or the so-called "back-door" coupling.

Regimes of interest span the domain of nuclear electromagnetic pulses (EMP) in which the frequencies extend up to several hundreds of MHz to microwave coupling (from 0.5 GHz to above 40 GHz). The latter is somewhat different because the wavelength is comparable to the size of the ports of entry (apertures, seams, cracks, protruding connectors, etc.). These ports of entry and the interior configuration of a vulnerable system are no longer below cutoff, and can permit significant penetration of the microwave energy into susceptible electronic systems. In fact, these coupling paths can be highly resonant at certain microwave frequencies, making the shielding against microwave threats difficult. Moreover, the dimensions of the coupled cavities and internal wires/cables are often tens or even hundreds of wavelengths.

This report is the second of a planned series which summarize efforts at Lawrence Livermore National Laboratory relating to phenomenology studies of electromagnetic back door coupling.

Part I dealt with coupling through apertures into large free-standing cavities having, at most, one interior cable [1]. These simple test objects were chosen chiefly to study the phenomenology of aperture coupling.

The data reported in Part I only covered the frequency range from 0.1 to 2.5 GHz because of the limitations of the Electromagnetic Transient Range Facility. This facility (now called EMPEROR) has since been upgraded in several ways. Most notably, these upgrades permit cw rather than transient measurements using an automatic network analyzer. The frequency range has now been extended from 0.1 to 18 GHz. As will be seen from the results herein, these enhanced capabilities equally enhance the phenomenological understanding.

This report builds on the phenomenology observed and reported earlier [1]. It gives broadband coupling data for free-standing cylinders having at most one interior coupling cable, various lossy and metal fill inside the cavity, and dielectrically loaded apertures. More complex test objects will be used as this work continues, namely, multiple cables with branching and protruding conductors, and slit-like apertures. Later, when the planned anechoic chamber is installed, testing of multiple apertures and multiple cavities will be done, including the measurement of radiation patterns and polarization effects. These long-term investigations will form the basis for understanding microwave coupling phenomenology.

ACKNOWLEDGMENTS

This work was funded in part by the Defense Nuclear Agency Task Code X99QMXVC (EMP Environments and Coupling), Work Unit 00019 (New Analytical Tools).

The long list of contributors to this report reflects the diverse talents needed to carry out these experiments. Ralph Boberg's expert technical assistance in the design and implementation of the new facilities made it all possible. The experiments were planned by Ray King, Karl Kunz, Pete Ludwigsen, and Gerry Hudson. Pete Ludwigsen implemented the control software for the instrumentation system and carried out the experiments, assisted by Dan Gnade, Gerry Hudson, Steve Pennock, and Jim Breakall. In addition, Dan Gnade, Steve Pennock, Pete Ludwigsen, Jeff Norris, Gerry Hudson, and Brian Daniels assisted in the installation of the new EMPEROR monocone, and in its characterization.

Likewise, many people contributed greatly to the phenomenological interpretation of the data, notably Karl Kunz, Ray King, Pete Ludwigsen, Gerry Hudson, Steve Pennock, Hriar Cabayan, and Jim Breakall. In particular, Karl Kunz conceived and wrote Section 4 on shielding/coupling effectiveness, and Pete Ludwigsen prepared the data in Section 5.

Finally, we acknowledge the excellent word processing of the text done by Linda Edinger and Barbara Sokoloski, the timely drafting support by John Danielson, and the cheerful assistance of the Secretary for the Microwave and EMP Group, Marcie March.

TABLE OF CONTENTS

<u>Title</u>	<u>Page</u>
Executive Summary.....	i
Preface.....	vi
Acknowledgments.....	viii
1. Overview.....	1
2. Summary of Phenomenology Observed in Part I.....	3
3. Experimental Microwave Coupling Facilities.....	9
3.1. The Emperor Monocone.....	10
3.2. Instrumentation.....	14
3.3. Performance of the Emperor Facility.....	16
3.3.1. Characterization of the Incident Field.....	18
3.3.2. Derivation of the Correction Factor.....	21
3.3.3. Spatial Variations in the Incident Field.....	25
3.4. Test Objects.....	26
3.4.1. Generic Models.....	26
3.4.2. Aircraft Models.....	28
3.5. Microwave Anechoic Chamber.....	28
4. A Simple Interior Coupling Decomposition Model: Its Development and Application.....	34
4.1. Introduction.....	34
4.2. Development.....	35
4.3. Discussion.....	39
4.4. Summary.....	40
5. Experimental Coupling Results.....	42
5.1. Introduction.....	42
5.2. Effects of Aperture Size.....	44
5.3. Varying Test Point Location.....	45
5.4. Varying the Size and Location of Metal Fill.....	47
5.5. Varying Cavity Height.....	57
5.6. Lossy Fill.....	58
5.7. Dielectric Loading in Aperture.....	64
5.8. A7 Scale Model Aircraft Tests.....	66
5.9. Concluding Remarks.....	68
6. Future Effort.....	71
6.1. Tests on Generic and Scale Model Test Objects.....	71
6.2. Broadband Field Mapping Homodyne System.....	74
6.2.1. Basic System.....	75
References.....	81

1. OVERVIEW

The vulnerability of electronic systems to high intensity electromagnetic fields is a long-standing problem which is becoming increasingly important under the threats of high altitude electromagnetic pulse (HEMP) and high power microwaves. This is an extremely complex problem involving many interdependent issues such as coupling, susceptibility, air breakdown, signal processing, and probabilistic failure analysis. Several threat parameters must be considered such as the intensity, polarization, angle of incidence, and spectrum of the EM field which is incident on the system. Many system parameters play important roles such as object shape; aperture size, shape and location; and the interior structure including cable layout. Further, stress parameters such as the interior field distributions, and voltages and currents induced at vulnerable pin locations are needed to finally predict the susceptibility of electronic components to malfunction or even burnout.

Modeling tools are essential to understand the phenomenology, whether they are analytical, numerical, or experimental. Combinations of these tools are complementary and serve to validate each other and the many phenomena. LLNL is approaching these problems from a phenomenology point of view, whereby analytical and experimental models are used to gain basic understanding of the individual effects, the end objective being to understand and predict vulnerability of the overall complex system. The current focus is on generic objects, the simplest of which permit analytical and numerical modeling to validate corresponding experimental models and vice versa. As the complexity increases, experimental tests may be the only alternative at the present time although finite difference super codes are being developed and implemented. These codes can be powerful tools for modeling complex systems.

The objectives are twofold:

- Programmatic: To develop experiments, test/signal processing techniques and validated modeling tools to evaluate electromagnetic coupling into systems, both front and back door.
- Technical: To phenomenologically determine how the test parameters (power, frequency, polarization, pulse length, incidence angle,

etc.) and the system parameters (entry ports, internal structure, cavity size and shape, etc.) relate to the observable responses (energy, voltage, or current).

The tools being used in the overall program are depicted in Fig. 1.1 which shows use of generic objects as experimental models, the experimental facilities for conducting the tests, the modeling tools, and the data processing tools which are available for analyzing and processing the data.

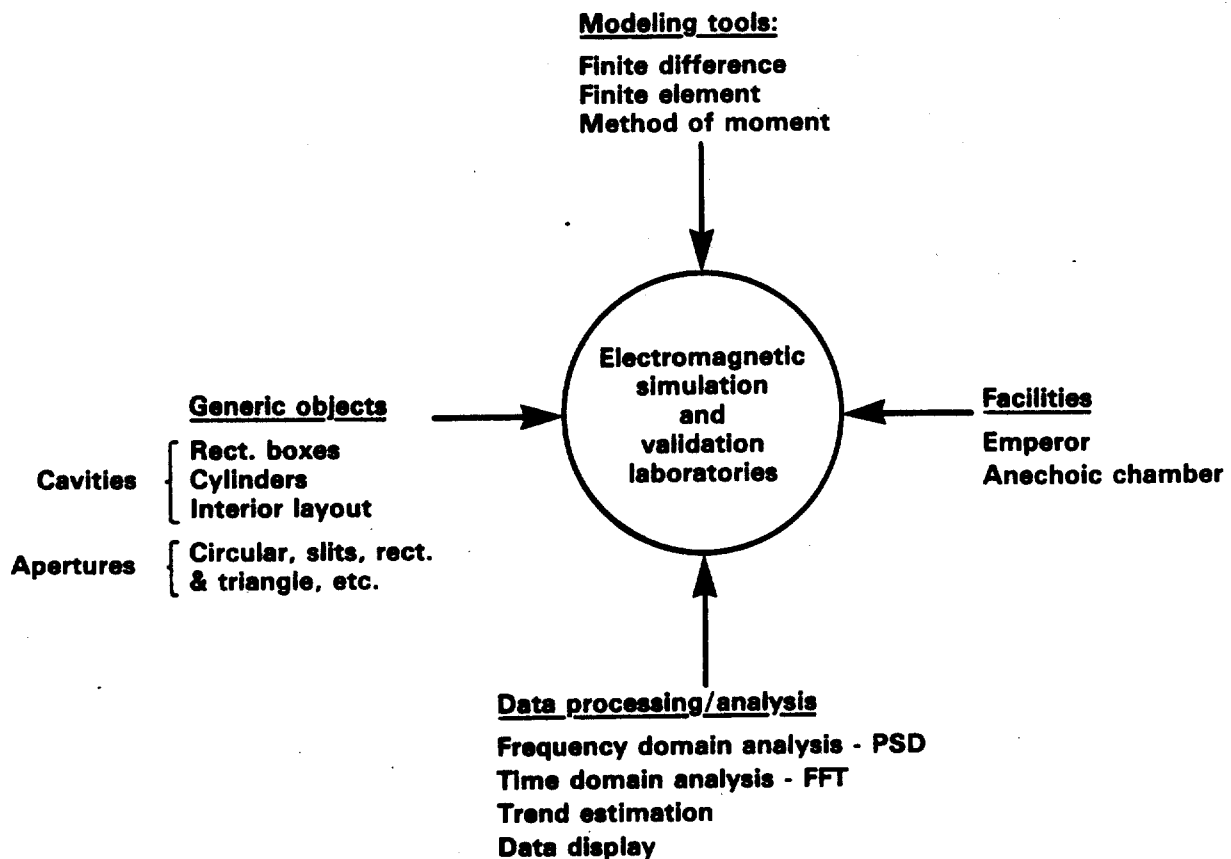


Figure 1.1 Development tools used in the LLNL Electromagnetic Simulation and Validation Laboratories.

2. SUMMARY OF PHENOMENOLOGY OBSERVED IN PART I

The initial electromagnetic coupling phenomenology studies described in Part I give results for relatively large stand-alone apertures and cavity-backed apertures using large simple boxes and cylindrical cavities as generic test objects having, at most, one interior coupling cable (wire) [1]. All of the experimental results reported there were obtained using the Electromagnetic Transient Range Facility (EMTRF) which is limited to 2.5 GHz at the upper frequency end. In these data, the source wave is a 360 ps pulse normally incident on the aperture since this presumably represents a worst case.

The salient features learned from these experiments for coupling through apertures were:

- (a) The onset of most significant coupling through an aperture occurs at the frequency, f_a , for which the perimeter of the aperture is about one wavelength, regardless of aperture shape. Typical data which illustrate these points are shown in Fig. 2.1. These data are for a \bar{D} probe located 5 cm behind various aperture shapes in a metal plane without a backing cavity. The apertures all have the same perimeter (40 cm with the ground plane image) and hence have the same frequency, f_a ($= 0.75$ GHz) where the perimeter is one wavelength. These data demonstrate the effect of the aspect ratio. Note that for the larger aperture aspect ratios (e.g., the 18 x 1 and 15 x 2.5 cm apertures) the transfer function peaks above that for the circular and square apertures, but falls below at frequencies somewhat above f_a . Above about $1.5 f_a$ the responses are all relatively constant with frequency. $T(f)$ for circular and square apertures are essentially the same. Other experiments showed that the field amplitude at f_a in the aperture is approximately cosinusoidal.
- (b) Coupling is strongest at f_a when the incident electric field is normal to the narrow dimension of the aperture, particularly when the aspect ratio of the aperture is large. In such cases, coupling

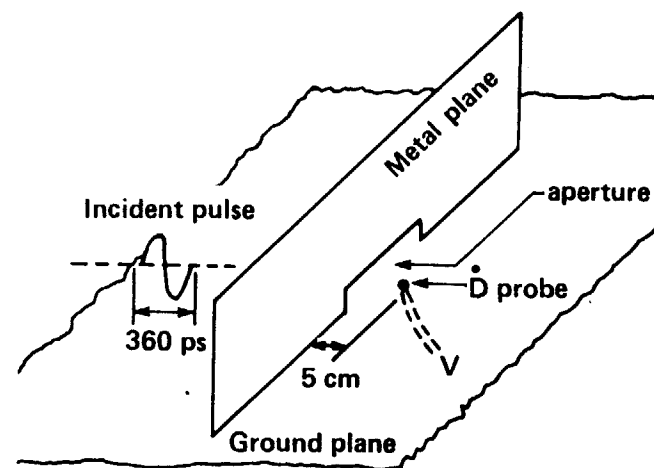
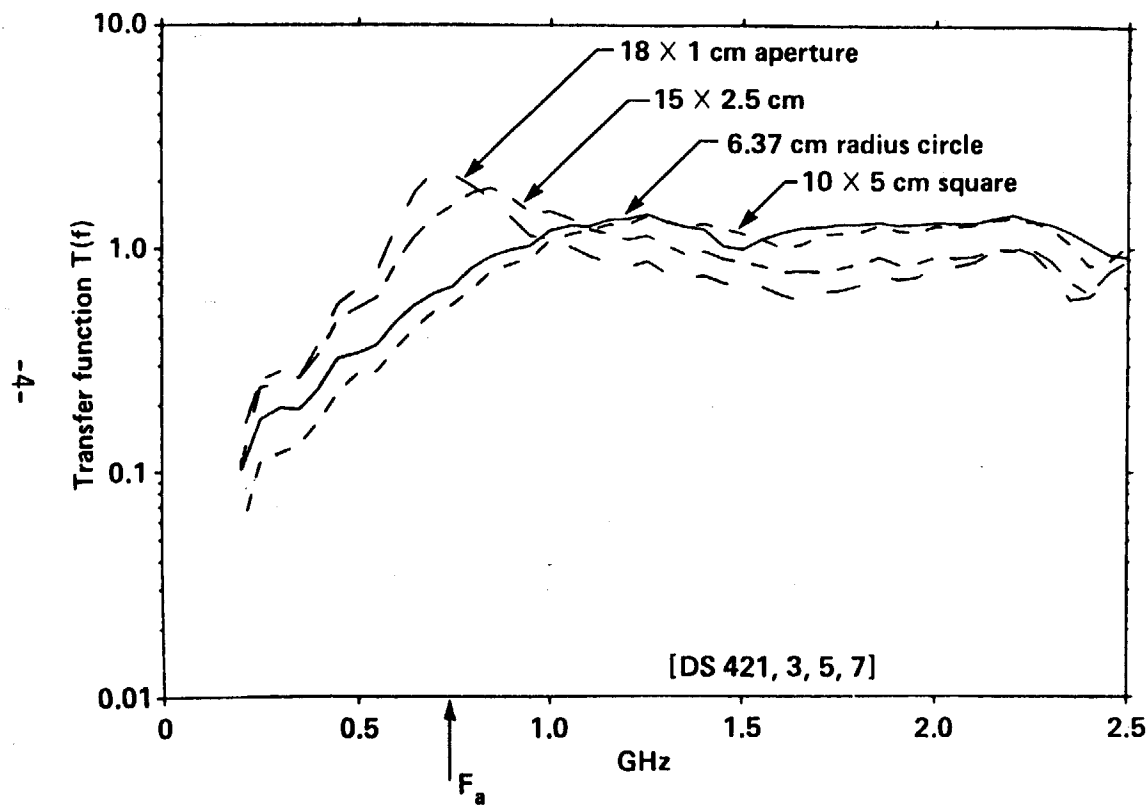


Figure 2.1. Transfer function for various aperture shapes in a metal plane. All apertures have the same perimeter and hence the same frequency f_a where the perimeter is one wavelength.

peaks at f_a followed by a decrease somewhat above f_a , eventually becoming relatively constant (energy "shines" through the aperture). This effect is most evident when the sensor is close to the aperture. Moving the sensor away from the aperture tends to reduce the coupling at all frequencies, but particularly at frequencies near f_a .

- (c) Apertures having a small aspect ratio (e.g., squares, circles, and apertures having the long dimension parallel to the incident E-field) have significantly reduced coupling at f_a , behaving much like a simple high-pass filter. At frequencies somewhat above f_a , the energy again appears to "shine" through.
- (d) When a large cavity backs an aperture, the main effect of the cavity is to add structure to the spectrum as shown in Fig. 2.2. As the length of the time record increases, this structure characterizes the buildup of modes. These modes may be due to either wall reflections or waves reflected along the length of internal cables. For very long time records, these modes evolve into high Q resonances resembling a "picket fence" spectrum.
- (e) Adding lossy material to the coupling probe can significantly reduce the coupling, particularly at the microwave frequencies (above 3 GHz). The effects of introducing lossy material is considered in Section 5.
- (f) Short time records for coupling through an aperture (whether backed by a cavity or not) predominantly characterize the aperture response (Fig. 2.3). The spectra for such short records may be useful to estimate current or voltage breakdown of electronic devices. As the length of the time record increases, both the structure and the mean level of the spectra increase since more energy is captured by the sensor. This type of spectral information is useful for estimating thermal breakdown of devices. In these data, "trend" refers to smoothing accomplished using a moving average of nine adjacent points.

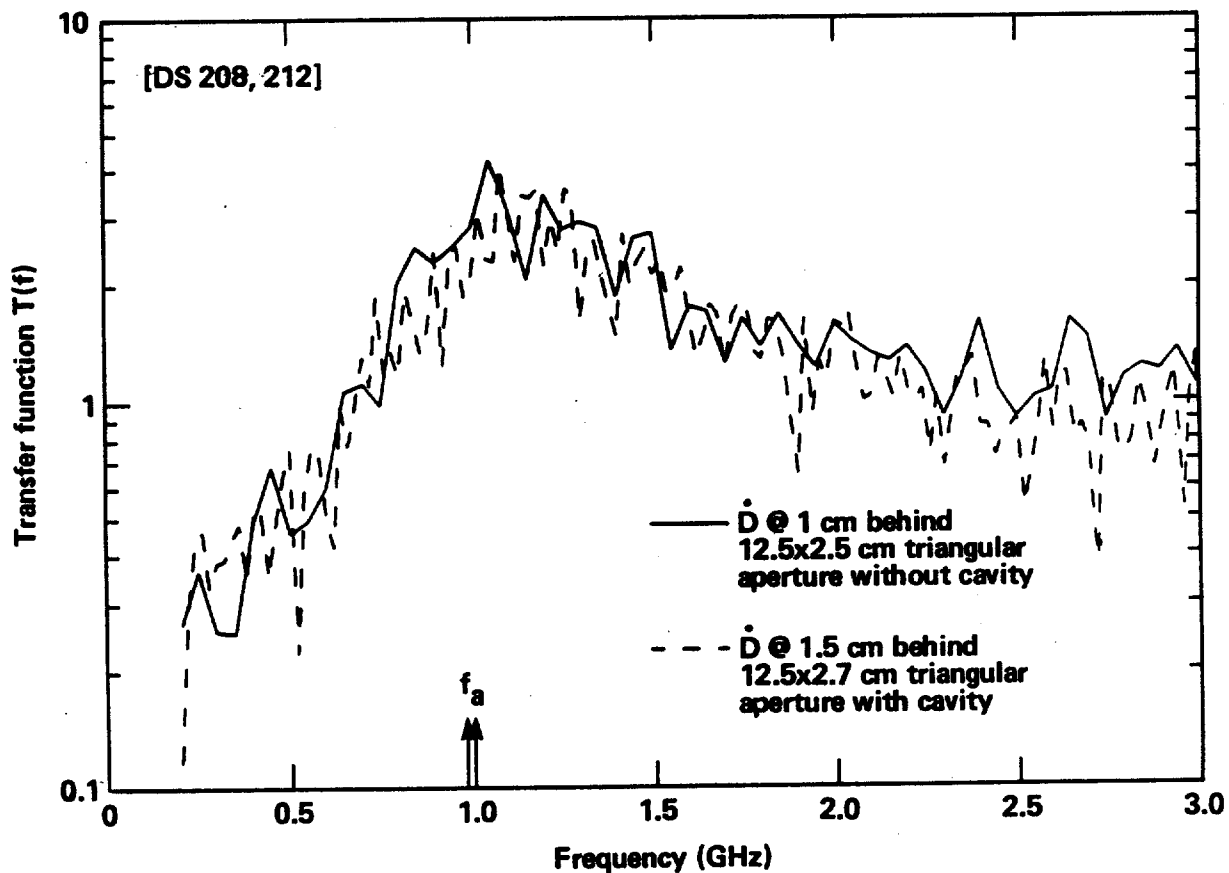
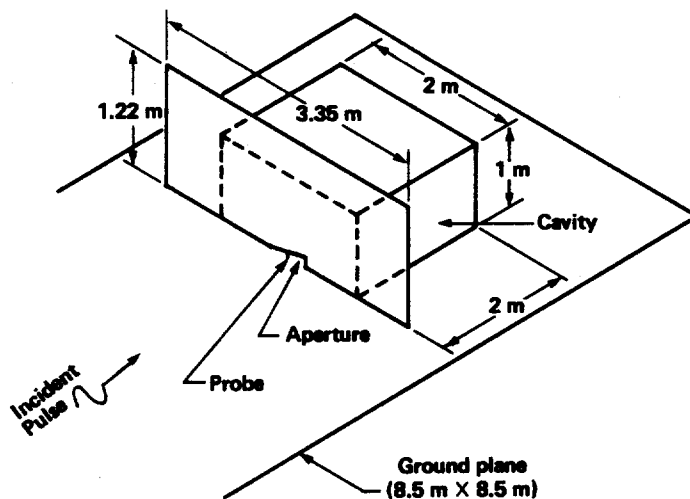


Figure 2.2. Comparison of transfer functions for a \dot{D} sensor behind nearly identical triangular apertures, with and without a large 2x2x1 m rectangular cavity. Note that the major effect of the cavity is that internal reflections add structure to the response (50 ns record). For a sufficiently long time record, the structure evolves to "mode" resonances.

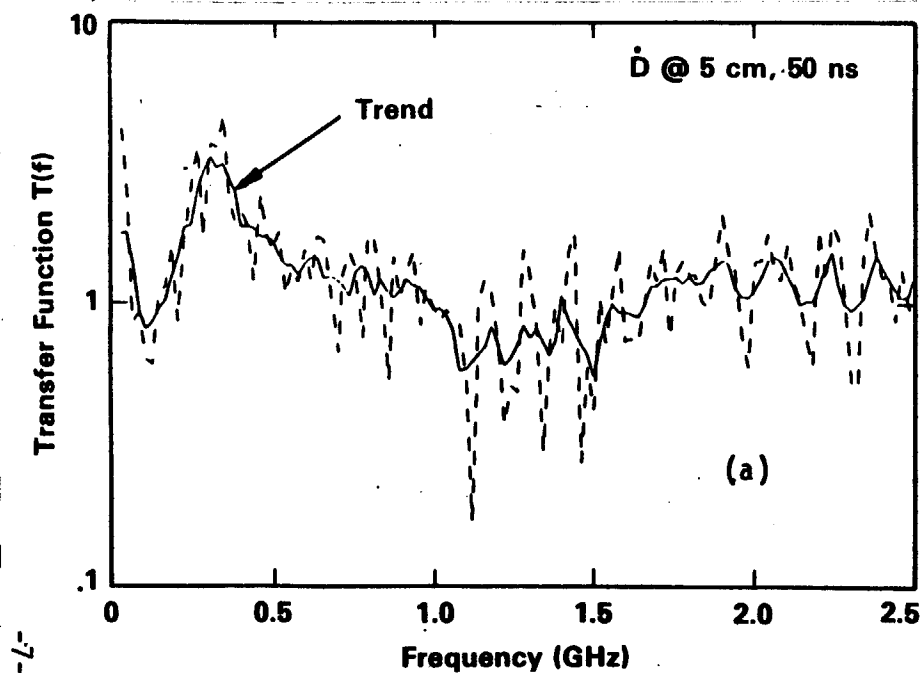
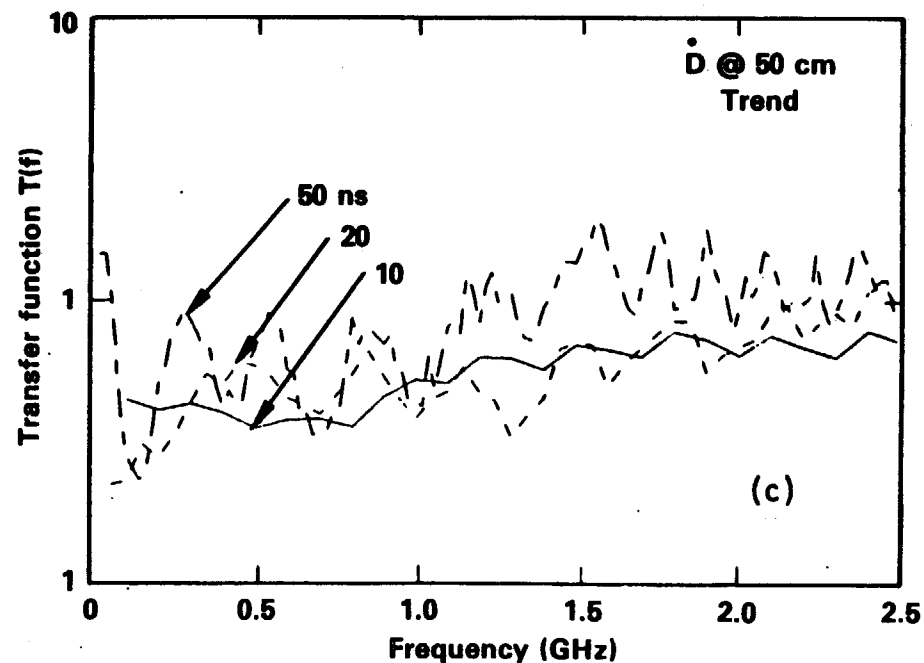
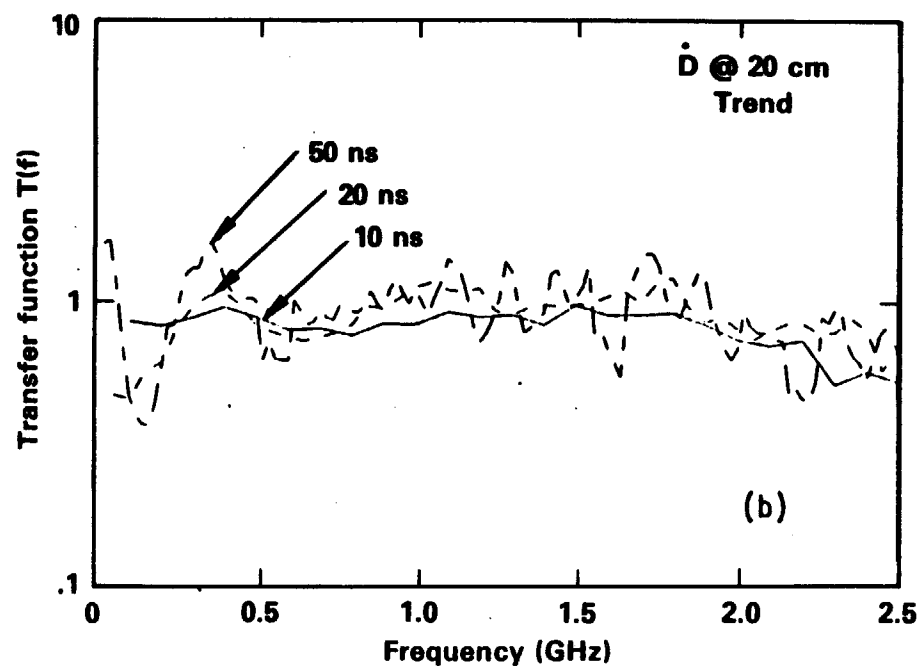
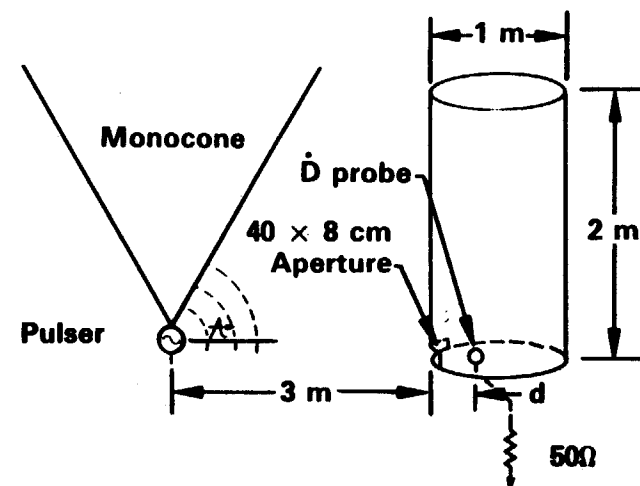


Figure 2.3 Transfer functions corresponding to time records of 10, 20, and 50 ns for a \dot{D} sensor inside a cylindrical cavity. Note the increase in structure and mean level of $T(f)$ for the longer time records.



The results in Part I clearly indicate the need to either extend the recorded response time so that the overall features of the total test object are observable, or else observe the response for continuous waves.

In the development of analysis codes, frequency domain codes based on a method-of-moments approach show little promise for handling interior coupling problems having dimensions greater than a few wavelengths. Available time domain finite difference and finite element codes are more promising, but they too are limited in the size of problem which can be economically handled. There is some hope, however, by incorporating clever algorithms. Moreover, the introduction of realistic dielectric losses may ease the computational requirements, especially at the higher microwave frequencies.

3. EXPERIMENTAL MICROWAVE COUPLING FACILITIES

The initial coupling studies reported in Part 1 were done in the time domain [1]. The facility was then known as the Electromagnetic Transient Range Facility (EMTRF). This facility had two major shortcomings. First, the rough surface of the monocone antenna and finite size of the range itself caused the incident time domain pulse to be severely contaminated by undesired scattering and reflections. Second, the frequency content of the state of the art high voltage pulser only extends up to about 2.5 GHz. This limited frequency coverage is hardly sufficient to yield a complete understanding of microwave coupling issues.

The first problem was very successfully solved by designing and installing a new monocone antenna shrouded by EM absorber. This indefinitely extended the free time for recording time responses. The second problem still remains when the facility operates in the time domain because of the limitations of the source pulser, but has been successfully solved by operating in the frequency domain using a sophisticated automatic network analyzer. Complete details on the time domain instrumentation and signal processing system are given in [1]. The following discussion focuses on the upgrade of this facility and its associated cw instrumentation system. This upgrade has resulted in a facility where highly repeatable exterior and interior measurements can be made on test objects for frequencies up to 18 GHz. Highly resonant interior responses, predicted by a time domain finite difference code, can now be resolved experimentally.

The cone is very nearly a true conic so that the radiated field has very small azimuthal variations. As would be expected from the use of a monocone, the field behaves as $1/r$ as shown in Section 3.3. The added frequency domain measurement capabilities make this facility unique, since both time and frequency domain measurements are possible using the same transmitting antenna.

3.1. THE EMPEROR MONOCONE

Dubbed EMPEROR (for EMP Engineering Research Omnidirectional Radiator), the monocone is mounted on an 8.5 x 8.5 m ground plane and suspended from the ceiling (Fig. 3.1). It consists of a solid cast aluminum base and an upper portion formed from sheet aluminum 0.050 in. thick attached to a girded framework. The upper portion is formed from five identical sectors bolted together. The seams are covered with conductive adhesive backed copper foil tape to form a smooth contiguous surface. The tolerances for this portion are on the order of ± 3 mm or 0.2λ at 18 GHz. Anywhere on the perimeter of the cone, the out-of-round deviation is approximately ± 1 cm. The 60 cm high base is machined to a 47 degree half angle and finished to a tolerance of ± 0.025 cm. The overall height is 3 m.

Since the monocone is supported from the ceiling, a "floating" connector arrangement (Fig. 3.2) allows a 0.5 m diameter portion of the floor to move up and down with the cone as the ceiling expands and contracts during the day. This motion is on the order of ± 3 mm and the impedance change is no more than 0.3 ohms. The connection from the 50 Ω coaxial feed line is through a modified, precision APC-7 to N adapter which is specified to operate up to 18 GHz.

In order to mitigate reflections from the walls, ceiling, and edges of the ground plane, commercial EM absorbers in the form of four-foot pyramidal carbon-impregnated urethane wedges were used to surround the EMPEROR antenna (Fig. 3.3). An additional wall of absorber was also placed behind the test volume which is where the white polystyrene object is shown. Figure 3.4 shows a 100 ns time domain record of a \dot{D} sensor at 2.4 m from the cone apex before and after absorber installation. The extent of the late time quieting (about 12 dB) and consequent extension of the facility "clear time" is clearly evident. The corresponding spectra for a 20 ns record are shown in Fig. 3.5. A more complete picture of the absorber effects at the low frequencies (10 to 500 MHz) is shown in Fig. 3.6. As can be seen, there are very significant variations below 100 MHz, which is the lowest frequency where reliable cw measurements can be made. The data with the absorber is for a 100 ns time record, while that without the absorber used a 20 ns record (to eliminate reflections).

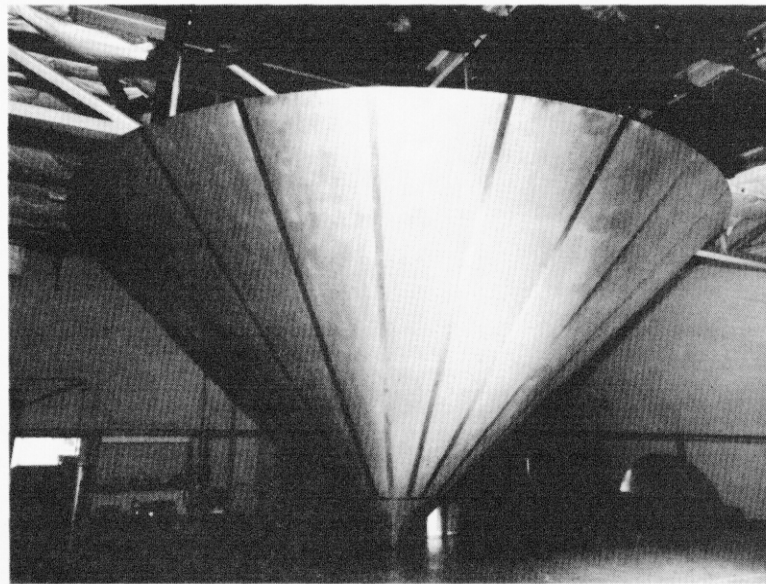


Figure 3.1. Photo of the EMPEROR monocone before the installation of absorbers.

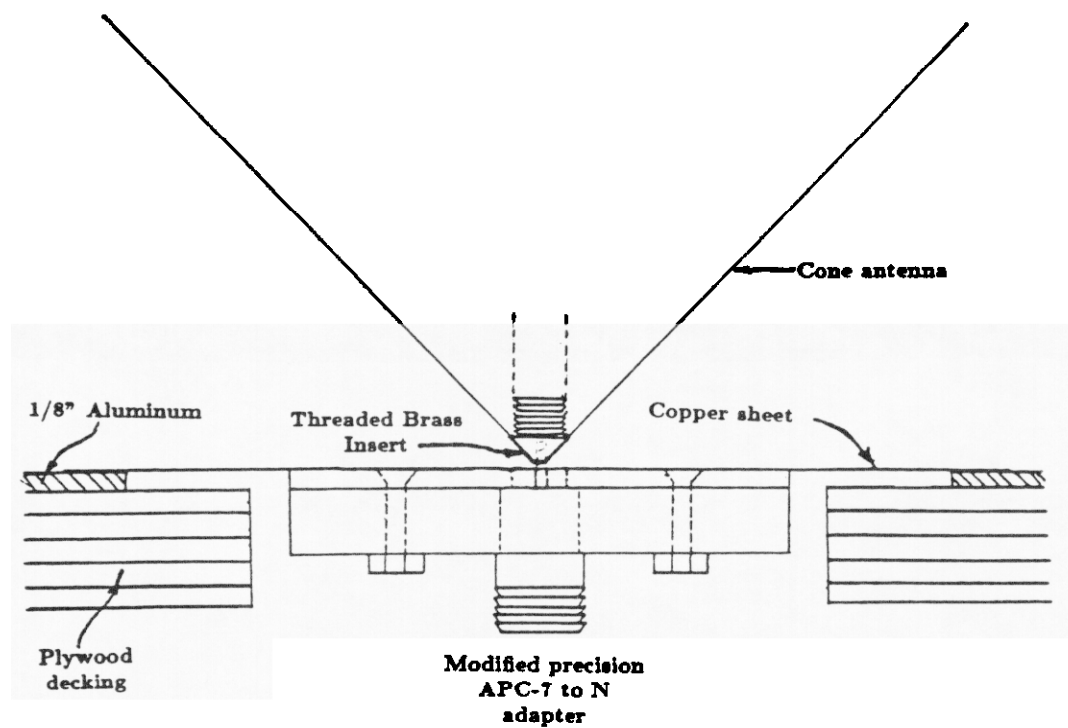


Figure 3.2. Side view of the "floating" connector. The copper sheet allows the floor to flex with the cone.

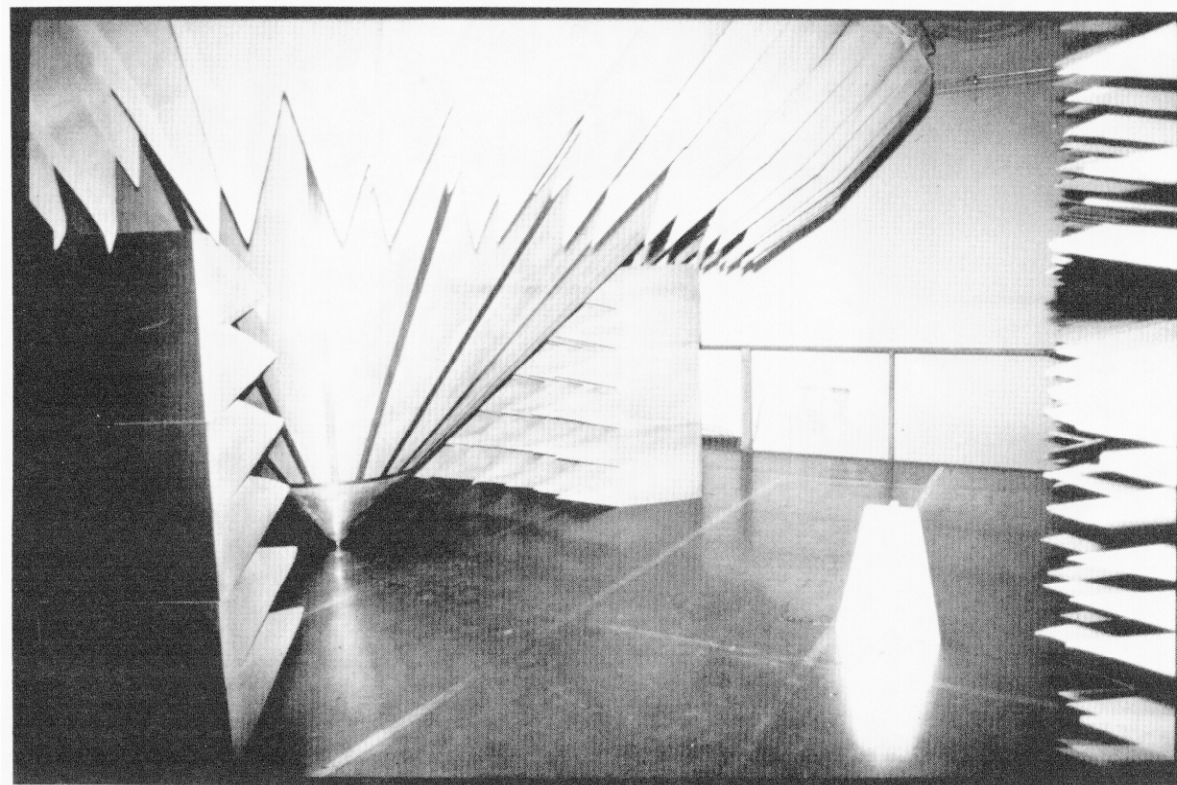


Figure 3.3. Photo of the EMPEROR monocone showing the microwave absorber.

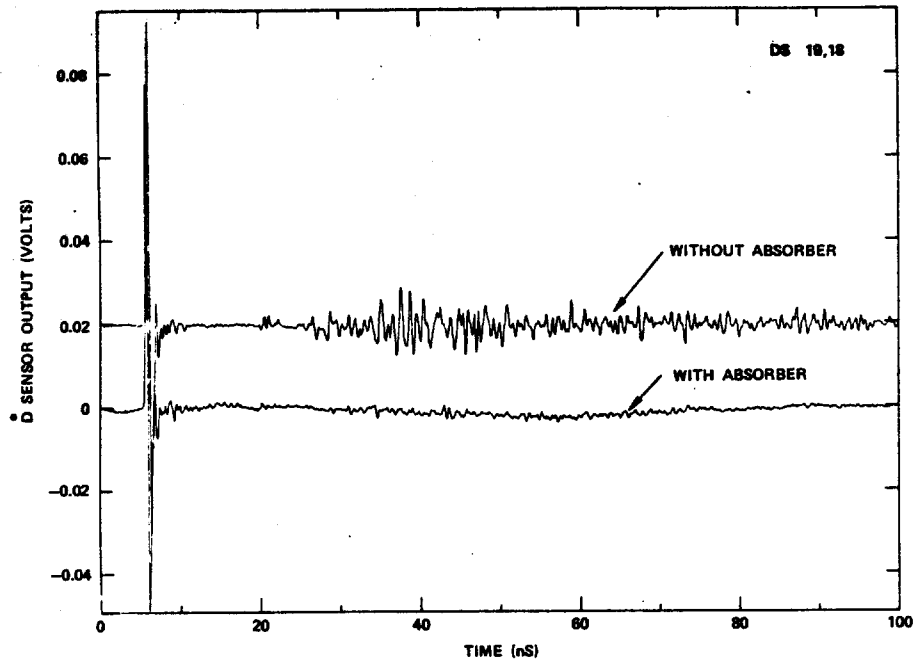


Figure 3.4. Incident field (100 ns) before (upper trace) and after (lower trace) absorber installation. Upper trace has been raised for clarity.

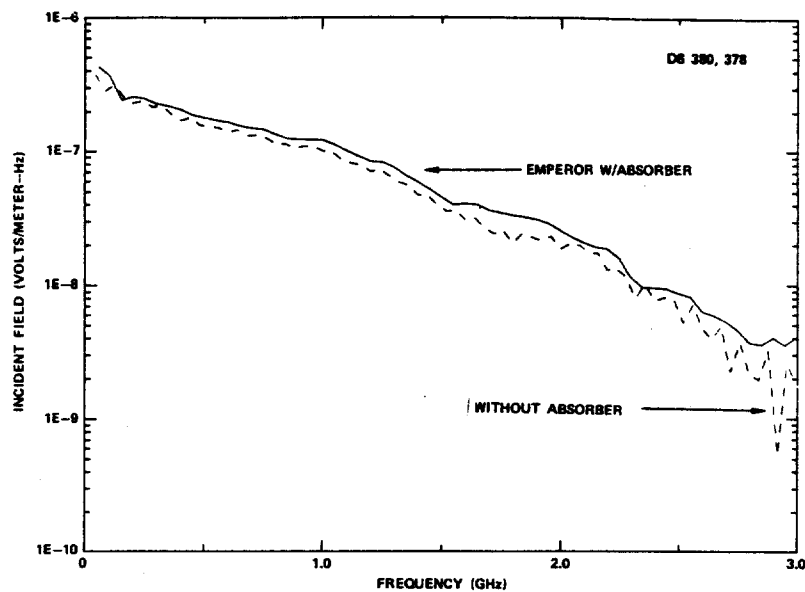


Figure 3.5. Incident field before (dash) and after (solid) absorber installation derived from a 20 ns time record.

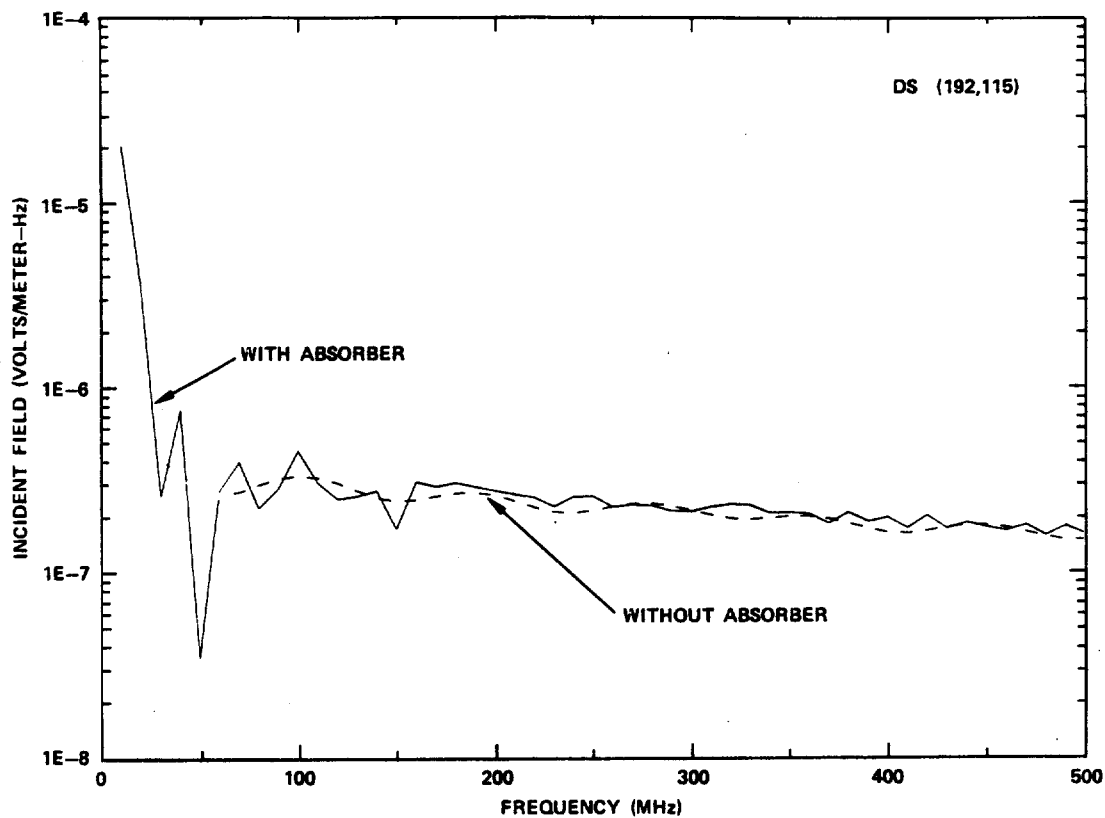


Figure 3.6. Change in low frequency components due to absorber installation on the EMPEROR Facility.

3.2. INSTRUMENTATION

The recently added cw frequency domain instrumentation system, called BEAMS for Broadband Electromagnetic Analysis Measurement System, uses a Hewlett-Packard (HP) 8510A vector network analyzer and an HP-8341A frequency synthesized source as key components. Figure 3.7 shows the entire EMPEROR test facility, including its associated instrumentation.

A block diagram of BEAMS is shown in Fig. 3.8. It can be resolved into three segments, data acquisition, processing and storage, and display. The data acquisition is composed of the HP-8510A, an HP-8512A transmission/reflection test set, and an HP-8341A synthesized sweep

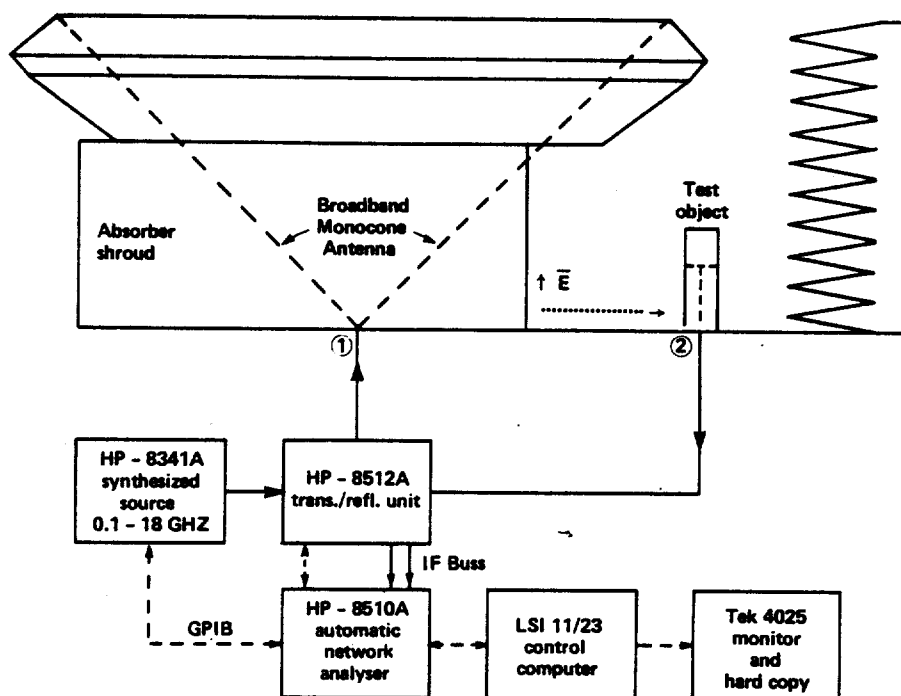


Figure 3.7. The EMPEROR Facility has been instrumented for broadband (0.10-18.0 GHz) cw microwave coupling studies.

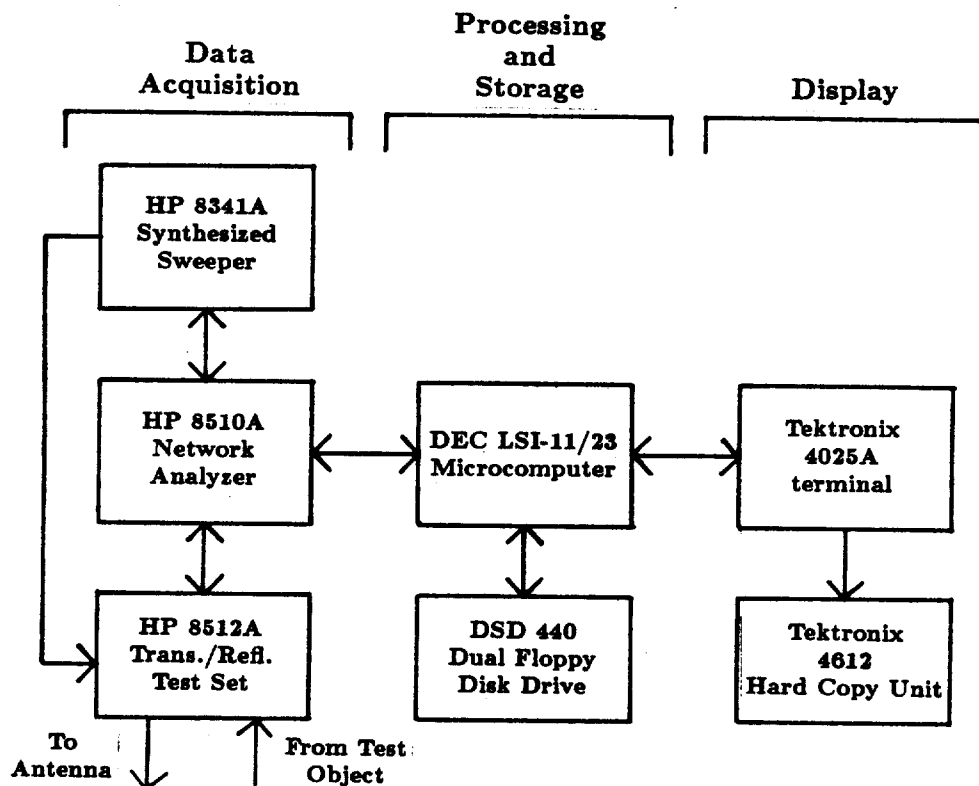


Figure 3.8. Block diagram of the Broadband Electromagnetic Analysis Measurement System (BEAMS) used for acquisition of frequency domain data.

generator. Processing and storage is accomplished by a Digital Equipment Corporation LSI-11/23 microcomputer and a Data Systems Design model 440 dual 8" floppy disk drive. The LSI-11/23 is configured to include a Tektronix CP4100 IEEE-488 interface for instrument communication. A Tektronix 4025A graphics terminal and a Tektronix 4612 hard copy unit are used for display purposes.

The HP-8510A vector network analyzer collects magnitude and phase information. The output of the HP-8341A synthesized source is split using a power splitter. Half of the power is fed to the EMPEROR antenna, and the other half serves as a -20 dBm reference to the HP-8512A converter, after being attenuated. Phase stable low attenuation cables are used throughout the system.

The processing and storage segment uses an LSI-11/23 microcomputer to control data acquisition and display. This segment also allows data to be stored on disk for transfer to a VAX-11/780 for further examination and processing. A Tektronix 4025A Graphics Terminal is the main device to display the acquired data as determined by the user. The 4612 hard copy unit can provide a permanent record if desired.

3.3. PERFORMANCE OF THE EMPEROR FACILITY

For these studies, knowledge of the amplitude and phase of the field incident on the test object is essential. This is because the measured response of a test object must be normalized by the incident field in order to remove any spatial or spectral variations of that field. Although the EMPEROR monocone is a very broadband (0.1 to 18 GHz) constant impedance (50 ohms) antenna having an essentially constant gain over the entire band, troublesome anomalies do appear in the incident field at some frequencies. They occur in two principal ways: in the VSWR which manifests itself in the input reflection coefficient, S_{11} , and in the transmission of the field into the test region, manifested as S_{21} . Figure 3.9a and b show S_{11} and VSWR, respectively, and Fig. 3.10 shows the amplitude and phase of the monocone input impedance. The most severe anomaly at 8 GHz is clearly evident.

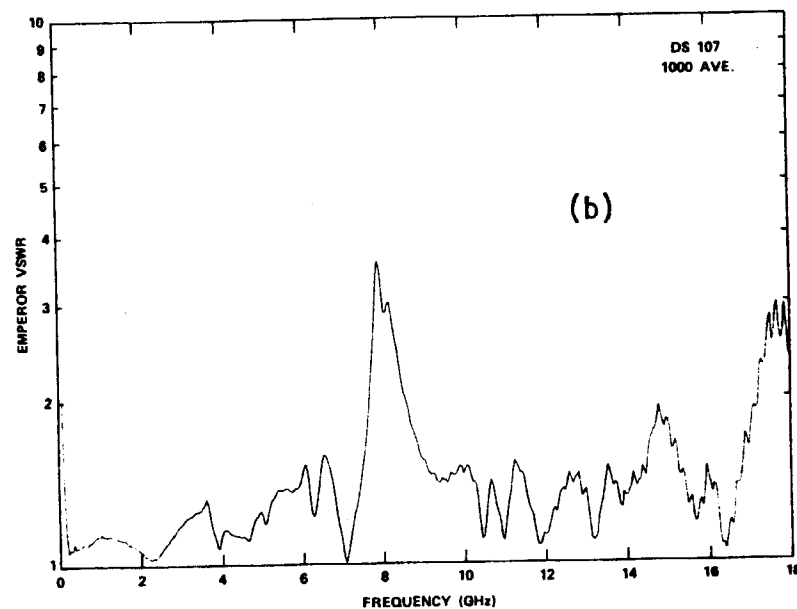
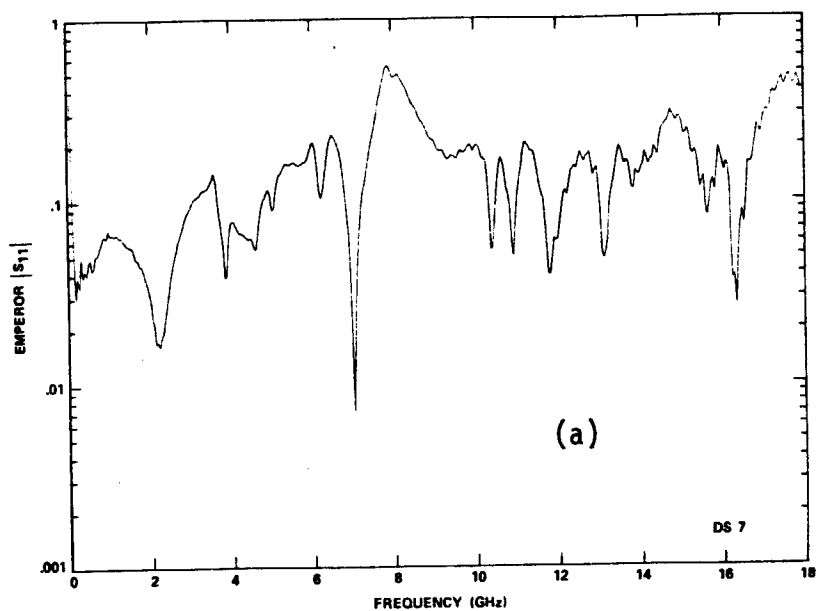


Figure 3.9. S_{11} and VSWR of EMPEROR Monocone Antenna.

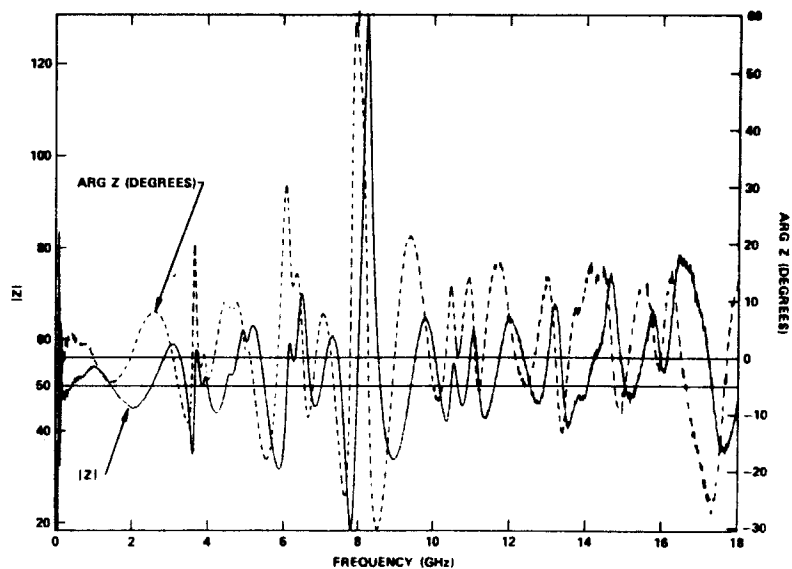


Figure 3.10. Magnitude and Argument of the input impedance to the EMPEROR Monocone antenna.

3.3.1. Characterization of the Incident Field

There is a decided lack of calibrated field sensors at frequencies greater than 6 GHz. For example, Fig. 3.11 shows the amplitude response of a Prodyne AD-10 \dot{D} sensor when located on the ground plane at 0.5 m from the apex of the EMPEROR monocone. The response increases linearly with frequency up to about 6 GHz, beyond which it still senses the field but is no longer calibrated. Pronounced notches in its response are clearly evident at 6, 8, 11, 14, and 16 GHz. While the exact causes of these anomalies are not known, it is likely that they are due to the monocone feed connector (see Fig. 3.2). Essentially, the same responses are seen for this sensor at locations ranging from 0.5 to 4 m from the cone apex, so it is unlikely that the anomalies are due to the absorber or scattering from the surface of the monocone. Similar anomalies are also seen for other sensors, including several wire monopoles. This suggests that the anomalies in Fig. 3.11 are present in the transmitted incident field itself, rather than being due to the sensor. For example, Fig. 3.12 shows the response of a 22.5 cm long monopole at 2.4 m from the apex of the monocone. The voltage at the base of the monopole was recorded by the BEAMS instrumentation (Figs. 3.7 and 3.8). These data were then normalized by an assumed incident field which behaves as e^{-jkr}/r , i.e., it assumes that there are no anomalies over the entire frequency range of 0.1 to 18 GHz. The ratio V_L/E_{inc} is therefore a measure of the effective height of the monopole in meters.

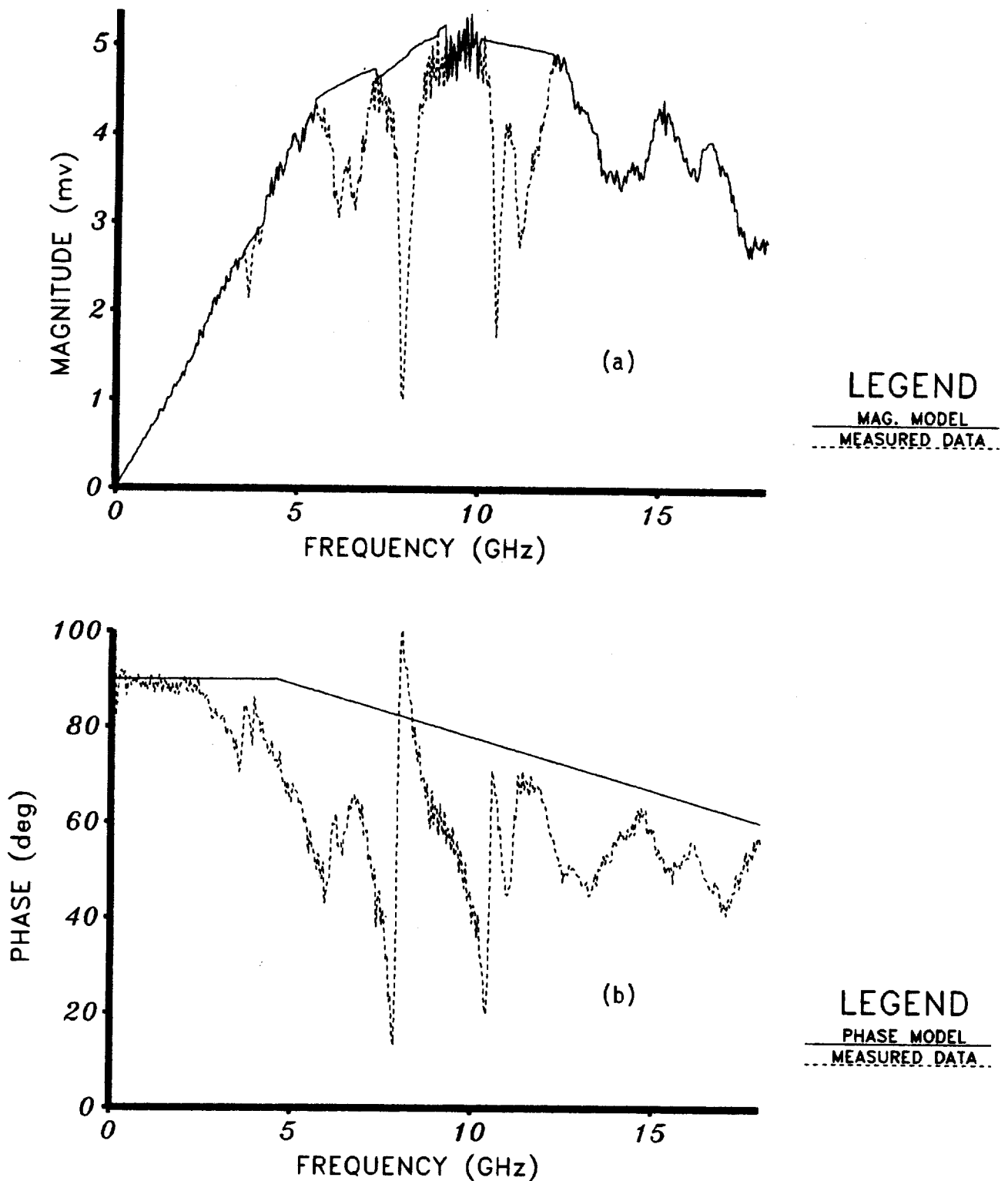


Figure 3.11. Voltage gain (a) and phase response (b) of a \dot{D} probe placed on the ground plane at 0.5 m from the apex of the EMPEROR monocone. The solid line estimates what the response of the probe should have been (model). The ratio of the estimated model data to the measured data gives an empirical correction factor shown in Figure 3.13.

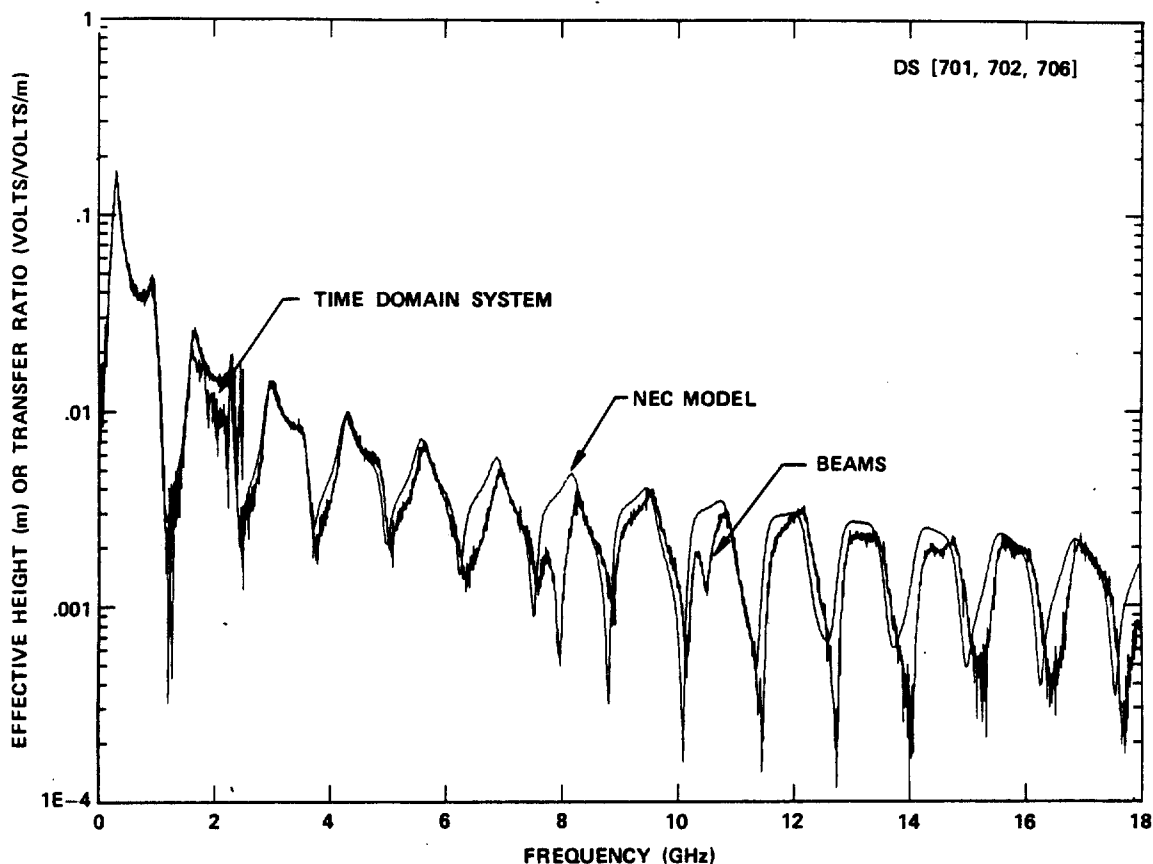


Figure 3.12. Comparison of the transfer ratio of a 22.5 cm monopole calculated using the NEC computer code, measured using BEAMS and measured using the Tektronix 7854 time domain system. Note that the time domain data does not extend above 2.5 GHz.

These data in Fig. 3.12 are compared with the results computed using a method-of-moments code known as NEC [2]. Also shown is the experimental data obtained using the time domain instrumentation system, which only extends to 2.5 GHz. The NEC and BEAMS data generally compare very well below 5 GHz. However, anomalies are seen in the vicinity of 6, 8, 11, 14, and 16 GHz, which are the same frequencies where anomalies were identified for the \dot{D} sensor in Fig. 3.11. It is therefore concluded that the anomalies are in the incident field itself rather than the sensors, and measures were taken to remove their effects, at least to a first order.

3.3.2. Derivation of the Correction Factor

A complex correction factor has been empirically derived to remove the major effects of these anomalies in the incident field up to 12 GHz. This factor was derived by estimating what the response of the \hat{D} probe should have been, as shown by the solid line (model) in Fig. 3.11. Over certain frequency ranges the amplitude of the measured response was judged sufficiently accurate that no correction was needed. Beyond 12 GHz, it is not clear that the deviations from a smooth amplitude response are due to the incident field, so no corrections were made. The modeled phase of Fig. 3.13(b) was assumed to be $\pi/2$ to 5 GHz, beyond which it tapers downward in a linear manner.

The ratio of the modeled to the measured data gives the complex correction factor shown in Fig. 3.13(a) and (b). Efforts are continuing to deduce a better way of correcting the incident field. Until this happens, this factor will be used. The experimental data given in Section 5 have been corrected by this factor. We now feel confident that these data are sufficiently accurate to permit reliable conclusions to be drawn.

The effectiveness of the correction factor can be estimated by comparing the measured response of a monopole antenna (with and without correction) to that computed by the Numerical Electromagnetics Code, NEC [2]. Figure 3.14(a) and (b) gives such a comparison for the magnitude of the response of a 5 cm high monopole. The removal of the anomaly near 8 GHz is clearly evident.

Since the EMPEROR/BEAMS cw system is capable of coherent measurements over a wide frequency range, it is possible to inverse Fourier transform the complex frequency domain data (normalized by the incident field) to yield the time domain impulse response. The same can be done to the numerical data as computed by NEC. Figure 3.15(a) and (b) compares the results of such a process, without and with the empirical correction to the normalizing incident field, respectively. These time domain results correspond to the frequency domain magnitude data shown in Fig. 3.14(a) and (b). The improvement in the fine structure of the corrected data in Fig. 3.15(b) compared to (a) is evident.

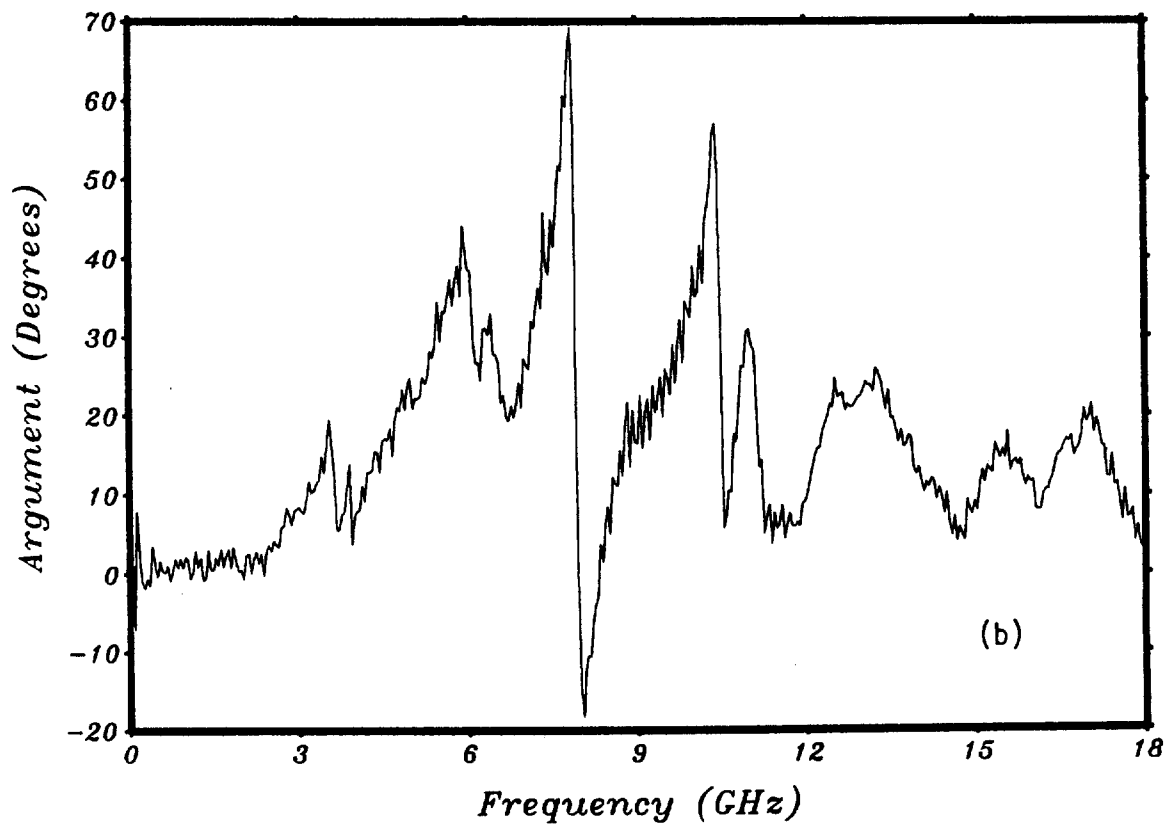
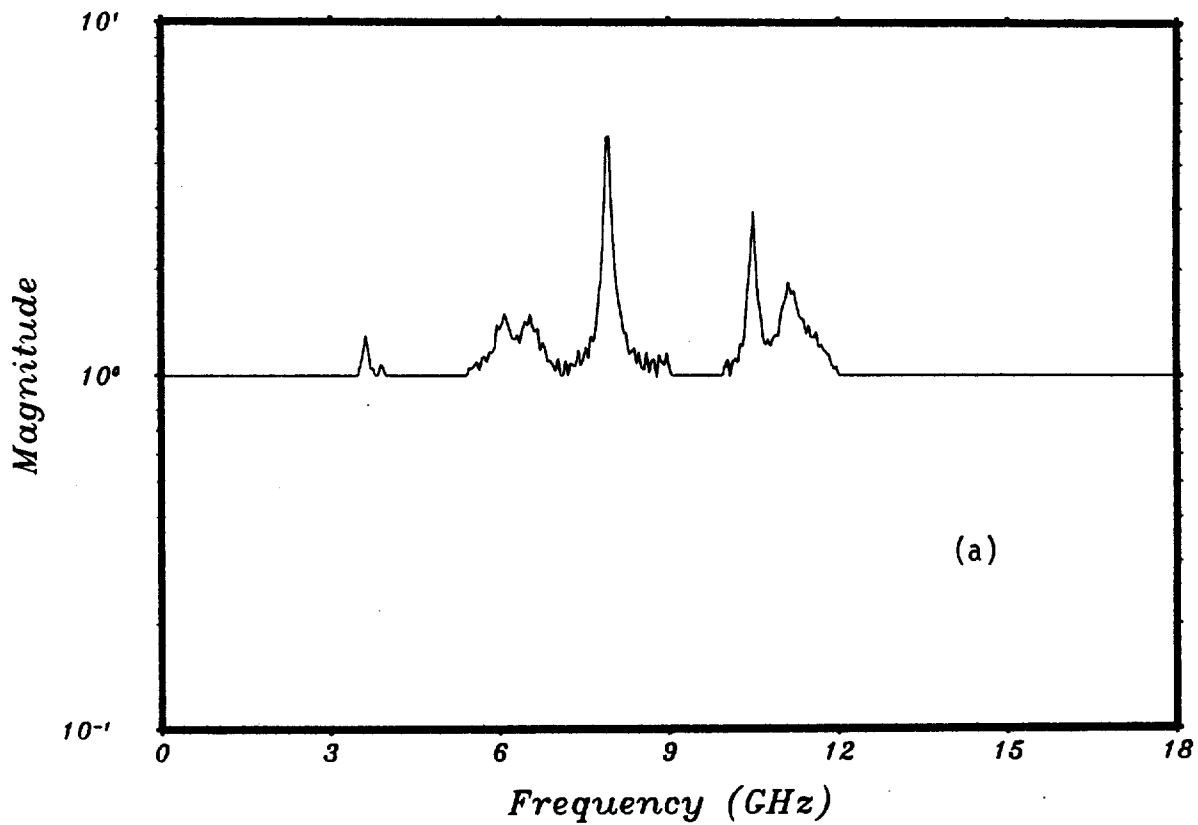


Figure 3.13. Emperically derived correction factor for the EMPEROR Facility
 (a) Magnitude (b) Argument. This factor has been applied to all of the
 experimental data given in Section 5.

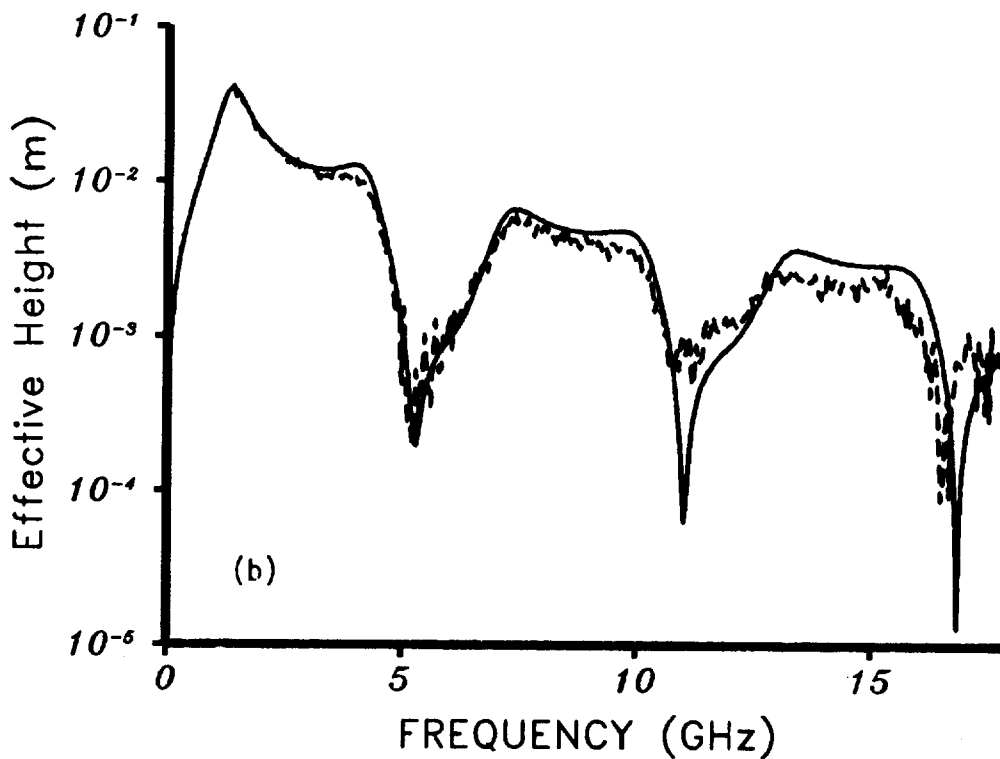
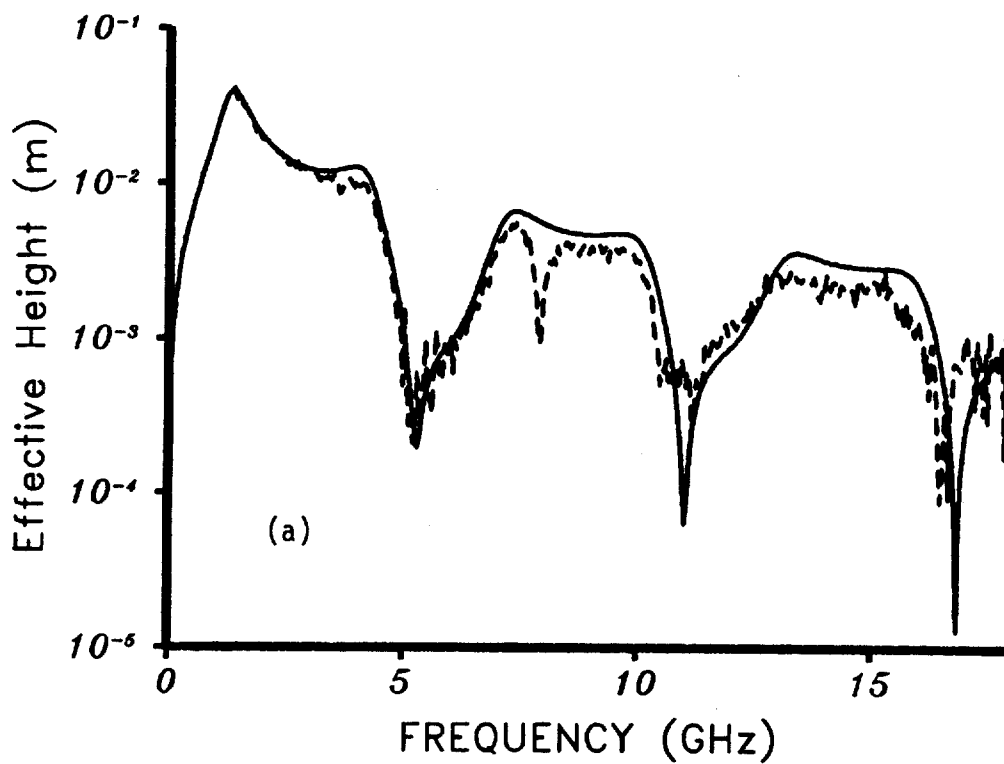


Figure 3.14. Amplitude of the response of a 5 cm high monopole. In (a) the normalizing incident field is uncorrected. In (b) the incident field has been corrected by the empirical correction factor shown in Fig. 3.13. The corresponding response computed using NEC is also shown.

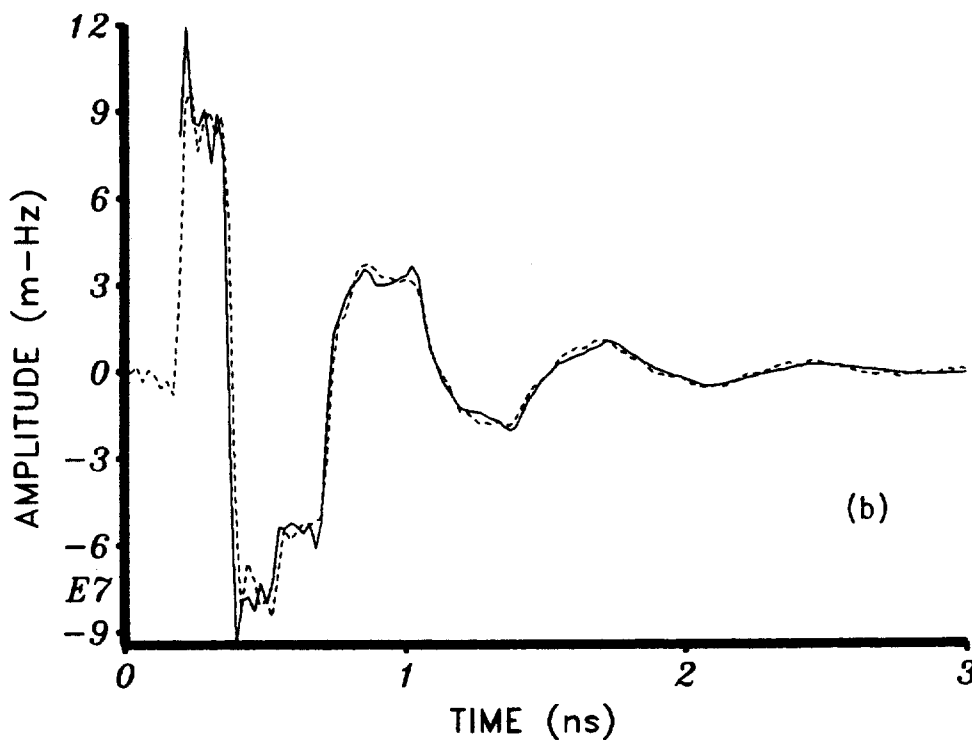
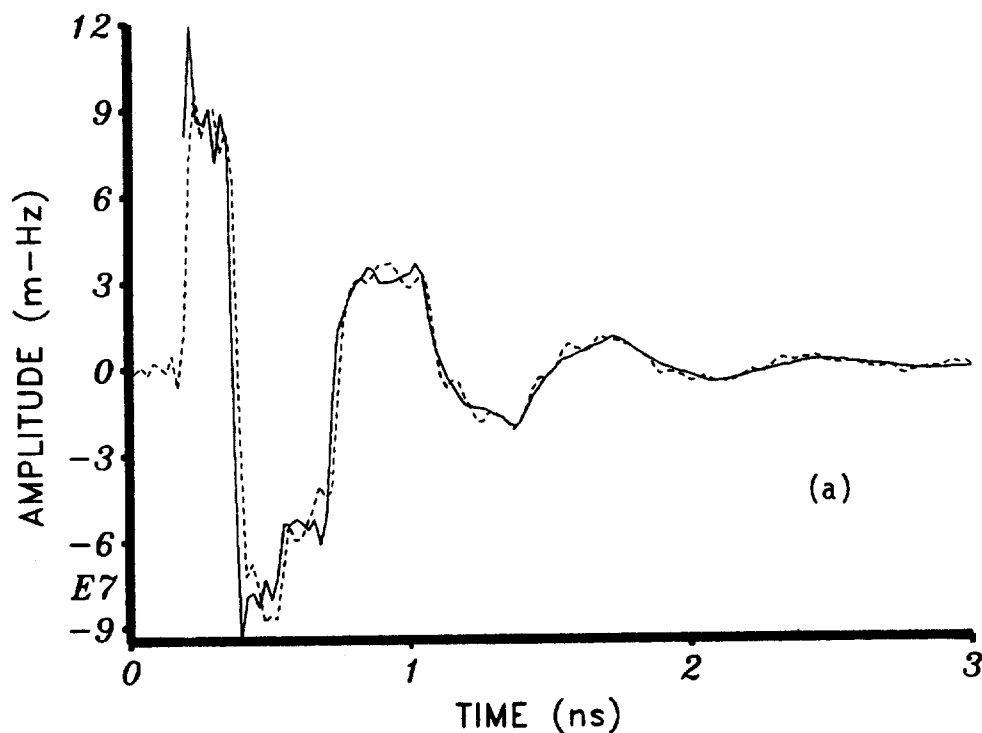


Figure 3.15. Comparison of the time domain impulse response of a 5 cm high monopole. In (a), the measured frequency domain data was normalized by the uncorrected incident field and then inverse Fourier transformed. In (b), the measured frequency domain data was normalized by the empirically corrected incident field and then inverse Fourier transformed. The corresponding response obtained by inverse transforming NEC calculated data is also shown for comparison.

3.3.3. Spatial Variations in the Incident Field

Tests were also made to quantify the spatial variations in the incident field within the test zone. Although the Prodyne AD-10 \dot{D} sensor is not calibrated above 6 GHz, it can be used to carry out relative measurements in which the correction factor discussed previously is not needed. Figure 3.16 shows the smoothed response (trend) of this probe at distances ranging from 1 to 4 m at 0.5 m increments from the apex of the monocone. Each data trace is normalized to the response of the same probe at 0.5 m, so any anomalies in the probe's own response and anomalies in the radiated field are cancelled, leaving just the variations in the intensity of the E_z field. The dB level of the horizontal lines for each trace depict the theoretical r^{-1} variations. These data show that the measured field deviates from r^{-1} by the order of ± 1 dB over the entire 0.1 to 18 GHz frequency range in the 1 to 4 m working range.

Tests to quantify the variations within a 60 degree sector comprising the test region show that the azimuthal variations are of the order of 2.5 dB over the same frequency range.

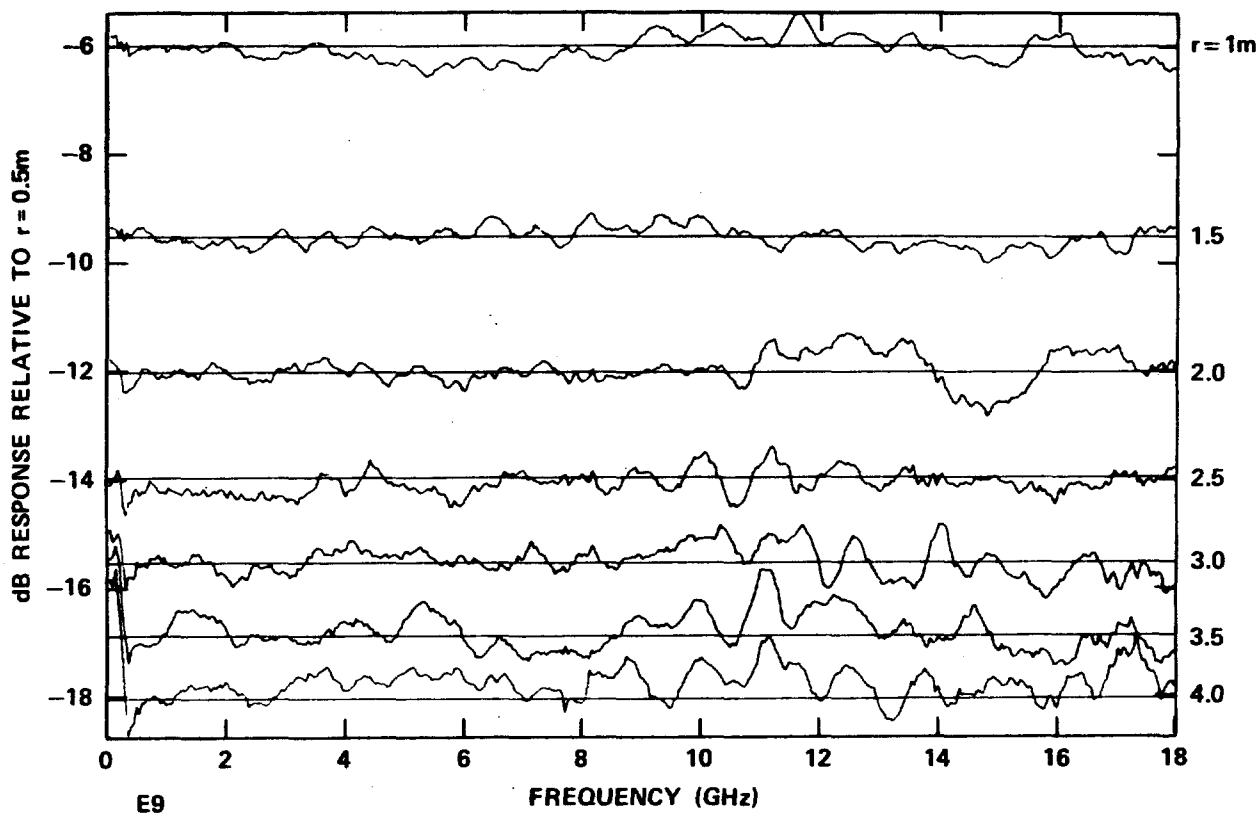


Figure 3.16. Response of the Prodyne AD-10 D probe at 1 to 4 meters, in 0.5 m increments, relative to the response at 0.5 m from the apex of the EMPEROR monocone.

3.4. TEST OBJECTS

3.4.1. Generic Models

As noted in Section 1, the Microwave Coupling Program focuses on understanding the phenomenology by studying simple generic test objects. Most of the results presented in Section 5 were obtained using PLUTO (Preliminary Livermore Universal Test Object) shown in Fig. 3.17. This object is a simple circular cylinder having a 10:1 length/diameter ratio (including the ground plane image) which simulate a scale model missile or fuselage of an aircraft. The program is chiefly concerned with interior coupling at microwave frequencies. It has consistently been observed throughout the

program that the exterior shape is of little consequence. Therefore, the absence of various protrusions such as fins, wings, etc., has little effect on the microwave energy which enters through apertures, cracks, seams, protruding conductors, etc.

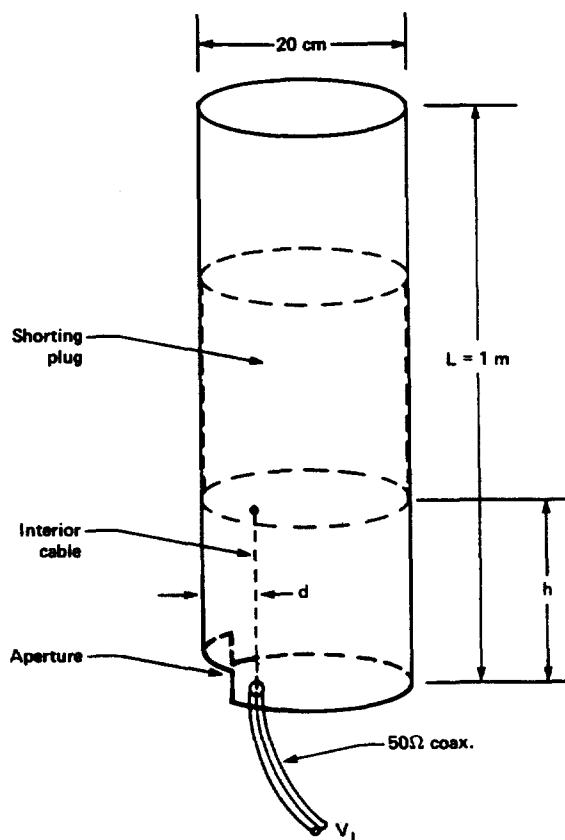


Figure 3.17. "PLUTO" (Preliminary LLNL Universal Test Object).

The interior cavities in PLUTO can be made substantially smaller than the exterior length using a shorting plug at height h . Various ports of entry (POEs) can be configured as needed; Fig. 3.17 shows a large aperture. Coupling wires (simulated cables) can be configured, either singly or in bundles, and these wires can be shorted at either end or terminated in a

load. Stiff piano wires are used for ease of assembly. Connection to any one of the coupling wires is through the ground plane using SMA connectors. Dielectric or dissipative materials can be added to suppress or otherwise alter the interior modes. Various metal objects and subcavities can be introduced into the main lower cavity to simulate multiple cavities with or without common coupling wires. Finally, multiple apertures can be introduced. All of these configurations will be studied during the course of the program. Figure 6.1 shows some of the configurations of PLUTO which will be studied.

The results in Section 5 focus on configurations using a single wire at various locations, a wire with absorber loading, a wire with metal fill in the cavity and dielectrically loaded apertures.

3.4.2. Aircraft Models

Testing of more complicated configurations are possible using 10:1 scale models of aircraft. In particular, Fig. 3.18 shows an A7 aircraft in which three cable runs are configured. Similar 10:1 scale models of F-14 and FB-111 aircraft are also available. While such cable layouts are not to be interpreted as exact scale models of the cables in an actual aircraft, the data gathered from such a model is indicative of the gross phenomenological features. The cables take devious routes with many bends, run through bulkheads, and near the hull. They therefore represent a complicated configuration like, but not equivalent to, that which might be encountered in an actual aircraft. Results for such a model are given in Section 5.

3.5. MICROWAVE ANECHOIC CHAMBER

LLNL is now installing a Keene/Ray Proof microwave anechoic chamber to support the Microwave Coupling program (Fig. 3.19). The chamber is scheduled for completion by mid-October 1985. Installation and check out of the positioner, controls, pattern plotter, and instrumentation will take about two months, making the total facility operational by January, 1986.

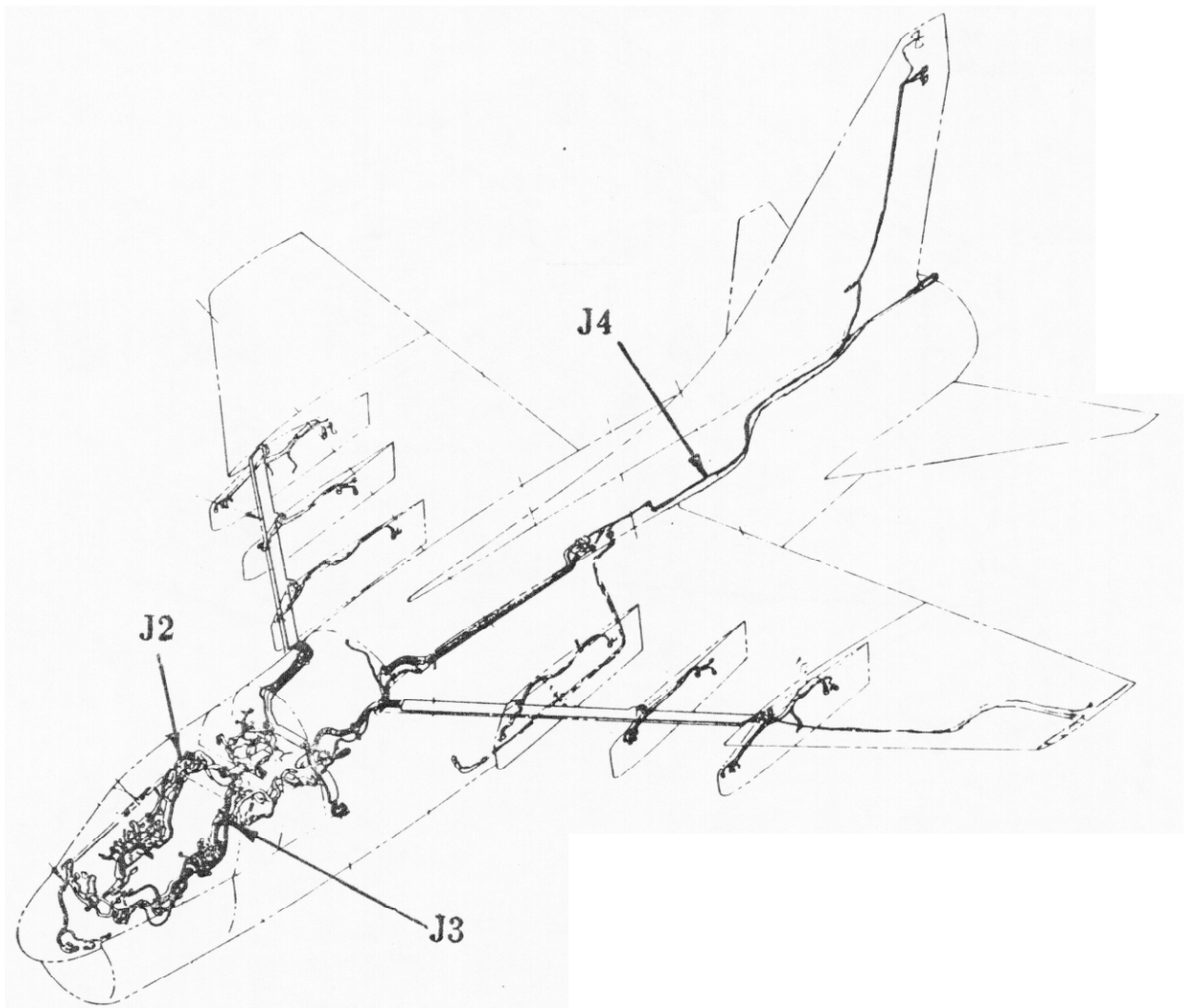


Figure 3.18. Scale (10:1) model of an A7 aircraft showing some possible interior cable layouts.

Quieting Zone: 12' diam., 6' high
 Shielding: 100 dB
 Frequency: 1 - 40 GHz
 Location: Bldg. 141, Bay 4

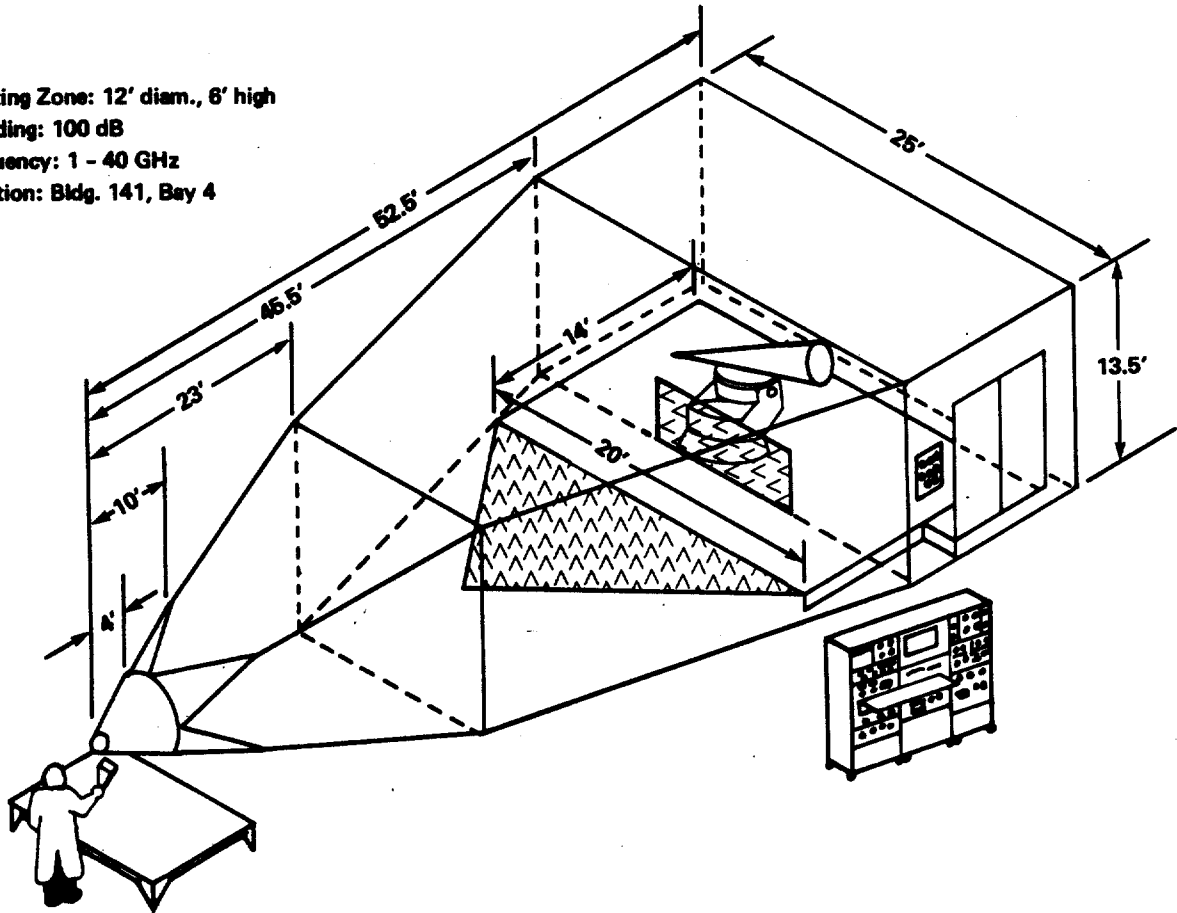


Figure 3.19. The LLNL microwave anechoic chamber.

This chamber is designed to operate from 1 to 40 GHz with 100 dB of shielding which will eventually be useful for high power use. Due to the limited height (13.5 ft.) of the room where the chamber will be installed, it was necessary to choose a tapered conical design to achieve the desired quieting (~ 30 dB) in the test volume. The cross-polarization is 30 dB down, and the axial ratio performance is 0.5 dB.

The Scientific Atlanta positioner/control/recording subsystem for the chamber is shown in Fig. 3.20. It is controlled by the same DEC LSI-11/23 computer which controls the microwave BEAMS subsystem shown in Fig. 3.8. A

block diagram of the BEAMS instrumentation system as configured for use in the chamber is shown in Fig. 3.21.

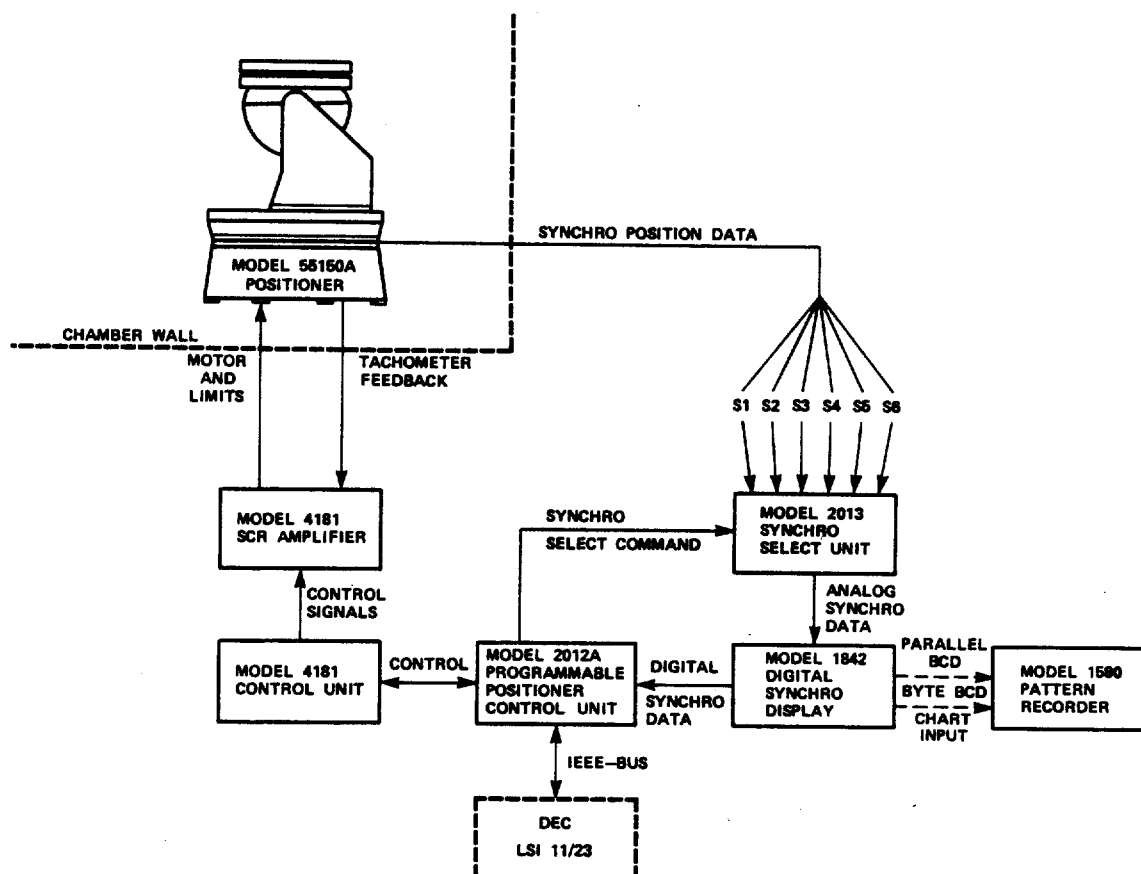
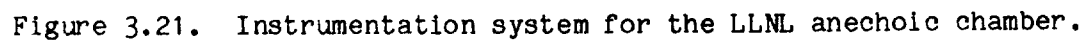


Figure 3.20. The Scientific Atlanta automatic position/control/recording subsystem.

Most of the microwave coupling experiments will be carried out in the anechoic chamber facility beginning in 1986, complemented by the existing EMPEROR facility. The chamber offers several advantages over the EMPEROR facility:



- Any polarization is permitted. Only one polarization is possible with EMPEROR.
- The quieting in the test volume is substantially better (-30 dB).
- Azimuth and elevation radiation patterns can be measured using the positioning subsystem.
- Large (2500 lbs.) test objects can be placed on the positioner.
- The size of test volume is substantially larger (12 ft. diameter x 6 ft. high).

The advantage of EMPEROR are its constant gain and its broad bandwidth (0.1 to 18 GHz). EMPEROR will also be instrumented with a second BEAMS system.

4. A SIMPLE INTERIOR COUPLING DECOMPOSITION MODEL: ITS DEVELOPMENT AND APPLICATION

4.1. INTRODUCTION

A simple interior coupling decomposition model has been developed as part of a long term study of electromagnetic coupling phenomenology. The model decomposes the response on an interior wire into the product of two factors, each with its own distinctive characteristics. These factors are shielding effectiveness (SE) [3], which represents the shielding effect of the exterior hull at low frequencies, and coupling effectiveness (CE), which represents the antenna-like $1/f$ rolloff in the current response of interior wires. The model is called SExCE for Shielding Effectiveness x Coupling Effectiveness. It describes the basic features in the envelope of the measured interior wire responses of simple generic test objects. The PLUTO test object (Fig. 3.15), was illuminated with both transient and cw fields in the newly installed EMPEROR facility [3; also see Section 3]. The response envelope manifested itself over a wide variety of test object configurations. These configurations included varying aperture sizes and orientations; varying wire lengths, number and terminations; varying cavity size; fill in the form of interior metallic cylinders, and various lossy materials in the interior.

The SExCE modeled response envelope is characterized by a suppressed low frequency response followed by a peak in the current response that falls off at $1/f$ at higher frequencies, or as $1/r^2$ in the power delivered to a load at the base of the wire. The location of the peak can be estimated from aperture size, wire and cavity length, and wire terminations. The peak typically occurs around $1/3$ to 1 GHz for small missile-like systems and 30 - 100 MHz for aircraft sized systems. Electromagnetic energy is most efficiently coupled into such systems at these frequencies and above by approximately a half decade. These characteristics strongly suggest what spectral components are most important in an incident waveform with respect to possible damage or upset in an aerospace system.

The extension of the SExCE model to aerospace systems is based on the belief that the envelopes observed in aircraft scale model measurements and on

the persistence of the envelope even under extreme PLUTO configuration changes will carry over to full scale systems. At most, configuration changes lowered the overall response by 12 dB, as when the wire was located behind a large interior cylinder that nearly blocked the aperture. More typically, reductions were on the order of 6 dB or less. Our conclusion is that SExCE is a robust model, suitable to a wide variety of systems. SExCE can now be used to predict the nominal responses of a variety of aerospace systems to a wide range of stressing electromagnetic fields. These predictions have application in the areas of aerospace system design, hardening, vulnerability and survivability. SExCE also provides a good intuitive framework for understanding interior coupling phenomenology. Future work will include numerical modeling of the perturbations introduced by the more important configuration variations that have been observed experimentally.

4.2. DEVELOPMENT

The first factor of the SExCE model is shielding effectiveness (SE), defined as the ratio of the wire current with the hull in place to the wire current without the hull in place. In PLUTO, the current is measured at the wire base (Fig. 3.15) since this is where the wire leads to a load for an unshielded wire or possibly to a leaky connector for a shielded cable. Current is monitored because it represents actual stress on the system that directly drives any sensitive electronic load. Ratioing the two current measurements accurately portrays the stress reduction. By definition, the wire is always terminated in the same manner with and without the hull, so both configurations share the same TEM wire resonances. With the hull in place, TM and TE cavity modes are also excited, but only the TM modes couple to the axial wire. These modes add a high degree of structure to the otherwise relatively smooth response envelope.

The salient characteristics of SE are that the stress is reduced below aperture cutoff, the frequency at which the wavelength is approximately equal to the aperture circumference. In this region the hull shields the system. Above aperture cutoff there is little stress reduction, and because of the cavity modes driving the wire when the hull is in place, the stress can

actually be greater with the hull than without the hull at some of the TM mode resonances. These characteristics persisted [4] over a wide range of PLUTO configurations. Thus, an idealized version of the SE is characterized by a low frequency region where shielding is effective. Above this region the SE nearly levels off at unity, indicating little or no shielding.

Shielding effectiveness is not the complete picture. As mentioned above, the lack of shielding at higher frequencies for the "shielded" system is important only to the degree that the response above aperture cutoff is large. Shielding effectiveness only measures the relative level, not the absolute level needed to characterize the importance of the response. Coupling effectiveness (CE) was therefore developed to complete the picture. It provides the absolute level of the wire response when multiplied by SE, and provides insight into how the wire's antenna-like properties influence the response.

Coupling effectiveness is defined in the following:

$$NWR = (SE) \times (CE) = \left(\frac{I_{\text{shielded}}}{I_{\text{unshielded}}} \right) \times \left(\frac{I_{\text{unshielded}}}{E_{\text{incident}}} \right) \quad (4.1)$$

where

- NWR = normalized wire response
- I_{shielded} = current at the wire base, shielded configuration with hull in place
- $I_{\text{unshielded}}$ = current at the wire base, unshielded configuration with hull removed
- E_{incident} = incident electric field
- (SE) = shielding effectiveness
- (CE) = coupling effectiveness

Therefore,

$$CE = \frac{I_{\text{unshielded}}}{E_{\text{incident}}} \quad (\text{mho} - \text{meters}) \quad (4.2)$$

and (SE) x (CE) yields the current on the interior wire in the shielded system, normalized to the incident field. This provides the absolute level required to assess the importance of the response. In the present formalism, CE (as given by 4.2) actually has the dimensions of mho-meter, while SE is dimensionless.

By itself, NWR represents the system response without any physical insight. Decomposed into a SE factor and a CE factor it becomes possible to predict NWR a priori, based on theoretically deducible SE and CE characteristics. The behavior of CE is expected to be $1/f$, based on the analogy between the wire and an antenna. This $1/f$ behavior holds for the TEM and cavity modes, since it is a property showing how the antenna sums the driving excitation along its length. The CE envelope curve (Fig. 4.1) is easily deduced by noting that f_0 is the lowest TEM resonance of the unshielded wire, and $CE(f_0)$ is its corresponding peak response. Multiplying the idealized SE behavior by the envelope of CE yields the overall SExCE modeled response envelope. The overall envelope is therefore characterized by a suppressed low frequency response followed by a peak and then rolls off as $1/f$ at higher frequencies (Fig. 4.1). As will be seen, this predicted behavior is observed throughout a wide range of PLUTO configurations and for a scale model aircraft. Further effort is needed to more precisely predict the SE response below aperture resonance although it appears to roll off as f^4 .

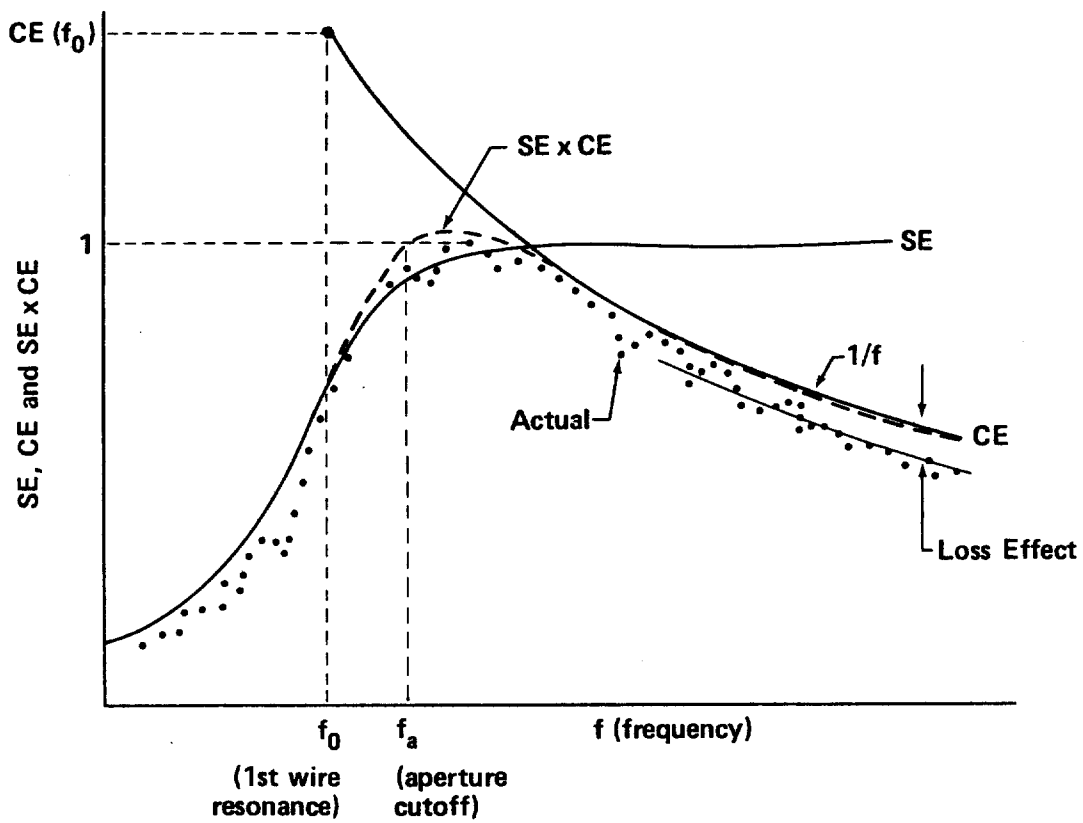
The preceding definition of NWR that embodies the SExCE model can be generalized further. This generalization explicitly accounts for interior cavity fill, in the form of conducting cylinders, boxes, other wires and cables, lossy materials, etc. The generalized definition is:

$$NWR = SE \times PE \times CE = \left(\frac{I_{\text{shielded}}}{I_{\text{unshielded}}} \right) \times \left(\frac{I_{\text{unshielded}}}{I_{\text{singlewire}}} \right) \times \left(\frac{I_{\text{singlewire}}}{E_{\text{incident}}} \right) \quad (4.3)$$

where

I_{shielded} = current at wire base, shielded configuration with hull and all interior fill in place

$I_{\text{unshielded}}$ = current at wire base, unshielded configuration with hull removed but all interior fill in place



SE x CE Modeled Response Envelope

Figure 4.1. SE x CE Modeled Response Envelope.

$I_{\text{single wire}}$ = current at wire base, hull and fill removed leaving only the single wire
PE = perturbation effect

For a cavity having only a single wire (4.1) and (4.2) are identical. With fill, the original definition interprets CE as the response of the wire of interest surrounded by the fill but not the hull and normalized by the incident E field. The generalized definition of NWR (4.3) substitutes (PE) x (CE) for (CE). Thus, (PE) is a measure of how much the fill alone perturbs the unshielded wire response compared to the unshielded wire response without the fill. If the perturbation is small, the insight offered by the original definition is good for a wide range of systems. If the perturbation is large but predictable, the original definition provides insight when combined with the necessary understanding of the perturbation effect. As will be seen in Section 5, the perturbations are generally modest (≤ 12 dB) to small (-3-6 dB) over most of the response frequency range. There has also been some success in predicting the larger perturbations. This ongoing work will be reported in subsequent reports. In short, the SExCE model appears to be quite robust and of broad applicability.

4.3. DISCUSSION

Studies are underway at LLNL to more fully characterize the SExCE model over a very wide range of configurations. At present we conclude that it does a good job of describing the internal wire responses. Rough estimates can be made as to the perturbing effects of fill, etc., so as to modify the basic SExCE predicted response. At the present stage of model development we observe that:

- SExCE without perturbations forms an upper bound on the internal wire response.
- It is difficult to suppress the overall internal wire response by more than 12 dB even when large amounts of fill and lossy material are present.

- The effects of fill can be roughly estimated, thereby improving the model accuracy.

Based on these observations we conclude that SExCE not only provides a physically intuitive and conceptually useful decomposition model, but that it also can be used to estimate reasonably well (≈ 12 dB error and typically ≈ 6 dB) interior wire response levels. The accuracy should improve as more is learned about the three factors, SE, PE and CE.

The SExCE model does not decompose the response into contributions from various coupling pathways. Rather, it views the hull and its penetration as a low frequency filter to the exciting waveform. The waveform after filtering, excites the interior wire(s) in approximately the same manner as if the interior were completely exposed, e.g., as a TEM mode. To this response there is added the highly structured resonances of cavity modes coupling to the antenna-like wires.

This decomposition could only be arrived at through a set of mutually supporting developments at LLNL. These developments include:

- A simple test object, PLUTO, that can be made progressively more complex.
- A precision monocone antenna, EMPEROR.
- The use of an EM absorbing shroud, removing clear time limitations (20 ns) on transient measurements and allowing CW operation as well.
- CW operation from ~ 100 MHz - 18 GHz with an Hewlett Packard 8510A Network Analyzer.

Further, the effort was supported by connector redesign to match the cone to at least 18 GHz, instrumentation upgrades and automation, a signal processing laboratory and a wealth of past experience. The resulting high quality data, extending over a very broad bandwidth (180:1 which is well in excess of any conventional full scale simulator), combined with physical intuition, allowed the pattern that SExCE models to be observed.

4.4. SUMMARY

Coupling effectiveness combined with shielding effectiveness completes the model of interior wire coupling. The model, known as SExCE, allows for

reasonably accurate characterization of a broad range of generic geometries. As such it is a robust model. It is being extended to more accurately model the response changes arising from interior perturbation effects. SExCE provides a solid foundation for understanding interior coupling as well as providing a useful predictive tool.

5. EXPERIMENTAL COUPLING RESULTS

5.1. INTRODUCTION

Extensive testing has been done on the EMPEROR Facility (Figs. 3.3 and 3.7) using the generic test object PLUTO (Fig. 3.17) and a scale model of the A7 aircraft (Fig. 3.18). The data given here summarize the most important features of the experiments conducted since Part I [1] was published. These data are interpreted in terms of the SExCE model discussed in Section 4.

In the PLUTO experiments, the parameters varied are:

- aperture size
- testpoint location
- metal fill (size and location)
- cavity height
- lossy fill (type and location)
- dielectric loading in aperture

The spectral data is typically presented as receiving cross section, σ , which is closely related to the normalized wire response (NWR) discussed in Section 4.

$$\sigma \equiv \frac{P_{\text{load}}}{S_{\text{incident}}} = \frac{I_{\text{shielded}}^2 R_L}{E_{\text{incident}}^2 / \eta_0} = \eta_0 R_L (\text{NWR})^2 \text{ sq. meters} \quad (5.1)$$

where NWR is defined in (4.1) and (4.3), S_{incident} is the incident power density, P_{load} is the power delivered to the load R_L at the terminals being measured and $\eta_0 = 120\pi$ is the intrinsic impedance of free space. In the present case, $R_L = 50 \Omega$, representing the input impedance to the coaxial line feeding the automatic network analyzer of BEAMS (Figs. 3.7 and 3.8). Thus, in the following plots of σ , $10 \log (\eta_0 R_L) = 42.75 \text{ dB}$ should be subtracted to get the $(\text{NWR})^2$ in dB.

In the following, most of the receiving cross section data plots have been smoothed 2.5% using a running average of nine adjacent data points (trend). Exceptions will be indicated. Without such smoothing, the highly

structured resonances of the TM modes in a cavity make evaluation of the trend difficult. Similarly, 10% smoothing has been applied to data plots showing the Perturbing Effect (PE) of adding absorbing materials into the cavity or dielectrics in the aperture of PLUTO. This degree of smoothing corresponds to computing the running average of 41 adjacent data points. All of the experimental data presented here has been corrected for anomalies in the incident field as explained in Section 3.3.2.

For reference, the PLUTO Test Point (TP) locations of the single wire which serves as the sensor are shown in Fig. 5.1. In all of the PLUTO data, the incident field is vertical (e.g., parallel to the axis of PLUTO) and normally incident on the aperture.

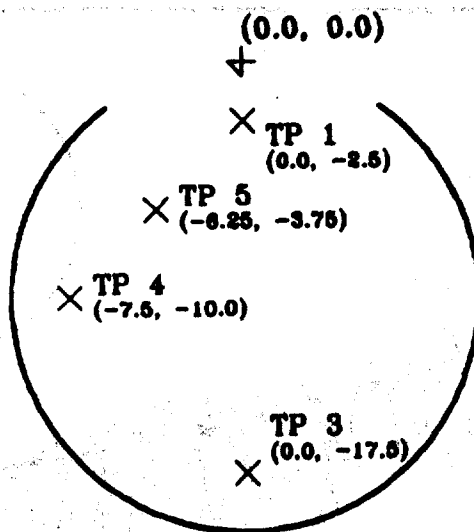


Figure 5.1. Test Point (TP) locations in PLUTO (See Fig. 3.17).

5.2. EFFECTS OF APERTURE SIZE

Figure 5.2 shows the receiving cross section, σ (or $(NWR)^2 + 42.75$ dB) of an open-ended long wire in PLUTO at TP1 which is near three sizes of apertures, all having a 10:1 aspect ratio. The wire is 22.5 cm long for which the first $\lambda/4$ resonance is at $f_w = 0.333$ GHz.

The unsmoothed response of the wire as a free-standing monopole (no shielding) and the f^{-2} Coupling Effectiveness (CE) curve (denoted as $1/n$ where $n = 1, 2 \dots$ is the TEM mode resonance number - actually $1/n^2$ for a σ -plot) are shown to bound the smoothed overall response in accordance with the SExCE model shown in Fig. 4.1. Aperture resonances occur at $f_a \approx 1, 2.5$ and 4.0 GHz, corresponding to when the perimeters (with images) of the three apertures are one wavelength. Also note that the Shielding Effectiveness (SE, see Fig. 4.1) improves about 5 and 10 dB respectively above f_a for the smaller two apertures.

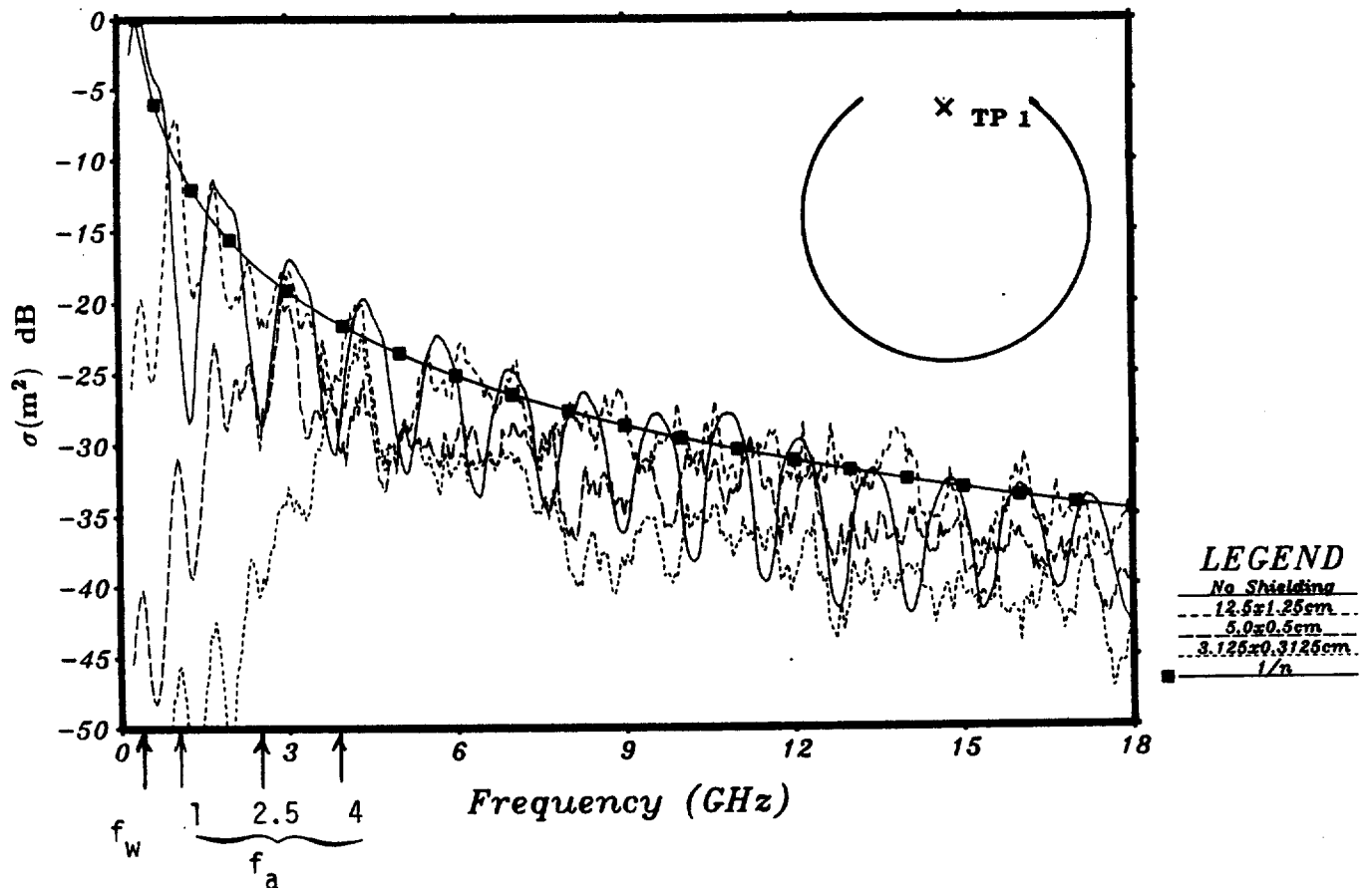


Figure 5.2. Effects of aperture size in PLUTO. The 22.5 cm wire sensor ($f_w = 0.333$ GHz) is located at TP1, $h = 30$ cm, smoothing = 2.5%.

5.3. VARYING TEST POINT LOCATION

Figures 5.3 and 5.4 show the smoothed response for a 22.5 cm long wire unshorted at the top ($f_w = 0.333$ GHz) at test points 1, 3, 4 and 5 in PLUTO. The aperture is 12.5×1.25 cm for which $f_a \approx 1$ GHz. The Coupling Effectiveness (CE) corresponding to the unshielded wire ($1/n$) is also shown.

There are two important effects to note. First, the Shielding Effectiveness (SE) is increased (curves are lower) near f_a when the wire is moved further from to the aperture. Second, the overall response somewhat above f_a is hardly effected by the location of the wire inside the cavity. Thus, SExCE is approximately CE as predicted by the SExCE model (Fig. 4.1). These effects are more easily observed by computing the perturbing factor shown in Fig. 5.4.

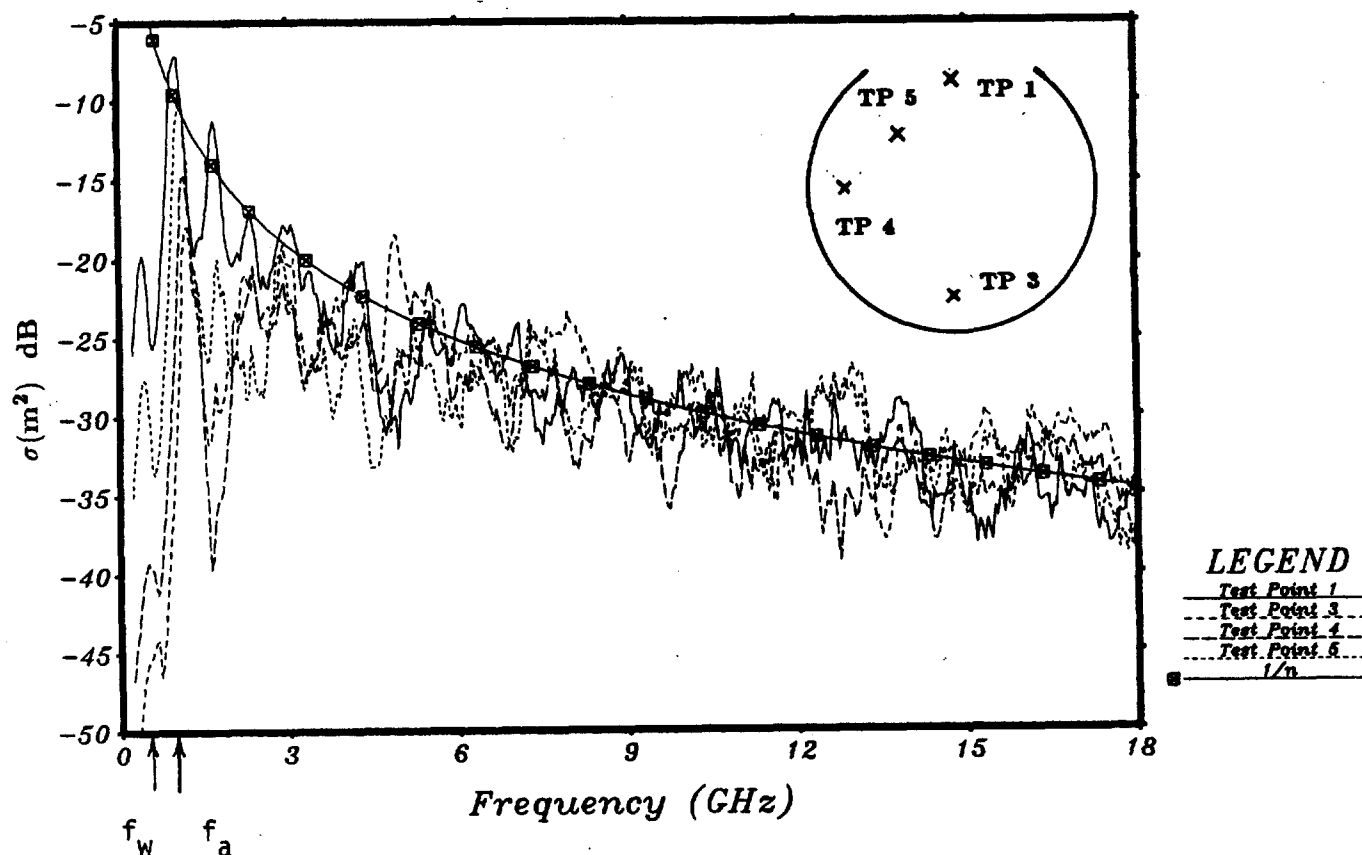


Figure 5.3. Effects of varying the test point location in PLUTO. Aperture = 12.5×1.25 cm ($f_a \approx 1$ GHz), $h = 30$ cm. The lowest resonance of the 22.5 cm wire sensor is $f_w = 0.333$ GHz. Smoothing = 2.5%.

The data of Fig. 5.3 is replotted as the Perturbing Effect in Fig. 5.4, relative to the response of the wire at TP1 near the aperture. Moving the sensor wire further from the aperture substantially increases the overall Shielding Effectiveness (lowers the curves) near f_a , but there is little effect for $f > 4f_a$. At these higher frequencies, the wire responds nearly the same for all locations in the cavity.

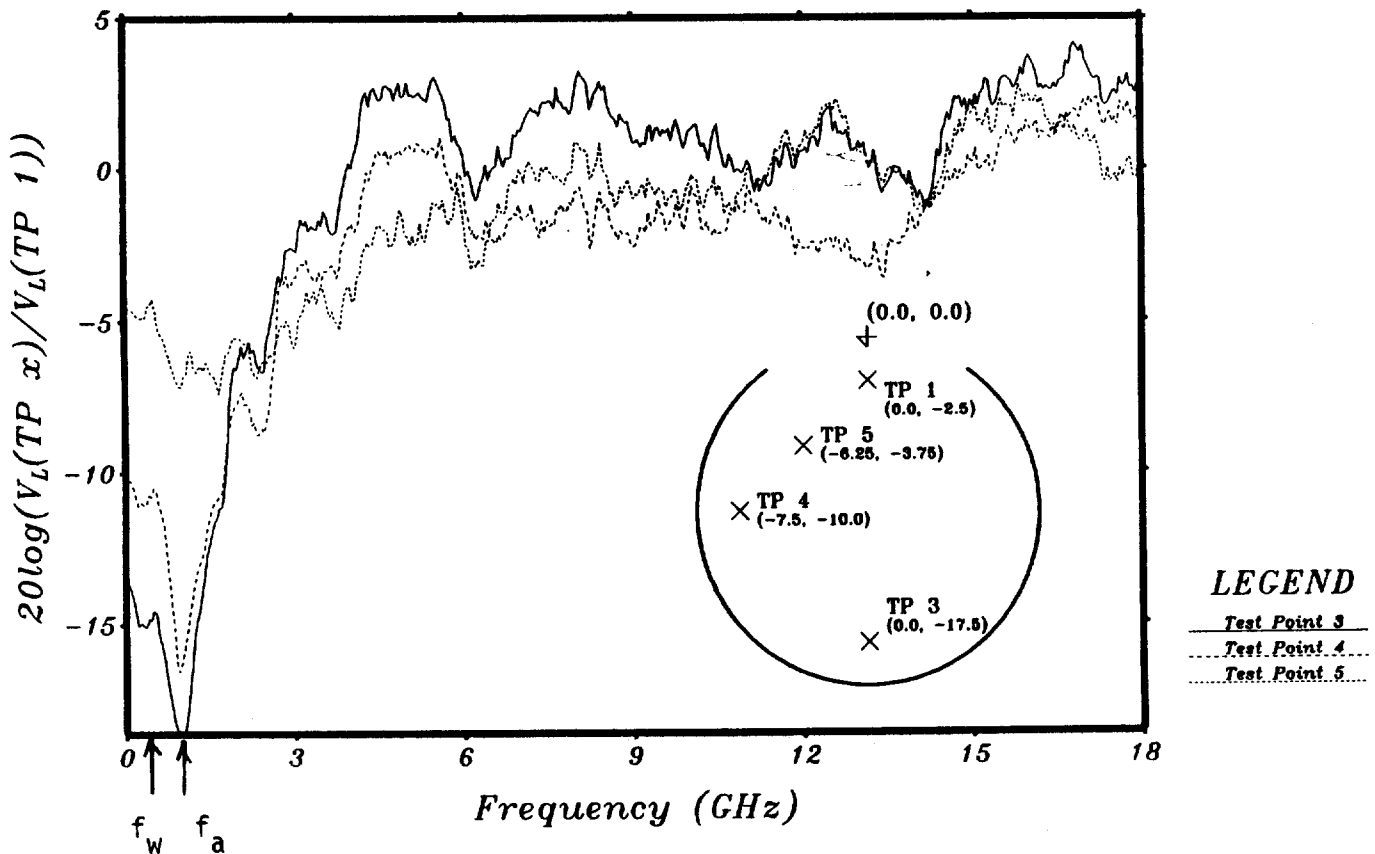


Figure 5.4. Perturbing Effect (PE) of moving the 22.5 long wire sensor ($f_w = 0.333$ GHz) away from TP1, using the data of Fig. 5.3. Aperture = 12.5×1.25 cm ($f_a = 1$ GHz), $h = 30$ cm, smoothing = 10%.

5.4. VARYING THE SIZE AND LOCATION OF METAL FILL

Figures 5.5 and 5.6 show the effect of introducing 30 cm high metal cylinders into the PLUTO cavity. Placement of the metal cylinders (perturbation) very near the aperture increases the Shielding Effectiveness (lowers the curves) and raises the aperture cutoff frequency, especially if the perturbation is large. This is attributed to blockage of the aperture so that it essentially becomes two apertures, each having a reduced perimeter with a corresponding increase of the cutoff frequency. Since the effective aperture resonance is raised by the perturbation, the Shielding Effectiveness is much smaller below f_a than in Fig. 5.3. Hence, the effect of the first wire resonance at f_w is less discernable. The envelope is bounded by the CE of the unshielded 22.5 cm monopole, in accordance with the SE_xCE model (Fig. 4.1).

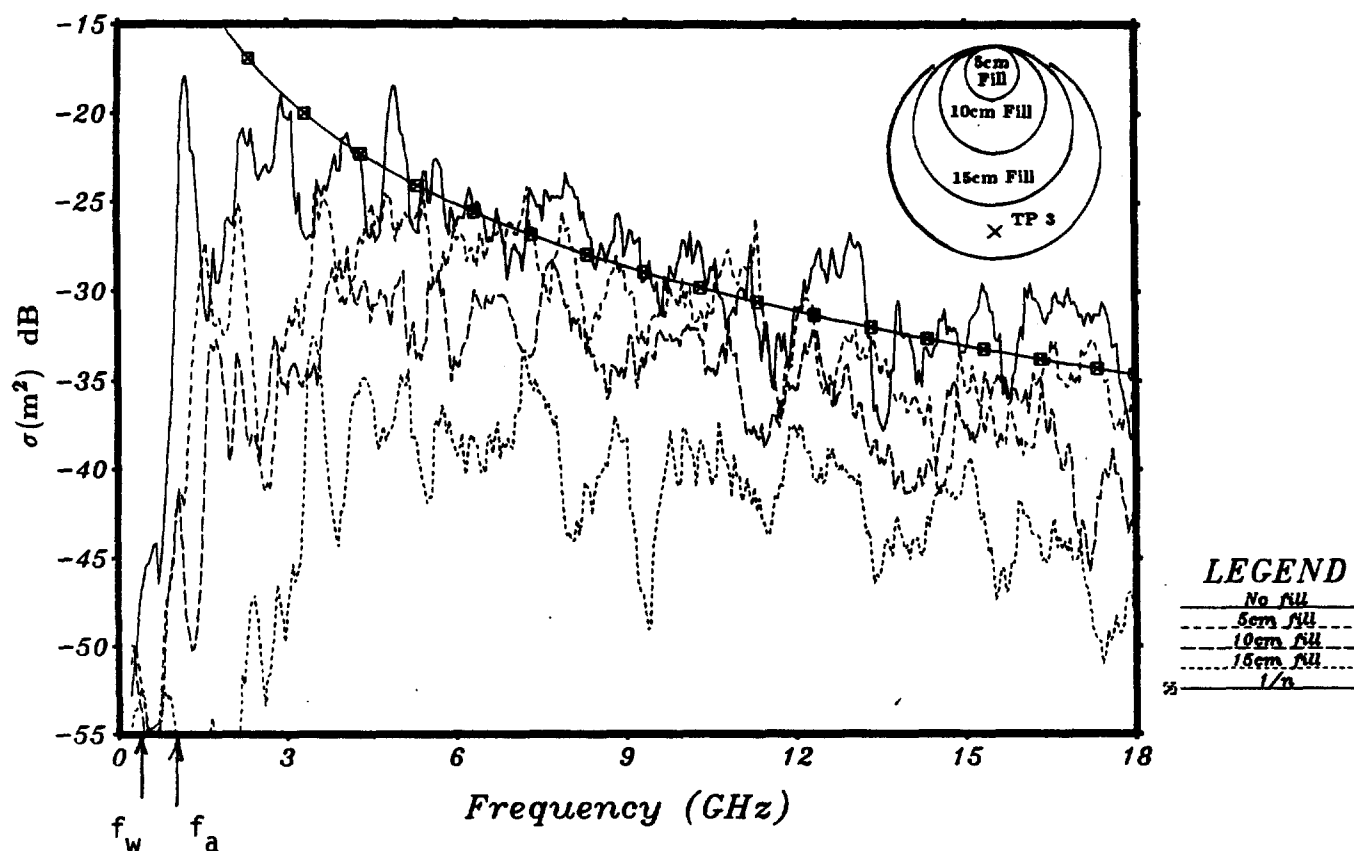


Figure 5.5. Effects of varying the size of cylindrical metal fill near the 12.5 x 1.25 cm ($f_a = 1$ GHz) aperture of PLUTO. The 22.5 cm open ended wire sensor ($f_w = 0.333$ GHz) is located at TP3, $h = 30$ cm, smoothing = 2.5%.

The data in Fig. 5.5 is replotted as the Perturbing Effect in Fig. 5.6. In accordance with (4.3), PE is the ratio of response with the fill present to that with no fill, everything else remaining the same.

From these data, the 5 cm fill near the aperture reduces the response about 7 dB near f_a , and 2-3 dB for $f > 4f_a$. The 10 cm fill reduces the response about 13 dB near f_a , and 5-6 dB for $f > f_a$, while the large 15 cm fill reduces the response more than 30 dB near f_a , and 10-15 dB for $f > 4f_a$.

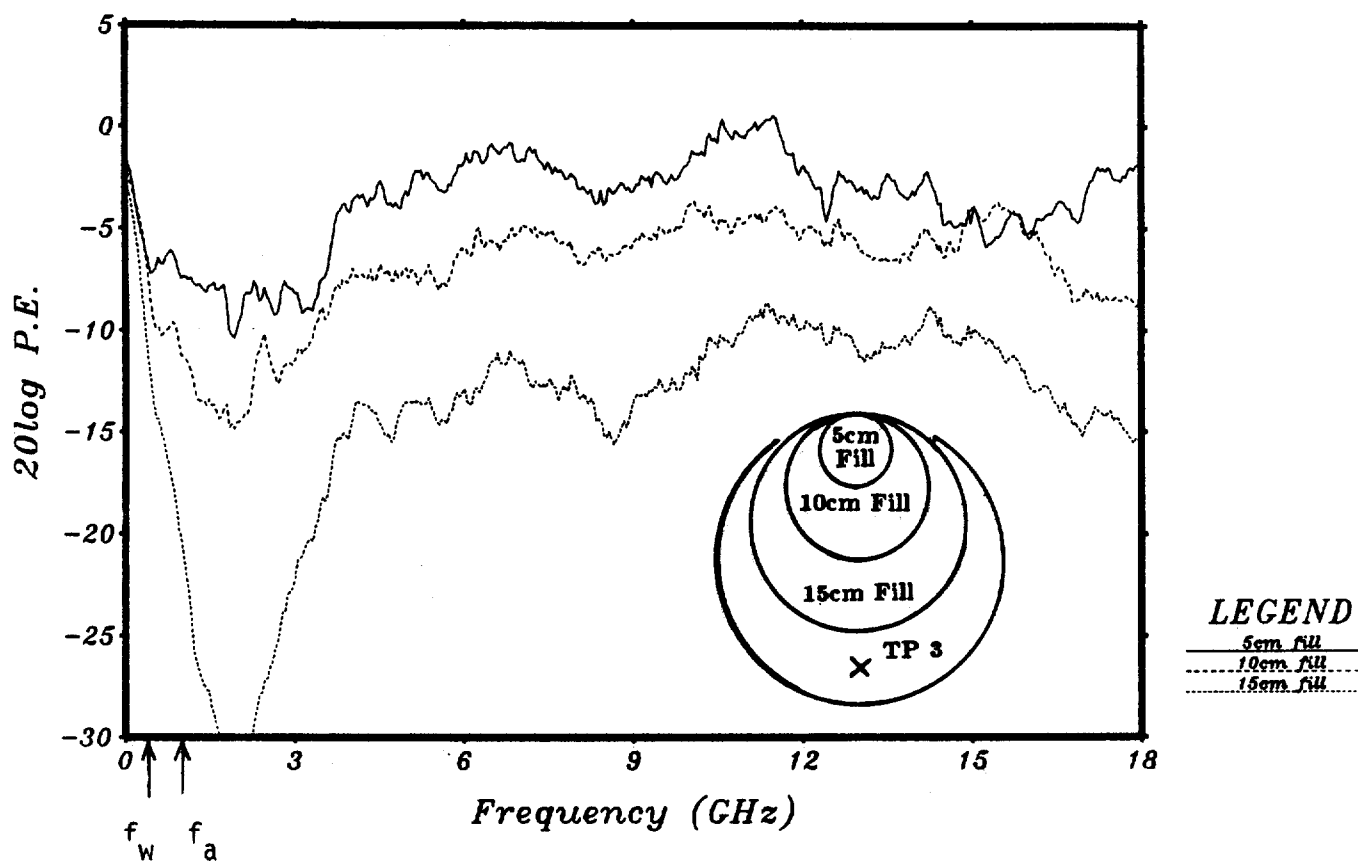


Figure 5.6. Perturbing Effect (PE) of varying the size of cylindrical metal fill near the 12.5 x 1.25 cm aperture ($f_a = 1$ GHz) in PLUTO. Data corresponds to Fig. 5.5. The 22.5 cm open ended wire sensor ($f_w = 0.333$ GHz) is located at TP3. $h = 30$ cm, smoothing = 10%.

When the metal perturbation does not block the aperture, the response is essentially unaffected for any location of the sensing wire. This important fact is illustrated in Figs. 5.7 through 5.14.

The effects of the three different 30 cm high metal fill cylinders located tangent to the back wall of PLUTO are shown in Figs. 5.7 and 5.8. Since the aperture is small ($f_a \approx 4$ GHz) the Shielding Effectiveness (SE) is less than unity above f_a (see Fig. 4.1). Therefore, for comparison, the Coupling Effectiveness (CE or $1/n$) curve has been shifted downward by 5 dB relative to that in Figs. 5.3 and 5.5. The overall responses for all three metal fill cylinders are essentially the same except for fine structure which are due to the TM mode resonances.

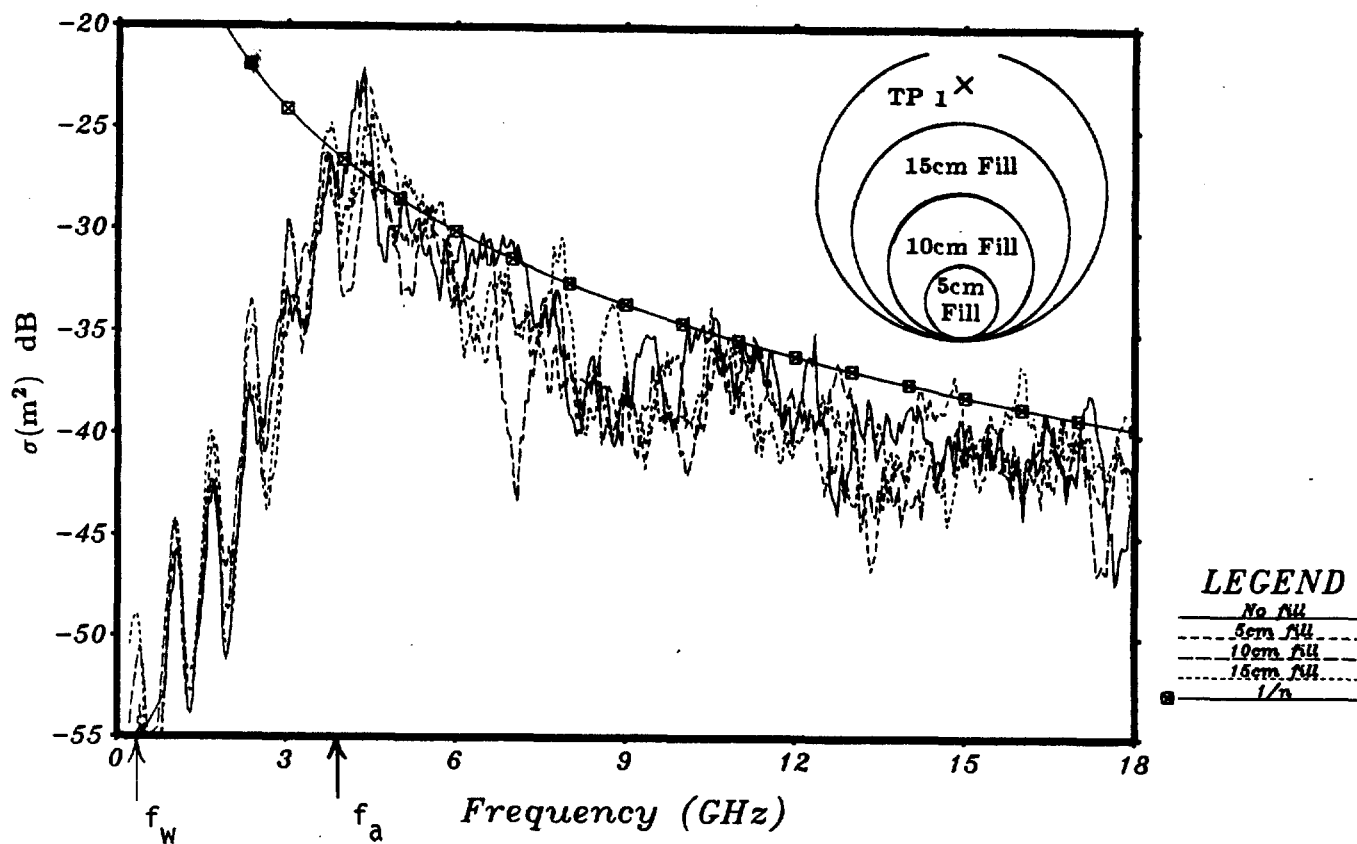


Figure 5.7. Effects of varying the size of cylindrical metal fill near the back wall of PLUTO. The 22.5 cm open ended wire sensor ($f_w = 0.333$ GHz) is located at TP1. Aperture = 3.12×0.312 cm ($f_a = 4$ GHz), $h = 30$ cm, smoothing = 2.5%.

The data of Fig. 5.7 is replotted as the Perturbing Effect in Fig. 5.8, relative to the response of the 22.5 cm wire at TP1 with no fill. In accordance with (4.3), PE is the ratio of response with the fill present to that with no fill, everything else remaining the same. Overall, if the fill is not near the aperture it has little effect on the response of a sensor located near the aperture.

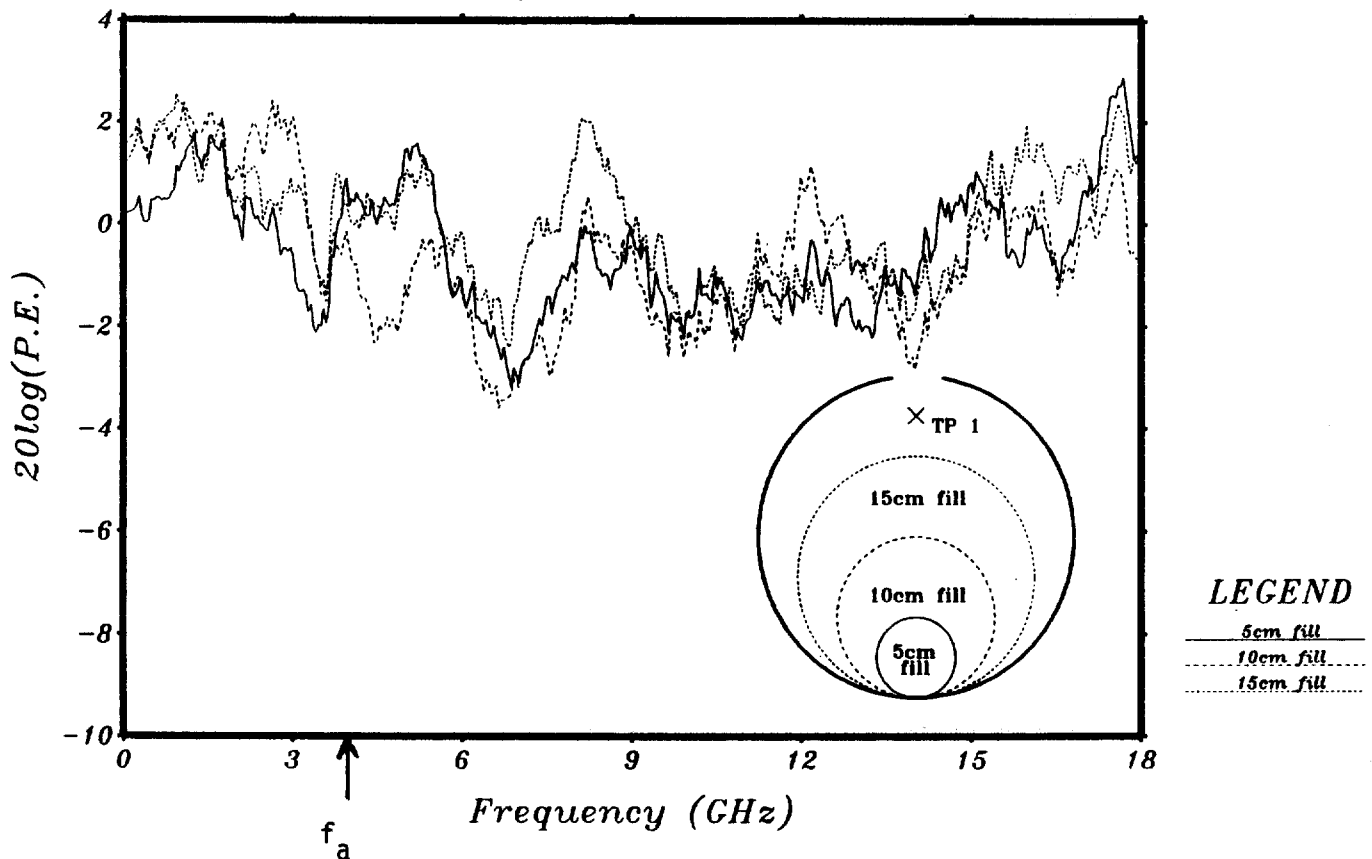


Figure 5.8. Perturbing Effect (PE) of adding three different metal cylinders tangent to the back wall of the cavity in PLUTO. Data corresponds to that of Fig. 5.7. The 22.5 cm open ended wire sensor ($f_w = 0.333$ GHz) is located at TP1. Aperture = 3.12×0.312 cm ($f_a = 4$ GHz), $h = 30$ cm, smoothing = 10%.

Figures 5.9 and 5.10 show the effects of metal cylindrical fill tangent to the side wall of PLUTO. Since the aperture is small (5 x 0.5 cm) the Shielding Effectiveness (SE) is less than unity above f_a . Therefore, for comparison, the Coupling Effectiveness (CE or $1/n$) curve has been shifted downward 5 dB relative to that in Figs. 5.3 and 5.5.

The overall coupling features are relatively unaffected for the small (5 and 10 cm) cylinders, but the Shielding Effectiveness is substantially increased (curve is lowered) near f_a for the 15 cm fill. This is due to aperture blockage such that the open region between PLUTO and the fill forms a high pass waveguide.

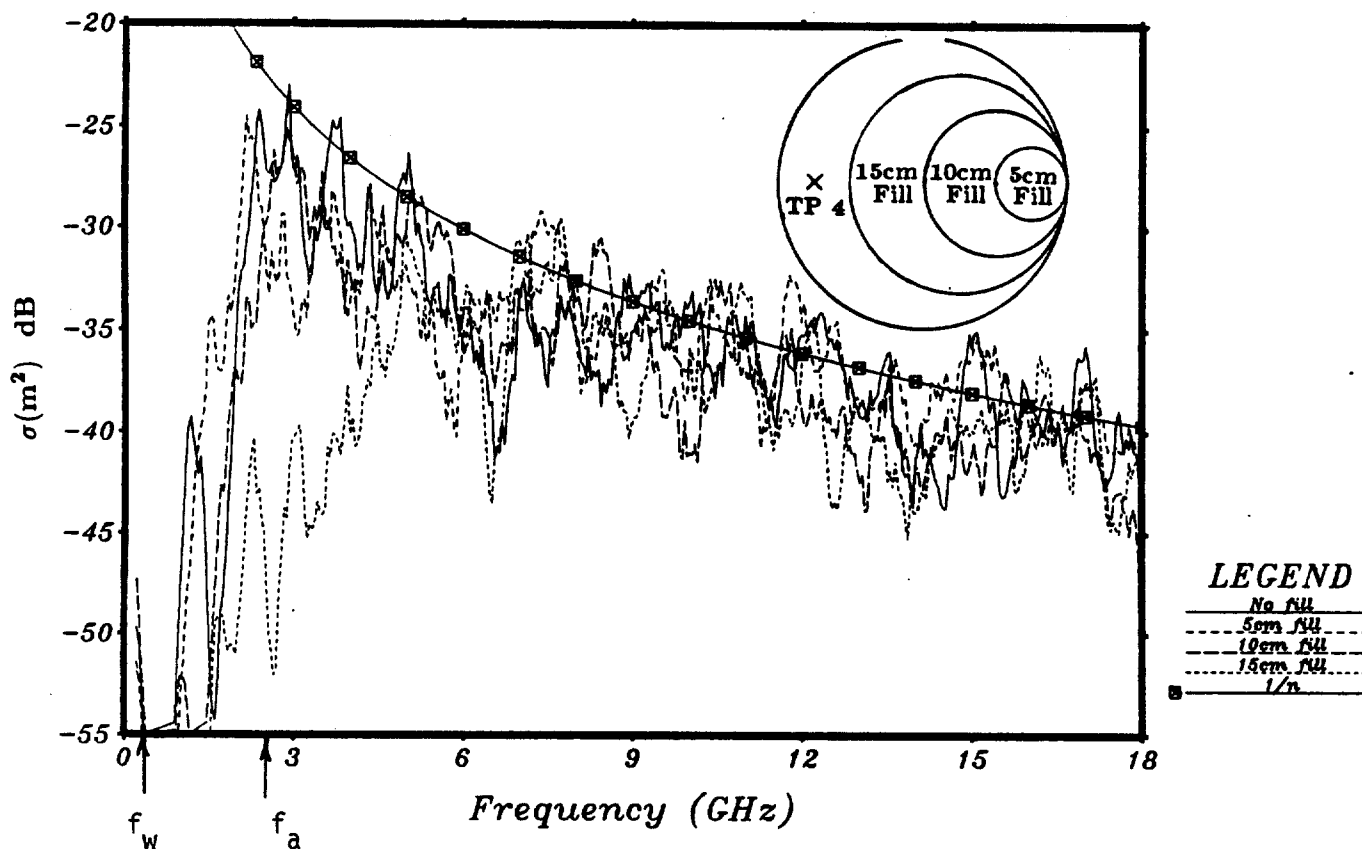


Figure 5.9. Effects of varying the size of cylindrical metal fill near the side wall of PLUTO. The 22.5 cm open ended wire sensor ($f_w = 0.333$ GHz) is located at TP4. Aperture = 5 x 0.5 cm ($f_a = 2.5$ GHz), smoothing = 2.5%.

The data in Fig. 5.9 is replotted as the Perturbing Effect in Fig. 5.10 relative to the response at TP4 with no fill.

As in Fig. 5.9, these data show that small fill (e.g., 5 and 10 cm cylinders) has little effect on the overall Shielding Effectiveness, but large fill which tends to block the aperture increases SE near the aperture cutoff frequency, f_a . This obtains because the open space between the large fill and the PLUTO cavity tends to form a high pass waveguide.

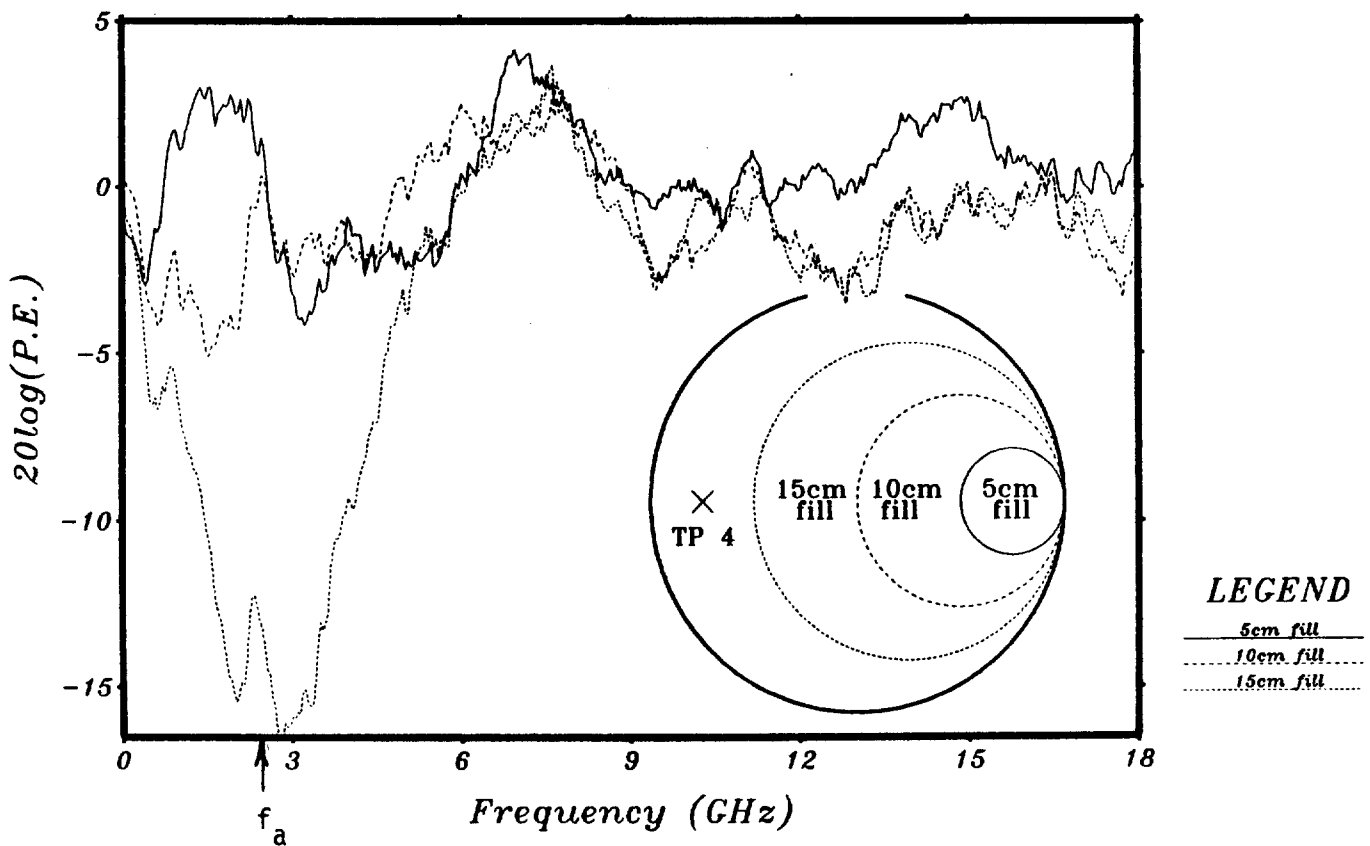


Figure 5.10. Perturbing Effect (PE) of varying the size of cylindrical metal fill tangent at one side wall of PLUTO. The 22.5 cm open ended wire sensor ($f_w = 0.333$ GHz) is located at TP4. Aperture = 5 x 0.5 cm ($f_a \approx 2.5$ GHz), $h = 30$ cm, smoothing = 10%.

The effects of placing 10 cm diameter metal cylinders near the side and back walls of PLUTO are shown in Figs. 5.11 and 5.12.

The Perturbing Effect of the fill tends to increase the Shielding Effectiveness (lower the curve) slightly near f_a , but has little effect above f_a except for changes in the fine structure due to the TM cavity modes. Above f_a the response decreases as f^{-2} in accordance with the Coupling Effectiveness (CE) of the long wire (Fig. 4.1). Also note the evidence of the first wire resonance at f_w . This resonance has been severely suppressed due to the Shielding Effectiveness (SE) of the aperture at frequencies below f_a .

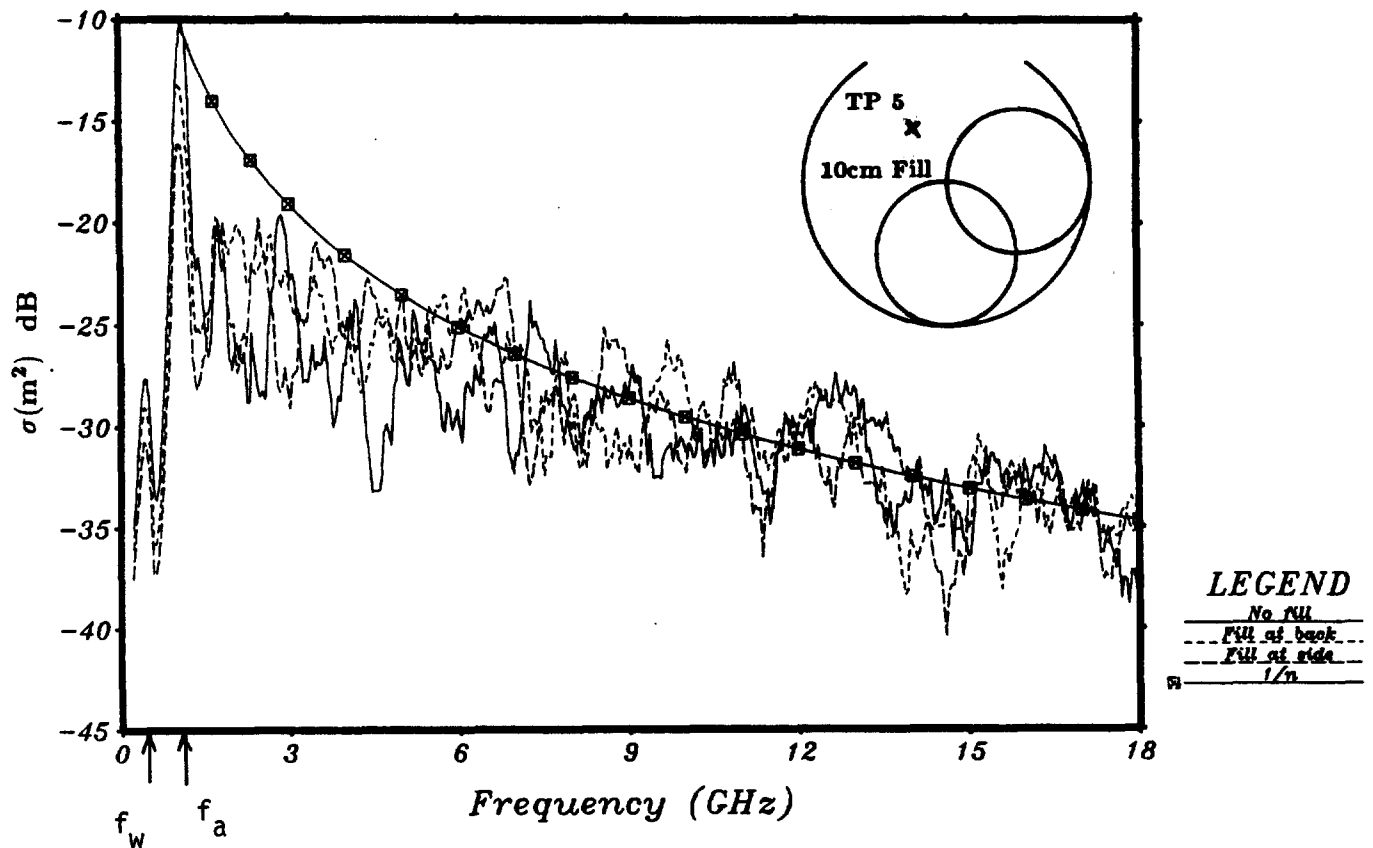


Figure 5.11. Effects of varying the location of a 10 cm cylindrical metal fill near the side and back walls of PLUTO. The 22.5 cm open ended wire sensor ($f_w = 0.333$ GHz) is located at TP5. Aperture = 12.5×1.25 cm ($f_a = 1$ GHz), smoothing = 2.5%.

The data of Fig. 5.11 is replotted as the Perturbing Effect (PE) in Fig. 5.12, relative to the response of the wire with no fill.

As in Fig. 5.11, the presence of the 10 cm cylinders tangent to the side and back walls of PLUTO effects the PE very little except for some slight reduction near f_a .

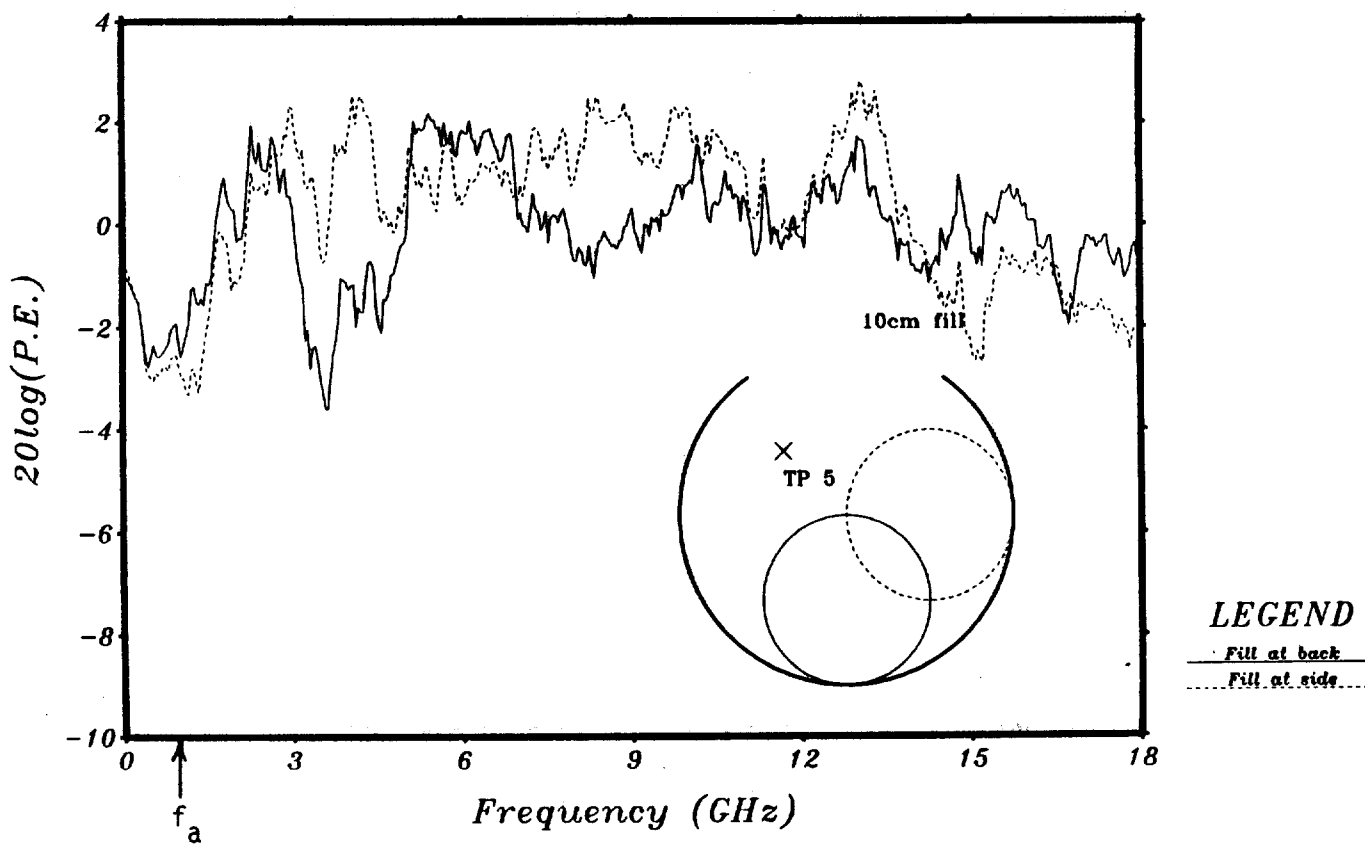


Figure 5.12. Perturbing Effect (PE) of varying the location of 10 cm cylindrical metal fill tangent to the back and side walls of PLUTO. The 22.5 cm open ended wire sensor ($f_w = 0.333$ GHz) is located at TP5. Aperture = 12.5 x 1.25 cm ($f_a = 1$ GHz), $h = 30$ cm, smoothing = 10%.

In Fig. 5.13, the 10 cm metal cylindrical metal fill (perturbation) is located near the front, side and back walls of PLUTO. Since the aperture is small (3.12×0.312 cm) SE is less than unity above f_a . Therefore, for comparison, the CE ($1/n$) curve has been shifted down 5 dB relative to that in Figs. 5.3 and 5.5

As in Figs. 5.7 through 5.14, there is little Perturbing Effect of the fill when it does not block the aperture. However, as in Figs. 5.5, 5.6, 5.9 and 5.10, when the fill blocks the aperture, the Perturbing Effect tends to decrease the overall normalized wire response (lower the curve). In Fig. 5.13, $f_w \ll f_a$, so the first resonance of the long wire has been severely suppressed.

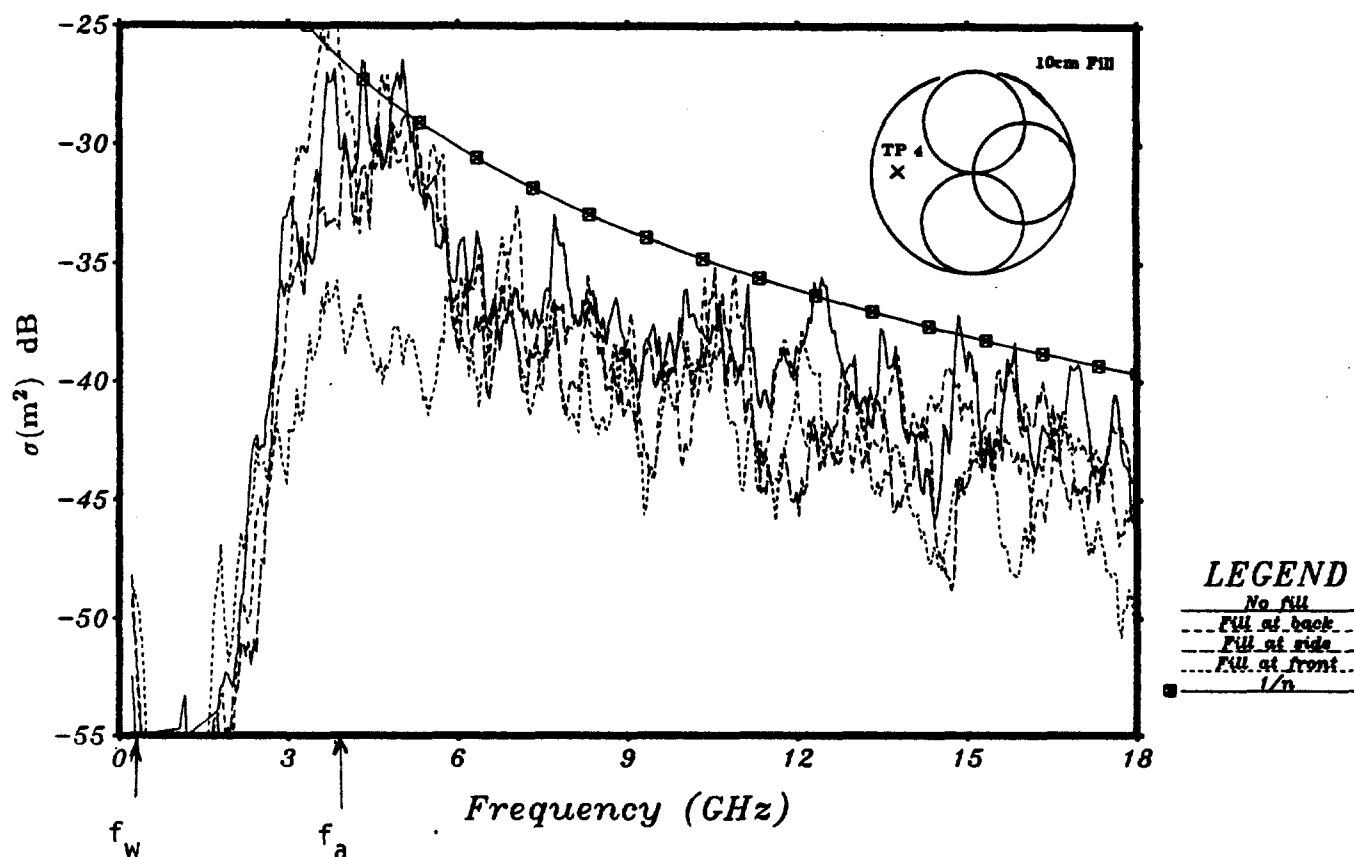


Figure 5.13. Effects of varying the position of a 10 cm cylindrical metal fill near the front, side and back walls of PLUTO. The 22.5 cm open ended wire sensor ($f_w = 0.333$ GHz) is located at TP4. Aperture = 3.12×0.312 cm ($f_a = 4$ GHz), $h = 30$ cm, smoothing = 2.5%.

The data in Fig. 5.13 is replotted as the Perturbing Effect in Fig. 5.14, relative to the response with no fill.

This data is similar to that of Figs. 5.11 and 5.12, except that the aperture is small ($f_a \approx 4$ GHz). Again, the PE is seen to be small (near zero dB) when the fill does not block the aperture. However, when the fill blocks the aperture the PE is significant near f_a (about 10 dB) and -3 dB for $f \gg f_a$.

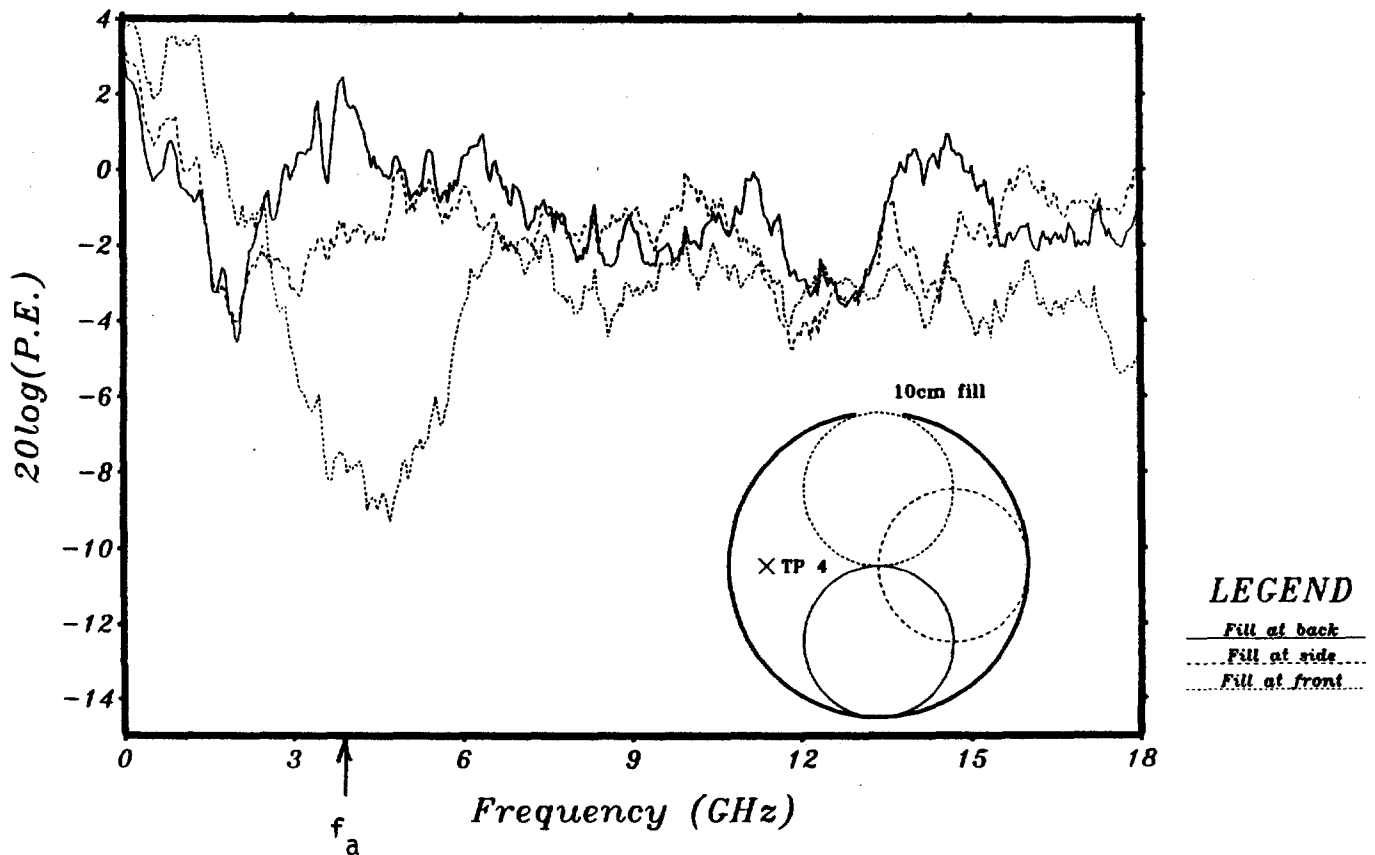


Figure 5.14. Perturbing Effect (PE) of varying the location of 10 cm cylindrical metal fill tangent to the front, side and back walls of PLUTO corresponding to Fig. 5.13. The 22.5 cm open ended wire sensor ($f_w = 0.333$ GHz) is located at TP4. Aperture = 3.12×0.312 cm ($f_a \approx 4$ GHz), $h = 30$ cm, smoothing = 10%.

5.5. VARYING CAVITY HEIGHT

The effects of varying the height, h , of the internal cavity in PLUTO is shown in Fig. 5.15. Below f_a , the Shielding Effectiveness is essentially independent of h . Since the aspect ratio (2:1) of the aperture is small, the Shielding Effectiveness below f_a is small. Consequently, the large Coupling Effectiveness of the wire at f_w ($= 0.5$ GHz) tends to enhance the overall coupling below f_a , in accordance with the SExCE model of Fig. 4.1.

Above f_a the presence of higher order TM cavity modes causes the response to be highly structured. There is little fall off with increasing frequency above f_a since the CE trend cannot be seen over the relatively narrow frequency range plotted here.

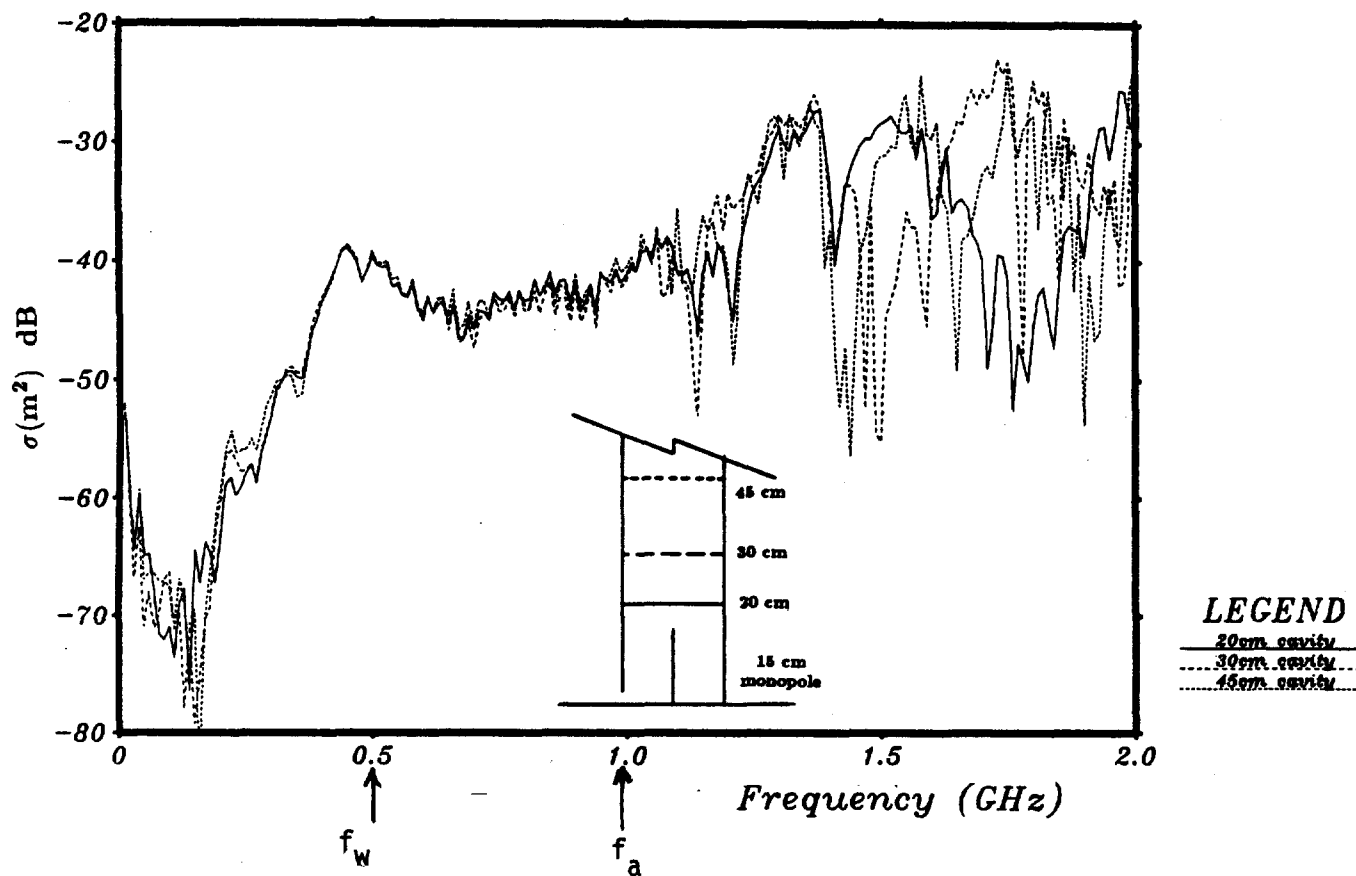


Figure 5.15. Effects of varying internal cavity height in PLUTO. The sensor is a 15 cm open ended wire ($f_w = 0.5$ GHz) at TP2. $h = 20, 30$ and 45 cm. Aperture = 7.5×3.75 cm ($f_a = 1$ GHz), smoothing = 2.5%.

5.6. LOSSY FILL

Figs. 5.16 and 5.17 show the effects of adding a small piece of ferrite (EMI Suppressant tubing LST-150; Capcon, Inc.) at the shorted end of the wire sensor in order to suppress the coupling above f_a . The Coupling Effectiveness of the 30 cm long wire (1/n curve) is also shown. Its first resonance occurs when $h = \lambda/2$, or $f_w = 0.5$ GHz. As seen, the ferrite effects the structure somewhat, but there is little effect on the overall response.

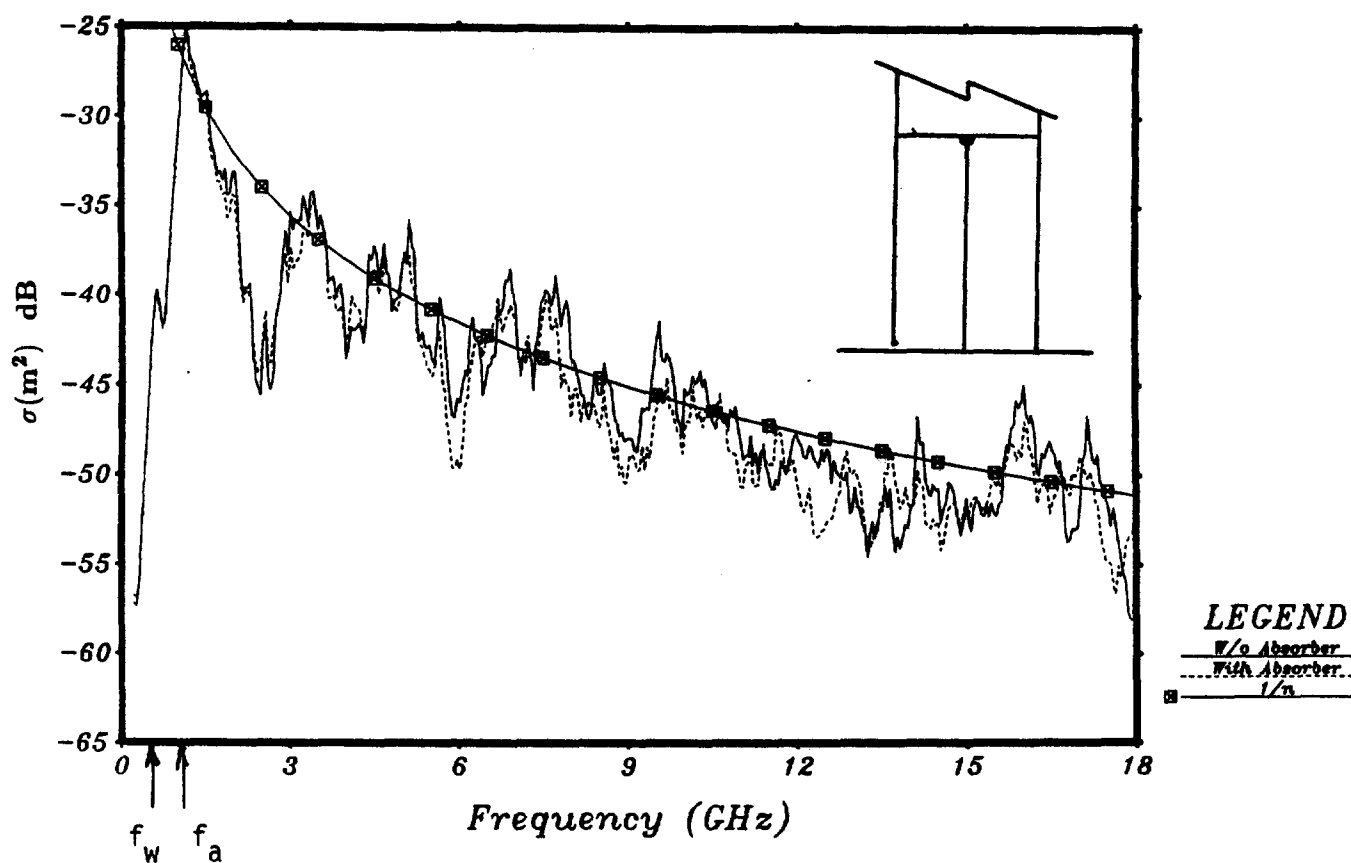


Figure 5.16. Effect of placing a small piece (length = 1 cm) of ferrite at the end of the 30 cm long wire sensor which is shorted at the top of the PLUTO cavity ($f_w = 0.5$ GHz). Wire is located at TP2. Aperture = 12.5×1.25 cm ($f_a = 1$ GHz), smoothing = 2.5%.

The data of Fig. 5.16 is replotted as the Perturbing Effect in Fig. 5.17, relative to the response with no ferrite absorber. PE is seen to be slight at the lower frequencies, becoming more (< 5 dB) above 9 GHz.

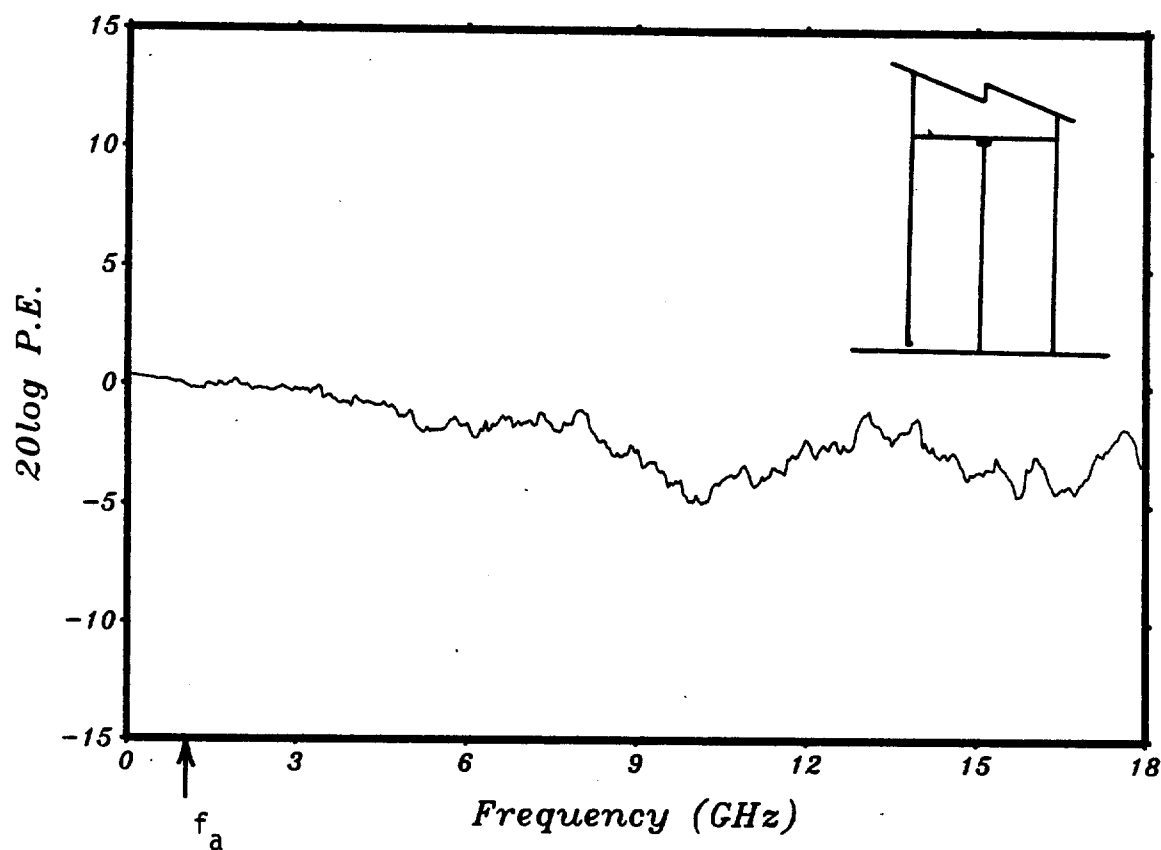


Figure 5.17. Perturbing Effect of a small ferrite bead (length = 1 cm) placed at the shorted end of the 30 cm long wire sensor ($f_w = 0.5$ GHz). Wire is located at TP2. Aperture = 12.5 x 1.25 cm ($f_a = 1$ GHz), smoothing = 10%.

Since the short piece of ferrite of Figs. 5.16 and 5.17 has little effect, an experiment was conducted in which a ferrite (EMI suppressant tubing LST-150; Capcon, Inc.) sleeve totally covered the long wire. Otherwise, the conditions were the same.

In this case, the Coupling Effectiveness decreases with increasing frequency in accordance with Fig. 4.1 and the SExCE model. The degree of decreased Coupling Effectiveness due to the ferrite sleeve is more clearly quantified by the Perturbing Effect plot shown in Fig. 5.19.

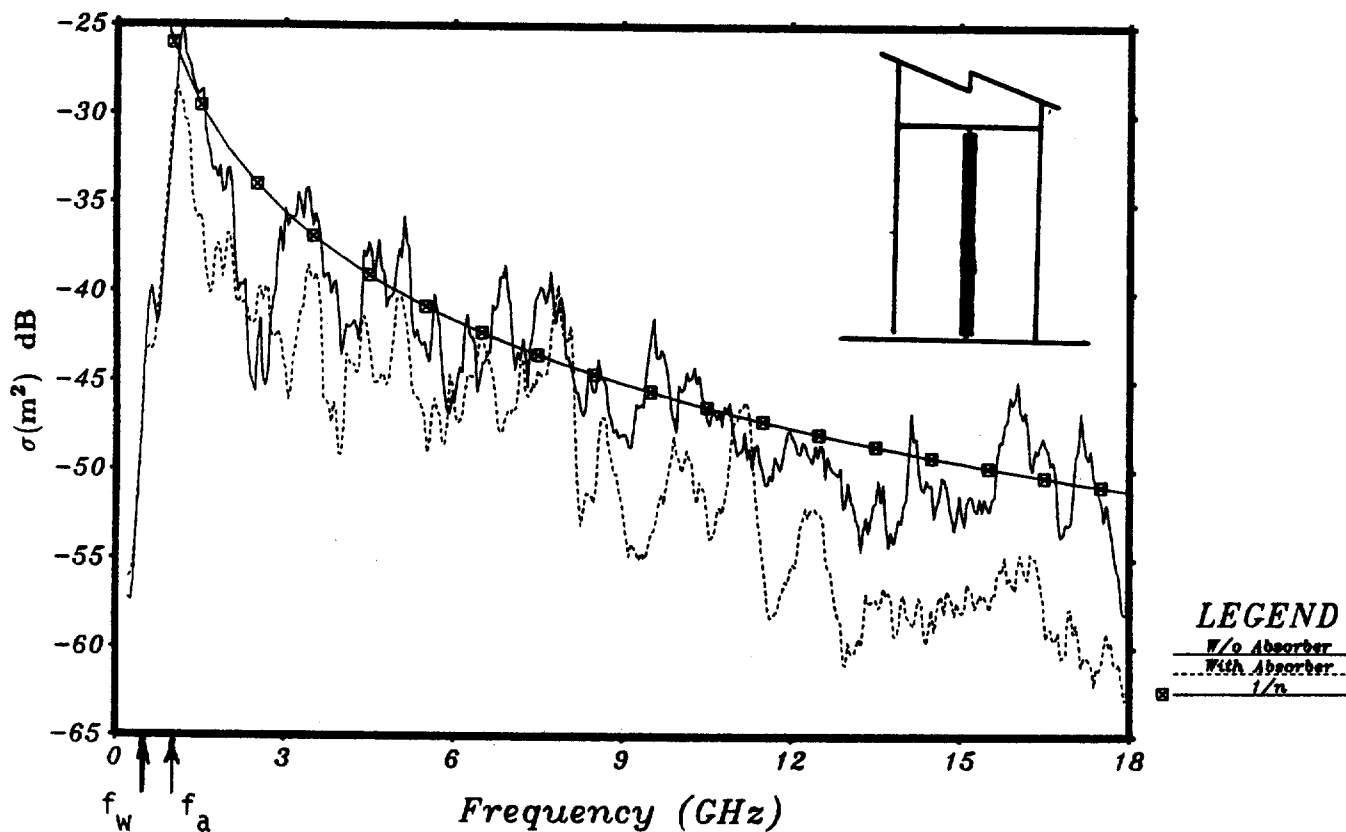


Figure 5.18. Effect of placing a ferrite sleeve over the 30 cm long wire sensor ($f_w = 0.5 \text{ GHz}$) located at TP2. Aperture = $12.5 \times 1.25 \text{ cm}$ ($f_a = 1 \text{ GHz}$), smoothing = 2.5%.

Although the ferrite does not have a major effect, it does tend to reduce the Coupling Effectiveness with increasing frequency. The cumulative reduction at 18 GHz is about 8 dB.

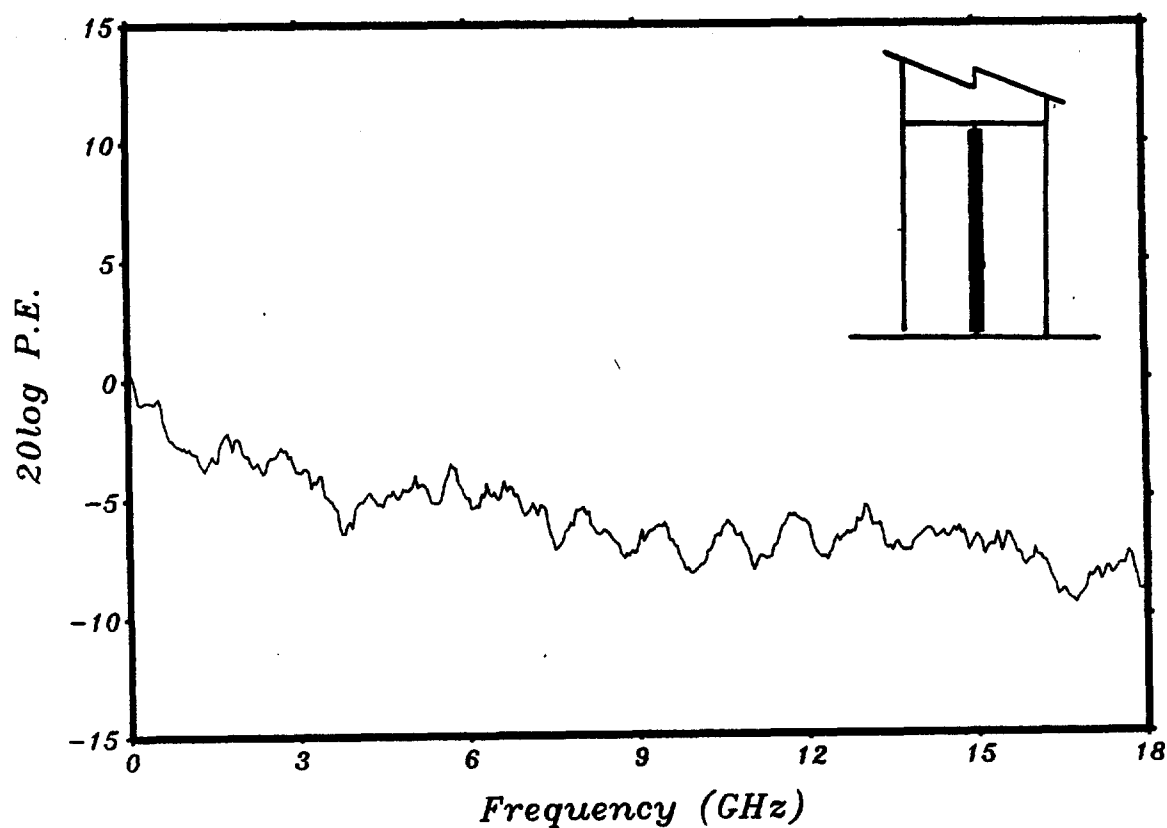


Figure 5.19. Perturbing Effect of placing a sleeve of microwave ferrite absorber over the 30 cm long sensing wire ($f_w = 0.5$ GHz). Aperture = 12.5 x 1.25 cm ($f_a = 1$ GHz), smoothing = 10%.

Figures 5.20 and 5.21 show the effect of adding an 8 cm thick piece of polyfoam microwave absorber (Emerson & Cuming VHP-2-NRL) at the top of the PLUTO cavity. It is seen that the Coupling Effectiveness is reduced somewhat with increasing frequency. This is more clearly quantified by the Perturbing Effect shown in Fig. 5.21. Note that the absorber fills about 25% of the cavity volume.

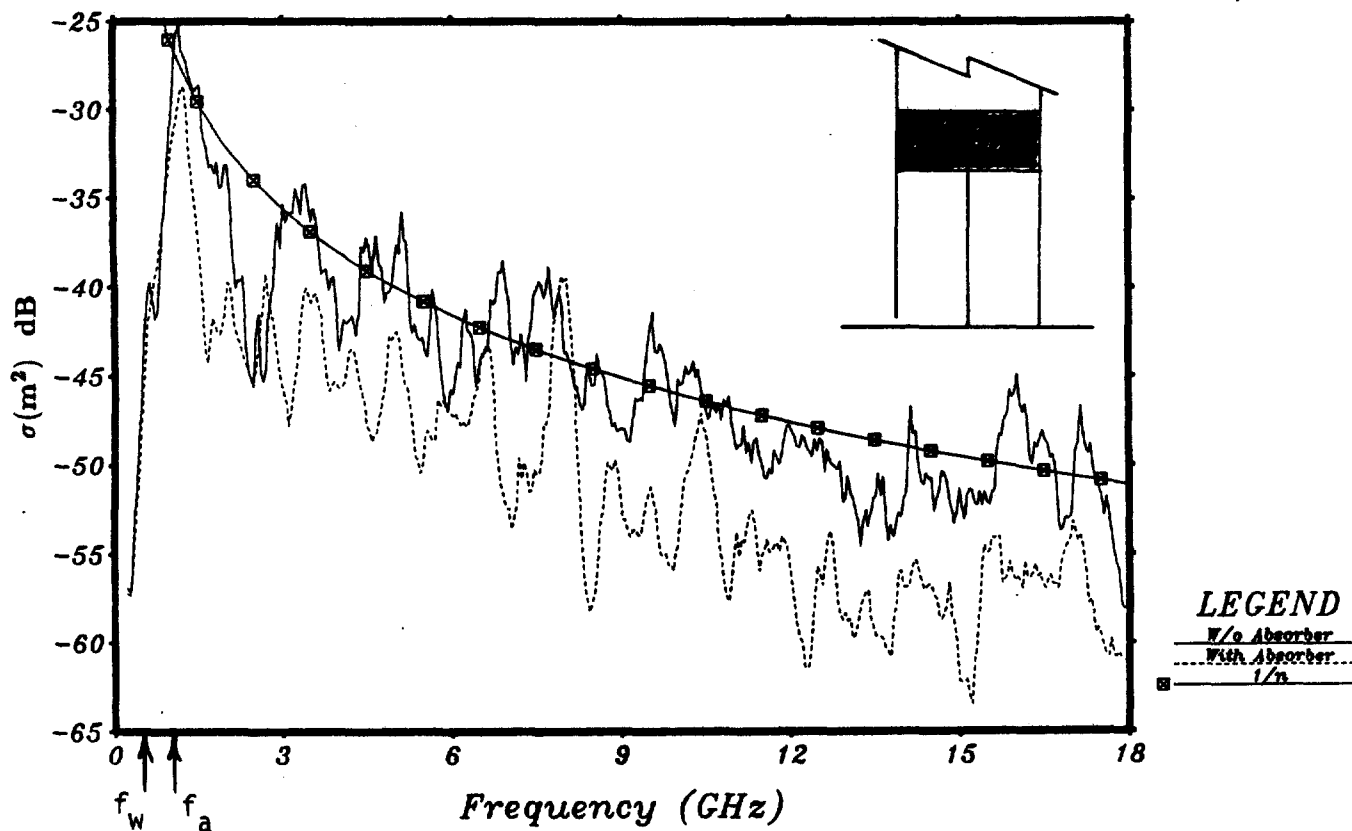


Figure 5.20. Effect of adding an 8 cm thick piece of carbon impregnated polyfoam microwave absorber at the top of the PLUTO cavity. The 30 cm long wire is shorted at the top ($f_w = 0.5 \text{ GHz}$). Aperture = $12.5 \times 1.25 \text{ cm}$ ($f_a = 1 \text{ GHz}$), smoothing = 2.5%.

The data of Fig. 5.20 is replotted as the Perturbing Effect of the absorber in Fig. 5.21. It is seen that the Coupling Effectiveness is reduced about 5 dB above 1 GHz, and 8 dB above 6 GHz.

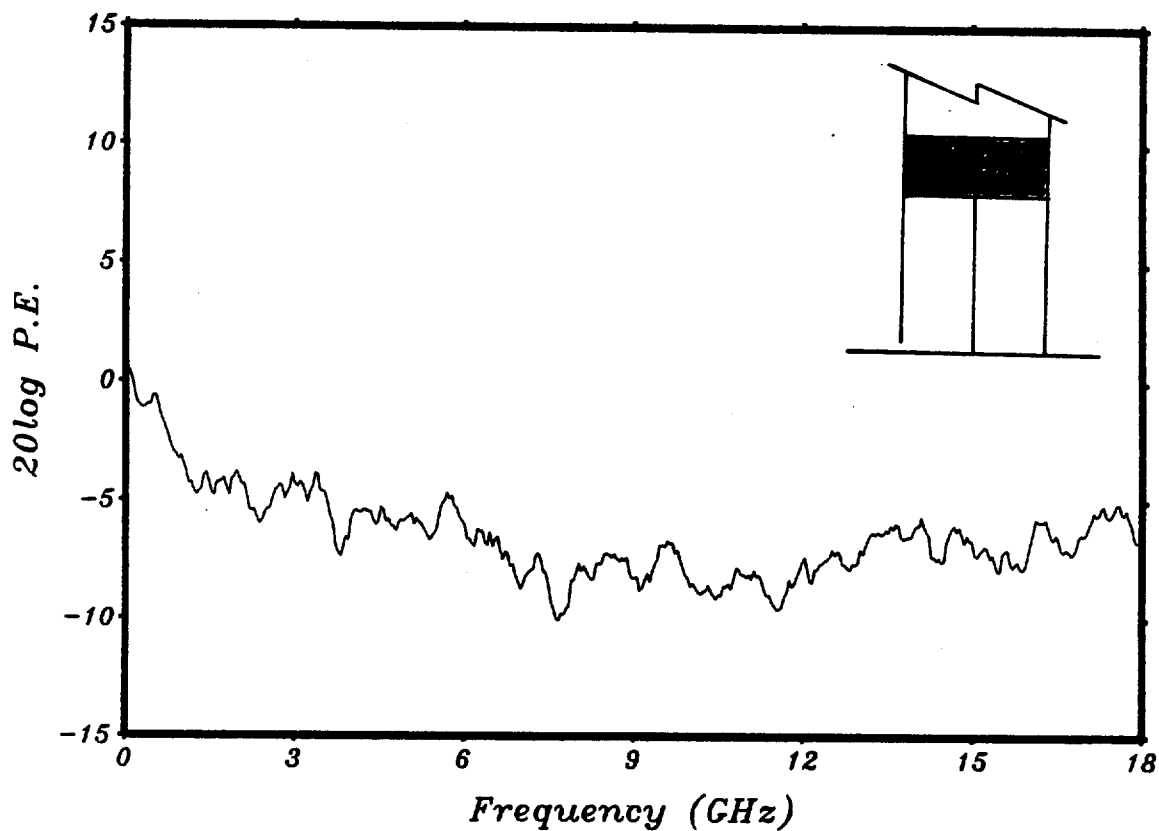


Figure 5.21. Perturbing Effect of an 8 cm thick piece of carbon impregnated absorber placed at the top of the PLUTO cavity. The 30 cm long wire is shorted at the top ($f_w = 0.5$ GHz). Aperture = 12.5×1.25 cm ($f_a = 1$ GHz), smoothing = 10%.

5.7. DIELECTRIC LOADING IN APERTURE

One would expect the Shielding Effectiveness offered by the aperture to be affected by the presence of a dielectric window. Accordingly, several experiments were carried out in which cylindrically shaped dielectrics having dielectric constant K were cut and placed in the aperture.

The results are shown in Fig. 5.22 for $K = 5$. The Perturbing Effects for $K = 3, 4$ and 5 are shown in Fig. 5.23. For $K = 5$, the coupling is enhanced somewhat near f_a (where the aperture is resonant in the absence of the dielectric window). However, this is not always the case as seen in Fig. 5.23 for $K = 3$. Somewhat above f_a the main effect is simply an alteration of the fine structure due to the TM cavity modes, the overall coupling being affected very little.

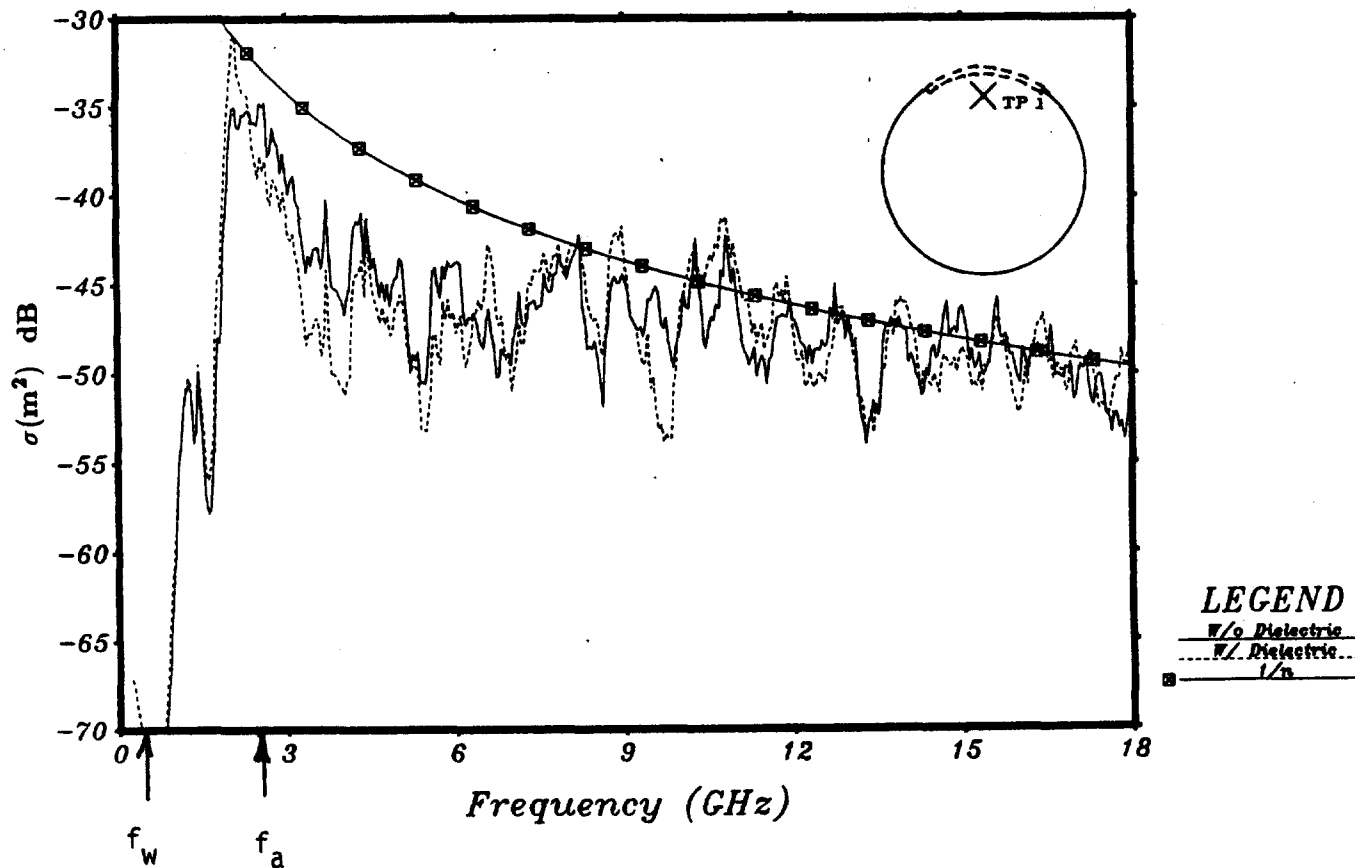


Figure 5.22. Effect of inserting a dielectric window in the aperture of PLUTO. $K = 5$. Aperture = $5 \times 0.5 \text{ cm}$ for which $f_a = 2.5 \text{ GHz}$ without the dielectric. The 30 cm long wire sensor is located at TP1 and shorted at the top of PLUTO ($f_w = 0.5 \text{ GHz}$). Smoothing = 2.5%.

The Perturbing Effect of the dielectric window for $K = 3, 4$ and 5 are shown in Fig. 5.23, relative to an air window. For $K = 4$, the coupling affects the response very little over the entire $100 \text{ MHz} \rightarrow 18 \text{ GHz}$ range. For $K = 3$, the coupling is reduced over the entire frequency range. For $K = 5$, the coupling is significantly enhanced below f_a . These results suggest that the coupling is increased below f_a for $K > 4$. Further studies are necessary to more carefully explain and quantify these effects.

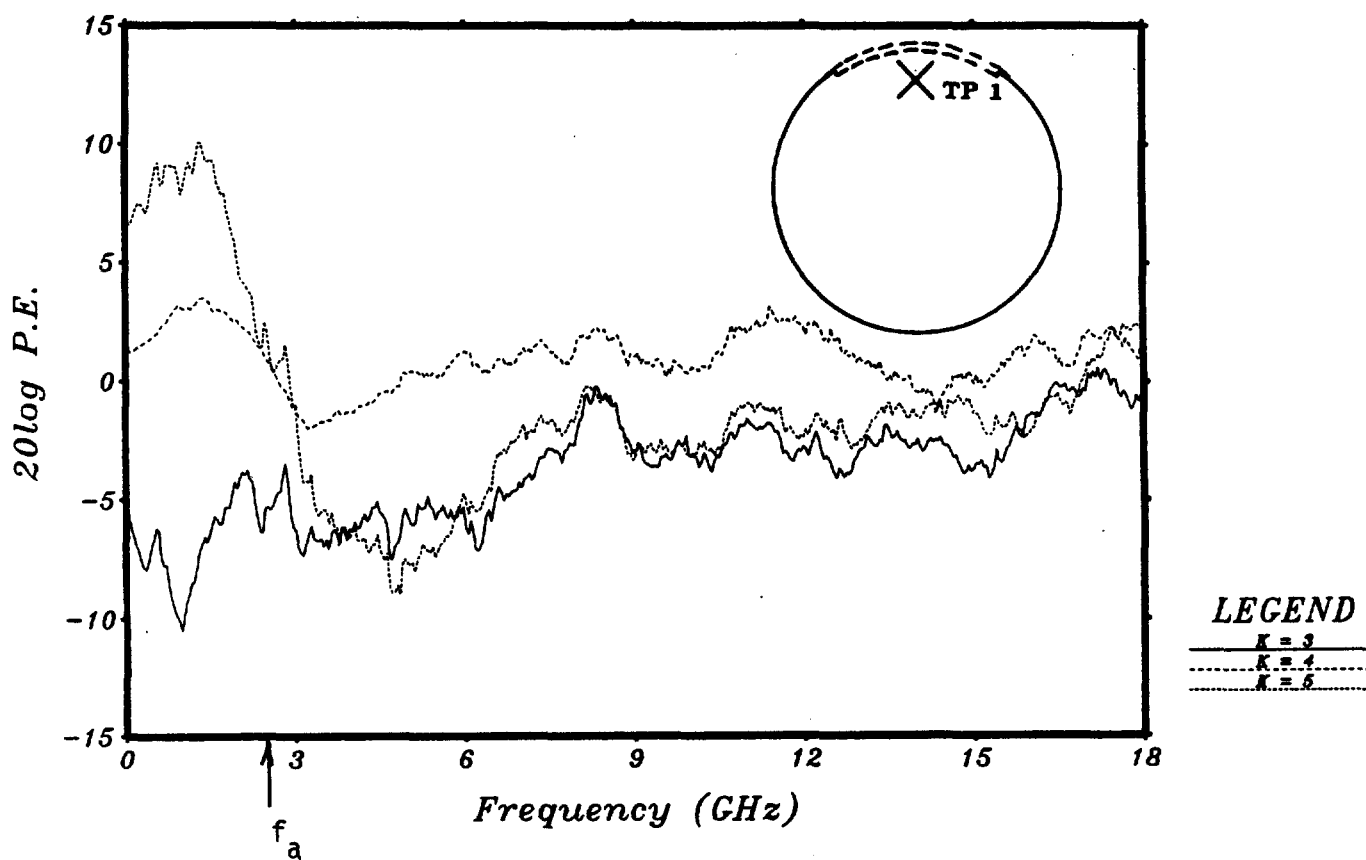


Figure 5.23. Perturbing Effect of a dielectric window in the aperture of the PLUTO cavity. Aperture = $5 \times 0.5 \text{ cm}$ for which $f_a = 2.5 \text{ GHz}$ without the dielectric. The 30 cm long wire is located at TP1 and shorted at the top of PLUTO ($f_w = 0.5 \text{ GHz}$). Smoothing = 10%.

5.8. A7 SCALE MODEL AIRCRAFT TESTS

Coupling tests were conducted on a 1/10 scale model A7 aircraft shown in Fig. 3.18. As explained in Section 3.4.2, this test object and its internal cables is not intended to be a true scale model of an actual aircraft. Rather, it should be considered to be a complex test object which will give many of the gross overall coupling features of a full scale aircraft. Of course, the frequency is scaled downward by the same 1/10 factor. For example, 10 GHz in the experiments on the scale model become 1 GHz when referred to a full scale aircraft.

In these tests the aircraft sits on the ground plane of the EMPEROR Facility and the field is incident on its broadside, the electric field being vertical. The response is measured at jacks J2, J3 and J4 located in the front wheel well (see Fig. 3.18).

Figure 5.24 shows the cw response of the A7 scale model aircraft as measured at J4. The cable is 90 cm long and shorted at its far end ($f_w = 0.17$ GHz). The Coupling Effectiveness for the wire ($1/n$ curve) is also shown for comparison with the SExCE model of Fig. 4.1. Both the raw data (corrected for the anomalies in the incident field) and the smoothed data (9 point trend or 2.5% smoothing) are given.

This test object has many possible ports of entry (cockpit, bomb bay, exhaust, cracks, seams, etc.) so it is impossible to identify the resonant frequency of a single aperture. Moreover, the wire runs a devious route through the aircraft (along the fuselage, through bulkheads, etc. with numerous bends). It is, however, significant that the overall coupling is greatest at f_w and tends to follow the CE ($1/n$ curve) except in the 1-3 GHz range where the overall coupling is reduced more. As in previous data, these results suggest that the general shape of the coupling is chiefly determined by the TEM mode resonances of the wire, while the presence of higher order cavity modes affects the fine structure.

Essentially the same conclusions are drawn from the smoothed responses as seen at J2 and J3 (Fig. 5.25).

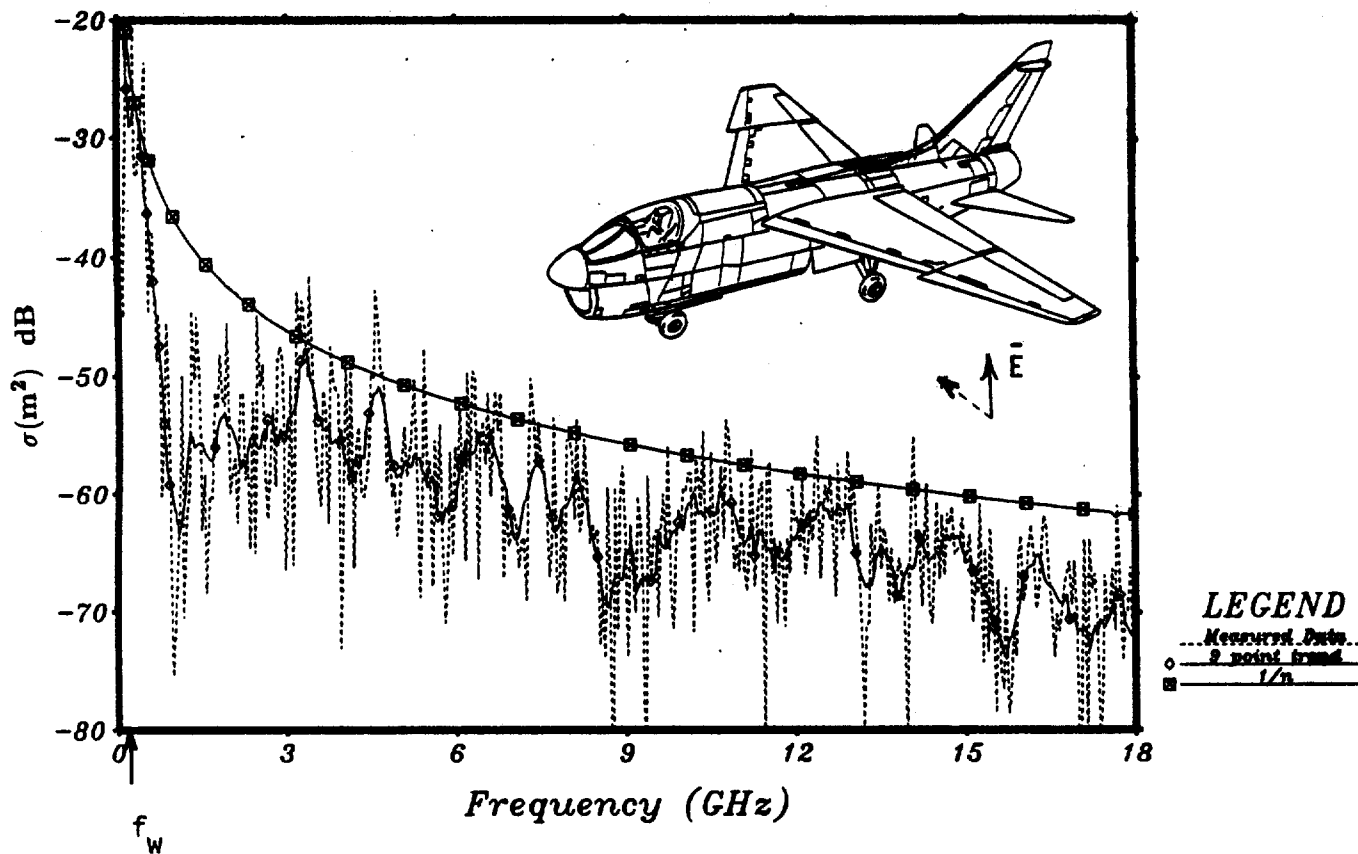


Figure 5.24. Response of the A7 1/10 scale model aircraft at terminal J4 (see Fig. 3.18).

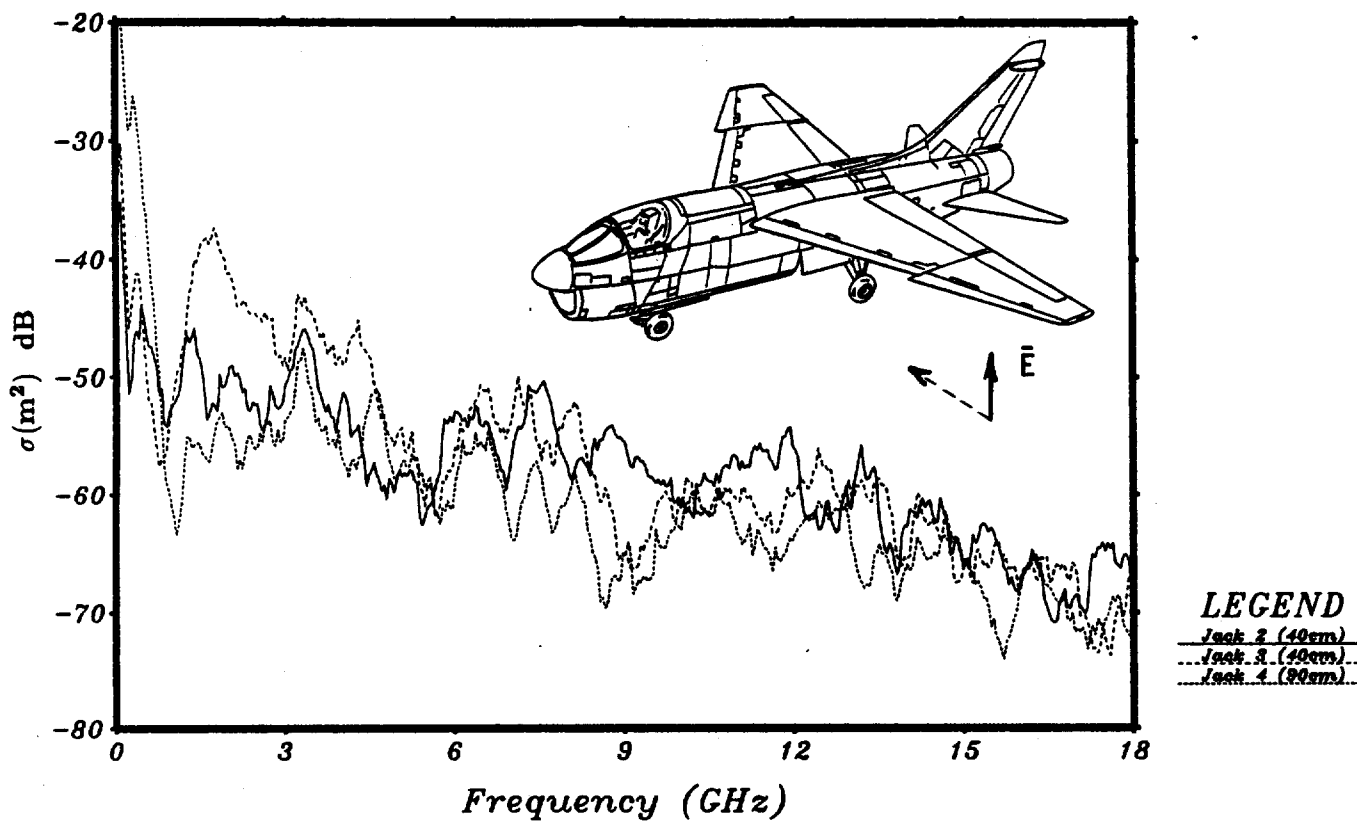


Figure 5.25. Response of the A7 1/10 scale model aircraft at terminals J2, J3 and J4 (see Fig. 3.18).

5.9. CONCLUDING REMARKS

The apparent reduction of SE below unity for $f \gg f_a$ and small apertures (see Fig. 5.2) or aperture blockage by metal fill (see Figs. 5.5, 5.6, 5.13, 5.14) needs further study in order to quantify and explain this effect. Part of this reduction may be due to frequency resolution in the raw experimental data. Small apertures or blockage of the aperture cause higher Q's of the cavity modes which are harder to adequately capture with the present sampling rate. As a result, the computed trends may be affected by the sampling rate.

The SExCE model discussed in Section 4 seems to bound the experimental results well, but considerably more effort is needed to quantify all of the possible interactions and effects. As this work progresses, a major goal is to be able quickly and easily sketch upper bounds on the overall receiving cross section or normalized wire response. Obviously, this is a very ambitious goal for an exceedingly complex problem, but thus far the results suggest that it is attainable. This will require many experiments on various configurations to determine the most important parameters and quantify their effects, in concert with numerical modeling. Hopefully, a model like SExCE can achieve this goal given a few simple geometric and electrical properties of the test object, e.g., port of entry size and shape, location, number and length of coupling wires/cables, size and location of metal and dielectric fill, presence of dielectric materials and lossy materials, etc.

From the previous data, the following general conclusions are drawn:

Aperture size and shape determine the shape of the Shielding Effectiveness (SE) curve (Fig. 4.1). Apertures generally behave as high pass filters having a cutoff frequency which is determined by the perimeter (Fig. 5.2). When the aspect ratio (length/width) is large (10:1 or greater) a pronounced peaking occurs at resonance, and this effect needs further quantification. Above resonance, the SE model appears to approach unity in accordance with Fig. 4.1 if the aperture is large (e.g., $> 12.5 \times 1.25$ cm in Fig. 5.2). For smaller apertures, SE above resonance is reduced below unity. Experiments and numerical modeling studies are currently in progress to more carefully quantify these observations.

Lengths of the coupling wires/cables largely determine the CE portion of the SExCE model, corresponding to when the wire is "unshielded." This curve decreases as f^{-1} above the first TEM wire resonance, or equivalently as n^{-1} where $n = 1, 2 \dots$ is the mode resonance number (in power such as σ or $(NWR)^2$, the curve decreases as f^{-2} and n^{-2} . This strongly suggests that the CE response envelope is chiefly determined according to TEM resonances as if the wire were unshielded, i.e., it behaves as a long wire antenna. The higher order cavity resonances simply add a "picket fence" like structure to the response. In the data presented here, this structure is smoothed 2.5% to permit observing the overall trend more clearly.

At frequencies near aperture resonance, coupling to the wire/cable is greatest when it is located near the aperture, and decreases as the wire is moved further inside the cavity. At frequencies far removed from aperture resonance ($f \geq 4f_a$), the location of the wire has little effect on the coupling (Figs. 5.3 and 5.4).

To date, there is little evidence that external resonances leak into the interior to any significant degree.

Metal fill in the cavity has little effect unless it tends to block the aperture (Figs. 5.6 through 5.14). When the fill is very near the aperture, it reduces the effective size of the aperture with a consequent increase in the aperture cutoff frequency and PE factor, especially if the fill is large (Fig. 5.6).

Height of the cavity has little effect on the overall coupling trend (Fig. 5.15), although the higher order cavity resonances add considerable structure to the response above aperture resonance.

Lossy fill inside the cavity can reduce the overall coupling to some degree, especially above 1 GHz. The reduction in coupling, however, is not dramatic (Figs. 5.16 through 5.21). More experiments are planned for a wider variety of absorbing materials.

Dielectric windows in the aperture can either increase or decrease the coupling near aperture resonance (Figs. 5.22 and 5.23). Further experiments

are also required here, and corroborating data from numerical modeling would be helpful.

Finally, tests on an A7 scale model aircraft conform to the CE of the SExCE model. This test object is so leaky, however, that it is not possible to identify a particular aperture resonance or the SE portion of the model.

6. FUTURE EFFORT

6.1. TESTS ON GENERIC AND SCALE MODEL TEST OBJECTS

As noted in Section 3.5, the anechoic chamber facility will become operational about January 1986. In the meantime, the experiments in which the EMPEROR facility is adequate will be carried out. Certain experiments must be done in the chamber, particularly those requiring a plane wave front and high sensitivity, because EMPEROR's wavefront is spherical and its gain is low. Also, those experiments calling for pattern measurements must be done in the chamber.

Figure 6.1 shows some of the PLUTO (generic test object) configurations which will be tested in the future, and Fig. 6.2 shows the timetable for carrying out those tests.

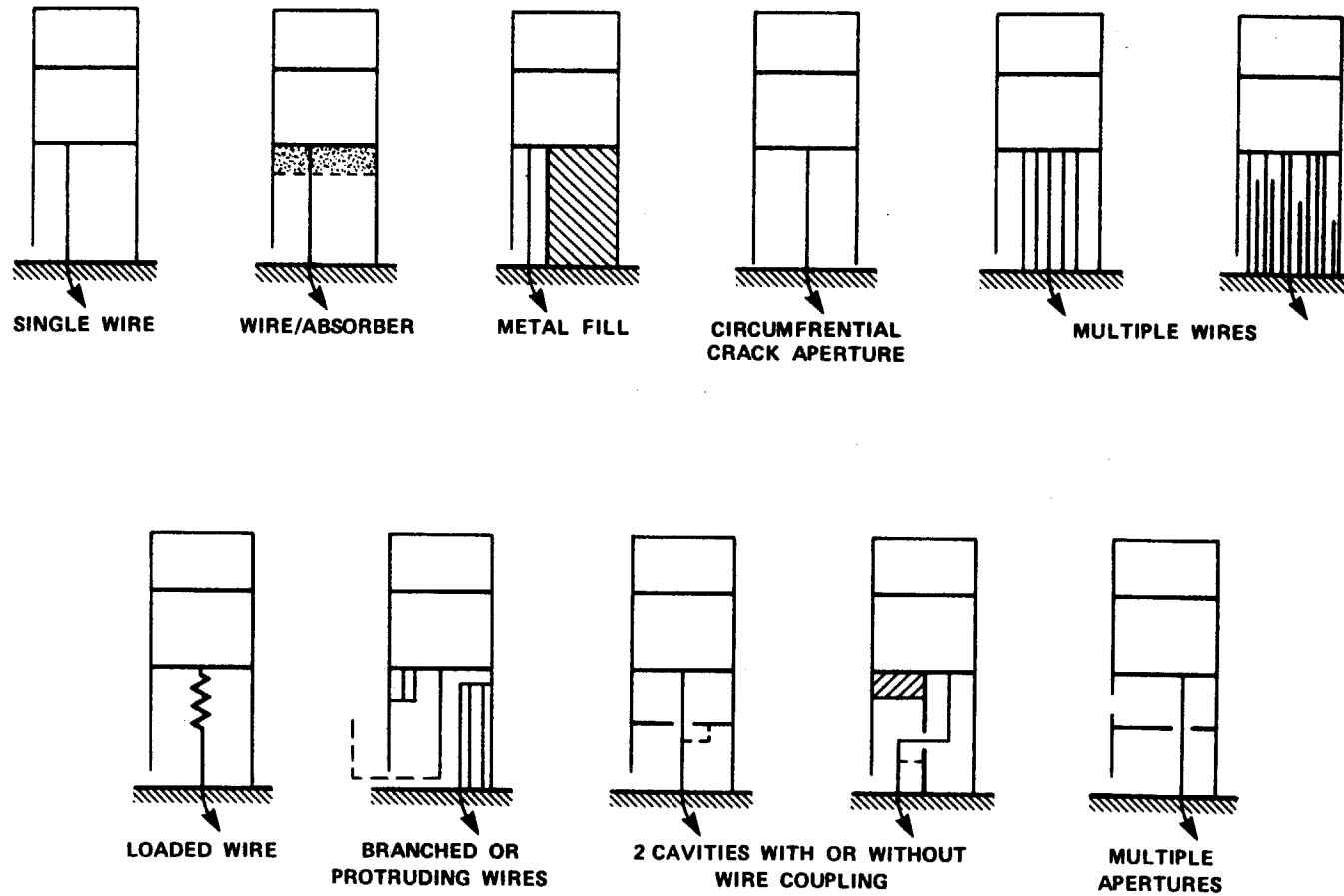


Figure 6.1. Some of the planned PLUTO configurations which will be tested during the course of these coupling studies.

PRELIMINARY TIMETABLE, HPM COUPLING
(22 May 1985)

1985

1986

M J J A S O N D J F M A M J J A S O N D

PHENOMENOLOGY

Characterize EMPEROR

Dielectrically shielded slot

Cable bundles and multiple wires,
branched bundles, external wires

Thin slot

"Lossy" fill

Multiple cavities and apertures

Loaded wires

Composite fill

Time domain synthesis

Anechoic chamber, install

Anechoic chamber, instrument

Seams/Connectors

ϕ , θ Variations

Multiple slits

Multiple cables

Multiple cavities

Homodyne field probe development

Field probe measurements

----- (Parts) -----

Reports

*

*

*

*

*

Figure 6.2. Preliminary Timetable, HPM Coupling (22 May 1985).

6.2. BROADBAND FIELD MAPPING HOMODYNE SYSTEM

A wideband (2-18 GHz) coherent detection (homodyne) system (Fig. 6.3) is being developed for mapping the amplitude and phase of microwave selected field components, particularly inside apertures and cavities. The probe is a small rectangular \dot{B} loop having a circumference which is small compared to the highest frequency used. This loop is loaded on two opposing sides by PIN diodes which are switched at 100 kHz, thereby amplitude modulating the normal \bar{H} -field component. By reciprocity, the scattered modulated field which finds its way back to the source antenna is coherently detected. Diode switching is accomplished via resistive leads which have negligible effect on the field being measured. Homodyne detection, besides being phase sensitive to permit phase as well as amplitude measurements, is also linear and has great sensitivity and dynamic range. The modulated probe arrangement avoids the use of cables and baluns which can disturb the field being measured and permits easy positioning and orientation of the probe for field mapping.

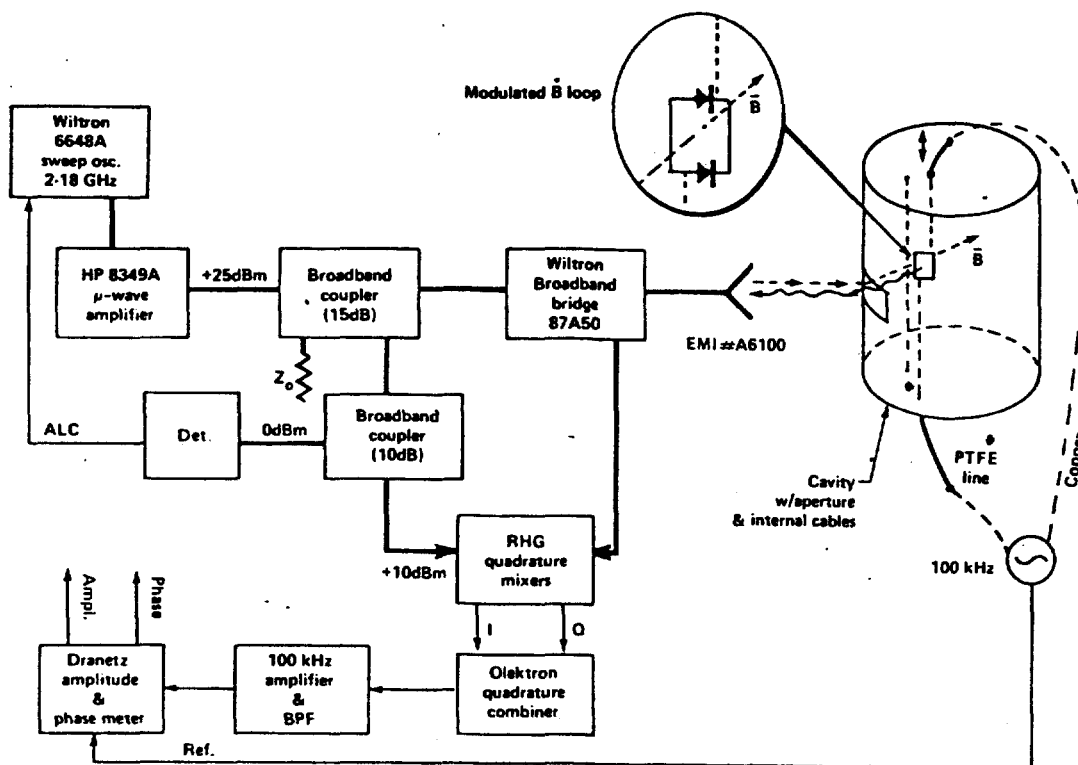


Figure 6.3. Broadband (2 to 18 GHz) homodyne system for mapping the amplitude, phase, and polarization of \vec{B} fields and currents inside cavities and apertures.

6.2.1. Basic System

The basic block diagram of the system is shown in Fig. 6.3. All microwave components are capable of operating over the 2-18 GHz range. The swept cw source drives an amplifier, and a portion of this output which serves as a reference signal, A, is coupled into the quadrature mixers. As with most mixers, this input is typically +10 dBm corresponding to the local oscillator input as specified by the manufacturer. Normally, it is desirable that this reference signal remain constant over the entire band, so a second broadband coupler is shown, the coupled output of which is detected and used as an automatic level control (ALC) of the swept source.

The main transmission path to the horn antenna is via a broadband bridge where the signal suffers a 6 dB loss before reaching the antenna. The cw field transmitted by the horn into the test object, in this case shown as a cavity with an aperture, is incident on a small printed circuit loop having a circumference somewhat smaller than a wavelength at the highest frequency used, e.g., 18 GHz. This ensures that the probe behaves as a \vec{B} sensor and scatters a field proportional to $j\omega\mu_0\vec{H} \cdot \vec{u}_l$ where ω is the angular frequency of the cw source, $\mu_0 = 4\pi \times 10^{-7}$, \vec{H} is the vector magnetic intensity and \vec{u}_l is a unit vector normal to the plane of the loop.

Two opposing sides of the loop are loaded with PIN diodes which are switched on and off by a low frequency (e.g., 100 kHz) sinusoidal oscillator via resistive (carbon impregnated PTFE) leads which are essentially transparent to the microwaves. The switching action amplitude modulates the signal scattered from the loop, and the leads are used to manipulate the position and orientation of the loop.

By reciprocity, a portion of this modulated signal finds its way back through the aperture where it is received by the transmitting horn antenna. It is then coupled into the quadrature mixers with another 6 dB of loss via the bridge. A precision bridge rather than a directional coupler, magic tee, or circulator was chosen for separating the modulated back-scattered signal from the outgoing cw signal because of its superior uniform amplitude and phase properties and exceeding by high directivity (36 dB) over the entire 2-18 GHz band.

While Fig. 6.3 shows the cavity being excited by an external source (horn), it can also be excited by direct injection, say by driving an internal coupling loop or wire. The principles of operation are the same in both cases.

Homodyne detection is accomplished by mixing the cw reference signal $A \angle 0^\circ$ with the double sideband amplitude modulated (DSBAM) signal $b \angle \phi^\circ$ in two mixers, one of which is in quadrature phase for say the reference signal. For a single mixer, this type of coherent mixing is called product for homodyne detection. Product detector is phase sensitive, which means that the amplitude of the detected signal depends on the phase, ϕ , between the

reference and information signals. While this is a useful feature in some cases, e.g., it is regularly used in very sensitive lock-in voltmeters, it is inconvenient for measuring the amplitude and phase of the information signal simultaneously and independently in real time, as is desired for the present application. For these reasons, a phase insensitive detector which is really the properly combined outputs of two homodyne detectors operating in phase quadrature, is used here to overcome these problems.

It is important to understand how phase-insensitive homodyne detection works, so the basic ideas are shown in Fig. 6.4. A comprehensive discussion on the principles of homodyne detection are given in [6]. First, consider the phase sensitive detector shown in the upper portion. For a sufficiently large A such that the mixer transfer characteristic is linear with slope K_h (conversion loss), the output at the angular modulation frequency, ω_m , is

$$e_{out} = K_h b \cos(\phi) \cos(\omega_m t) \quad (6.1)$$

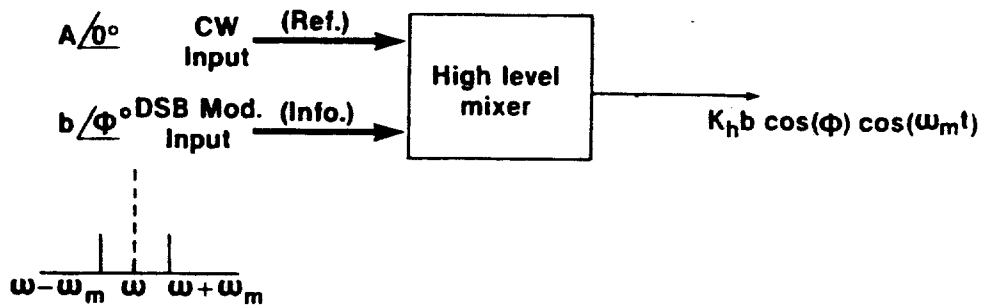
for DSB amplitude modulation. Harmonics of ω_m are omitted since they are easily removed by filtering. Equation (6.1) is clearly phase sensitive, i.e., the amplitude is $b \cos \phi$ so that the amplitude and phase information are contained as a product. They are not easily separable in a dynamic measurement.

This problem is circumvented by using two parallel identical mixers (except for the quadrature shift of the reference signal into one of the mixers) as shown in the lower portion of Fig. 6.4. The lower mixer has an output of the same form as (6.1) except for an additional factor of $1/2$ because of the power division between the two mixers. The upper mixer has an output

$$e_{out} = \frac{K_h}{2} b \sin(\phi) \cos(\omega_m t) \quad (6.2)$$

since the phase of the reference signal has been shifted by 90 degrees. Now, if the phase of $(\omega_m t)$ in (6.2) is also shifted by 90 degrees, it becomes

Phase-sensitive detector:



Phase-insensitive detector:

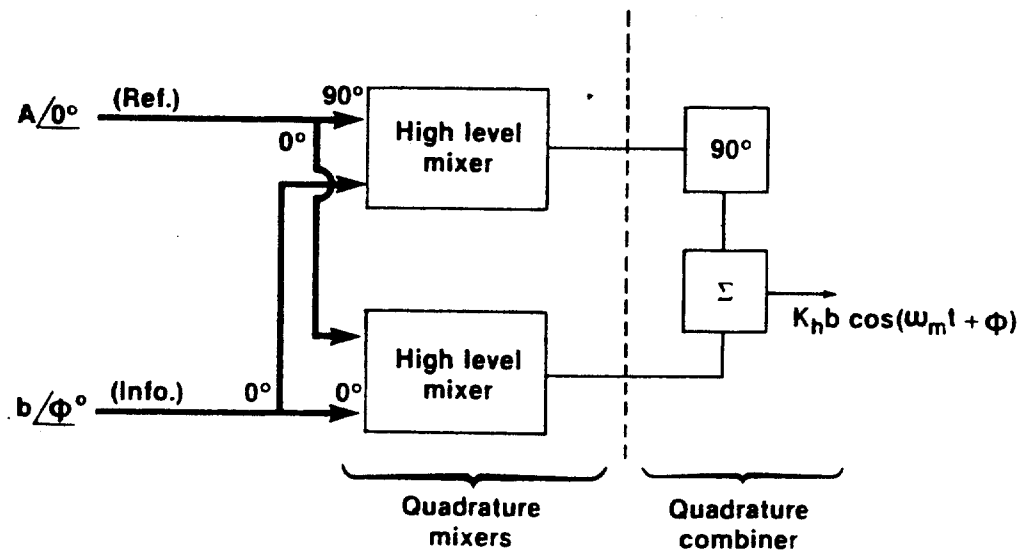


Figure 6.4. Basic phase sensitive and phase insensitive homodyne detectors.

$$e'_{\text{out}} = \frac{K_n}{2} b \sin(\phi) \sin(\omega_m t) \quad (6.3)$$

Summing the outputs of the lower mixer and (6.3) gives (via a trigonometric identity)

$$e_{\text{out}}^{\text{total}} = K_n b \cos(\omega_m t + \phi) \quad (6.4)$$

which is in the desired form to be able to measure the amplitude and phase simultaneously and independently in real time.

Of course, the above assumes that the amplitudes of both mixer channels are identical and that the phase shifts indicated are exactly 90 degrees. Small unbalances lead to amplitude and phase measurement errors. A full analysis of these errors and ways to mitigate them are given in [7].

Referring back to the basic system shown in Figs. 6.3, the ω_m output of the quadrature combiner (6.4) is amplified (typically 60-80 dB) and bandpass filtered to remove the low frequency mixer noise below ω_m and the harmonics of ω_m . This bandwidth (typically 3-5 kHz) should be sufficient to accommodate the anticipated rate of change of b and ϕ as the source is swept or the \vec{B} probe is moved. The amplitude and phase are then measured using a phase meter and a reference signal from the ω_m -modulating oscillator. The analog amplitude and phase signals can then be recorded digitally or graphically for analysis.

The basic principles outlined above are well understood, and building the system as shown is straightforward. However, a major problem remains which must be dealt with. The above assumes that the carrier signal entering the mixers through the information branch is small compared to the carrier entering the mixers through the reference branch. Such an undesired carrier, called A' , can originate as leakage through the broadband bridge (which typically has a directivity of 35 dB), but the most troublesome sources of A' are reflections from the feed of the horn and from the test object. Thus, A and A' combine to give an effective carrier which interacts with the sidebands in a very complex way. Since A' probably cannot be reduced to insignificant

levels (compared to A) over the entire 2 + 18 GHz band, a possible solution is to insert a YIG tracking notch filter into the information branch before the mixer. This will require the use of a higher modulating frequency, say 10 MHz, to avoid filtering the desired sidebands. This and other possible solutions are being considered for future implementation.

This system is not yet operational, although all of the components are on hand. The above discussion on the operation of the system is included here since the microwave coupling community has conveyed the need for such a capability. At present, this community has no tools for mapping fields and measuring currents on wires and conducting surfaces above a few GHz.

REFERENCES

1. R. J. King, J. K. Breakall, H. G. Hudson, J. J. Morrison, K. S. Kunz, V. G. McGevna, and D. K. Gnade, "Phenomenology of Microwave Coupling, Part I," LLNL UCID-20215, November 1984.
2. G. J. Burke and A. J. Poggio, "Numerical Electromagnetics Code (NEC) - Method of Moments," NOSC Technical Document 116, January 1980.
3. K. S. Kunz, H. G. Hudson, J. K. Breakall, R. J. King, S. Pennock and A. P. Ludwigsen, "Lawrence Livermore National Laboratory Electromagnetics Measurement Facility," UCRL-20416, April, 1985.
4. K. S. Kunz and H. G. Hudson, "A Shielding Effectiveness Characterization for Highly Resonant Structures Applicable to System Design," UCRL-92015, January, 1985.
5. J. K. Breakall and H. G. Hudson, "The Equivalent Current Measurement Technique and its Comparison with Current Probe Measurements," UCRL-91905, April, 1985.
6. R. J. King, Microwave Homodyne Systems, Peregrinus Press, 1978.
7. R. J. King, "Error Analysis of Phase-Insensitive Coherent (Homodyne) Detectors," IEEE Trans. on Instrumentation and Measurement, IM-31(3), September 1982, pp, 212-214.

